GL-TR-89-0266

Ion and Electron Interactions at Thermal and Suprathermal Energies

David Smith
Nigel G. Adams
Charles R. Herd

University of Birmingham
School of Physics and Space Research
Birmingham B15 2TT, UNITED KINGDOM

30 September 1989

Scientific Report No. 2

GEOPHYSICS LABORATORY
AIR FORCE SYSTEMS COMMAND
UNITED STATES AIR FORCE
HANSCOM AIR FORCE BASE, MASSACHUSETTS 01731-5000

"This technical report has been reviewed and is approved for publication"

JOHN F. PAULSON
Contract Manager

JOHN E. RASMUSSEN
Branch Chief

FOR THE COMMANDER

ROBERT A. SKRIVANEK
Division Director

This report has been reviewed by the ESD Public Affairs Office (PA) and is releasable to the National Technical Information Service (NTIS).

Qualified requestors may obtain additional copies from the Defense Technical Information Center. All others should apply to the National Technical Information Service.

If your address has changed, or if you wish to be removed from the mailing list, or if the addressee is no longer employed by your organization, please notify GL/IMA, Hanscom AFB, MA 01731. This will assist us in maintaining a current mailing list.

Do not return copies of this report unless contractual obligations or notices on a specific document requires that it be returned.

Unclassified
SECURITY CLASSIFICATION OF THIS PAGE

REPORT DOCUMENTATION PAGE

1a. REPORT SECURITY CLASSIFICATION Unclassified	1b. RESTRICTIVE MARKINGS
2a. SECURITY CLASSIFICATION AUTHORITY	3. DISTRIBUTION / AVAILABILITY OF REPORT Approved for public release; Distribution unlimited
2b. DECLASSIFICATION / DOWNGRADING SCHEDULE	
4. PERFORMING ORGANIZATION REPORT NUMBER(S)	5. MONITORING ORGANIZATION REPORT NUMBER(S) GL-TR-89-0266
6a. NAME OF PERFORMING ORGANIZATION University of Birmingham 6b. OFFICE SYMBOL (If applicable)	7a. NAME OF MONITORING ORGANIZATION European Office of Aerospace Research and Development
6c. ADDRESS (City, State, and ZIP Code) School of Physics & Space Research Birmingham B15 2TT, UNITED KINGDOM	7b. ADDRESS (City, State, and ZIP Code) 223/231 Old Marylebone Road London NW1 5TH, UNITED KINGDOM
8a. NAME OF FUNDING / SPONSORING ORGANIZATION Geophysics Laboratory 8b. OFFICE SYMBOL (If applicable) LID	9. PROCUREMENT INSTRUMENT IDENTIFICATION NUMBER AFOSR-87-0355
8c. ADDRESS (City, State, and ZIP Code) Hanscom AFB Massachusetts 01731-5000	10. SOURCE OF FUNDING NUMBERS PROGRAM ELEMENT NO: 62101F; PROJECT NO: 2303; TASK NO: G1; WORK UNIT ACCESSION NO: AJ
11. TITLE (Include Security Classification) **Ion and Electron Interactions at Thermal and Suprathermal Energies**	
12. PERSONAL AUTHOR(S) David Smith, Nigel G. Adams, Charles R. Herd	
13a. TYPE OF REPORT Scientific #2 13b. TIME COVERED FROM _____ TO _____	14. DATE OF REPORT (Year, Month, Day) 1989 September 30 15. PAGE COUNT 122
16. SUPPLEMENTARY NOTATION	
17. COSATI CODES FIELD / GROUP / SUB-GROUP	18. SUBJECT TERMS (Continue on reverse if necessary and identify by block number) Electron attachment Dissociative recombination Ion-molecule reactions Flowing afterglow/Langmuir probe Selected ion flow tube

19. ABSTRACT (Continue on reverse if necessary and identify by block number)

The flowing afterglow/Langmuir probe (FALP) apparatus has been used to study (i) dissociative electron attachment reactions of several haloethanes; (ii) the neutral products of the dissociative recombination reactions of several ground state polyatomic ions (using the FALP together with LIF and VUV spectroscopic techniques). The selected ion flow tube (SIFT) apparatus has been used to study (iii) the reactions of ions in the series PH_n^+(n=0 to 4) and the reactions of Kr^+, Xe^+, Kr_2^+ and Xe_2^+ with several molecular gases. Details of these studies are given in seven appendices to the report.

20. DISTRIBUTION / AVAILABILITY OF ABSTRACT ☐ UNCLASSIFIED/UNLIMITED ☐ SAME AS RPT ☐ DTIC USERS	21. ABSTRACT SECURITY CLASSIFICATION Unclassified
22a. NAME OF RESPONSIBLE INDIVIDUAL John Paulson	22b. TELEPHONE (Include Area Code) 22c. OFFICE SYMBOL GL/LID

DD FORM 1473, 84 MAR — 83 APR edition may be used until exhausted. All other editions are obsolete.

SECURITY CLASSIFICATION OF THIS PAGE
Unclassified

PREFACE

PREFACE

This work is part of a larger programme of ionic reaction studies at thermal energies conducted by the senior authors of this report. The overall programme includes studies of ion/neutral reactions, electron attachment, electron/ion recombination, ion/ion recombination, and other plasma reaction processes. The work is largely intended as a contribution to the physics and chemistry of natural plasmas, such as the ionosphere and the interstellar medium, and of laboratory plasma media, such as gas laser systems, etchant plasmas and combustion plasmas. A great deal of relevant data has been obtained principally by exploiting the variable-temperature selected ion flow tube (VT-SIFT), the variable-temperature selected ion flow drift tube (VT-SIFDT) and the variable-temperature flowing afterglow/Langmuir probe (VT-FALP) techniques which were developed in our laboratory. Part of the overall programme is supported by a grant from the Science and Engineering Research Council.

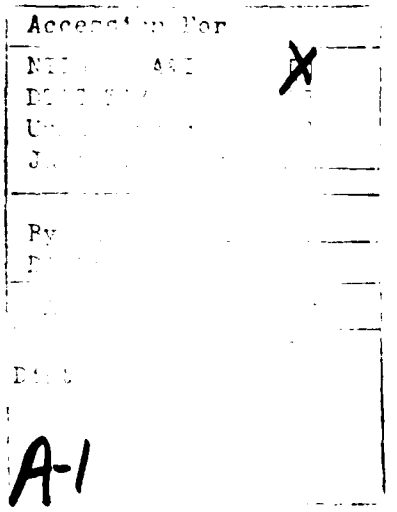

I INTRODUCTION

Our major commitment under the terms of the current grant is to study various gas-phase ionic reaction processes at thermal and near-thermal energies, with special reference to processes that may occur in the terrestrial atmosphere and in combustion and discharge plasmas. Such processes include ion/neutral reactions, electron attachment, electron/ion recombination and ion/ion recombination (mutual neutralization). All these processes can be studied in our laboratory following our development and construction of the very versatile selected ion flow drift tube (SIFDT) and flowing afterglow/Langmuir probe (FALP) techniques. Using these techniques, rate coefficients and ion products of reactions can be determined in many cases over the wide temperature range 80-600K and at reactant ion/reactant neutral centre-of-mass energies up to about one electron volt in some cases. Numerous reactions have been studied during the past few years and many have been presented in previous reports and research publications. The relevance of much of our experimental work to the terrestrial atmosphere, interstellar gas clouds and laboratory etchant plasmas is explained in the brief review paper which is presented as Appendix 1 to this report.

During the period covered by the current grant, we have added laser and vacuum ultraviolet spectroscopic techniques to the already versatile FALP apparatus and this has greatly extended the processes that we can study. In this report, we refer to

the further studies we have made of electron attachment, electron/ion recombination, specifically the neutral products of some such reactions, and some ion/molecule reactions. Details of much of this work are given in the reprints and preprints of research papers which are included as Appendices 2-8 of this report. A brief summary of the most important results is given in the next section.

II SUMMARY OF RESULTS

(a) Electron Attachment

In the previous Interim Scientific Report No.1, we mentioned the results of our study of the attachment reactions of C_6F_5Cl, C_6F_5Br and C_6F_5I. The detailed results of this study are given in this report as Appendix 2. Also mentioned briefly in the previous report was our study of the attachment reactions of methyl and ethyl triflate and the details of this study are presented in Appendix 3.

More recently, we have completed a study of the dissociative attachment reactions of four haloethanes, CH_3CCl_3, $CH_2ClCHCl_2$, CF_3CCl_3 and $CF_2ClCFCl_2$, which was carried out under truly thermalised conditions at 298, 385 and 470K using our flowing afterglow/Langmuir probe (FALP) apparatus. In all four reactions the only product ion was Cl^-; in the majority of the reactions the attachment rate coefficient, β, increases rapidly with increasing temperature. The values of β obtained have been compared with those derived from non-thermal swarm and photoionization techniques in which the β are observed to decrease with increasing mean electron energy, $\bar{E}$, at a fixed gas temperature of 298K. The different senses of the variations

of β with temperature and with $\bar{E}$ are discussed, and are rationalised in terms of the thermal and non-thermal nature of the different experiments, in Appendix 4 to this report.

Our most recent attachment study has involved some bromomethanes and bromoethanes. The surprising result of this study is that dissociative attachment reactions between these molecules results in the production of not only Br^- ions as expected but also a significant fraction of Br_2^- ions. The details of these observations will be discussed in a research paper which is now in the draft stage.

(b) Electron/Ion Dissociative Recombination

We have previously used the FALP apparatus to determine the dissociative recombination reaction rate coefficients, α, for a wide variety of polyatomic ions and the data have been presented in several research papers and in previous scientific reports. During the last year, we have begun a programme of measurements to determine the neutral products of the dissociative recombination reactions of some polyatomic ions. This has been made possible by the application of laser induced fluorescence (LIF) and vacuum ultraviolet (VUV) spectroscopic techniques to recombining FALP plasmas consisting of electrons and one ionic species only. In the first measurements, we have determined the fraction of OH molecules (by LIF) produced in the recombination with electrons of the ions HCO_2^+, N_2OH^+, O_2H^+ and H_3O^+. The intensity of the LIF from OH radicals was calibrated against the OH number density by first creating a swarm of H atoms in the flow tube in the absence of ionization, determining the number density of H atoms in the plasma (by utilizing VUV absorption) and then converting all of the H atoms to OH radicals using the

reaction $H+NO_2 \rightarrow OH+NO$. The details of the experimental approach to this interesting study are given in Appendix 5 to this report. The fractions of OH generated following dissociative recombination of the above-mentioned ions are reported in the preprint given as Appendix 6 to this report.

These data on the neutral molecular products of dissociative recombination of ground state polyatomic ions are the first ever obtained. Work is proceeding to determine the fractions of H and O atoms produced in the above recombination reactions. Preliminary data have been obtained and these will be consolidated and then presented in research publications and future reports.

(c) Ion/Neutral Reactions

We have continued to exploit our versatile selected ion flow tube (SIFT) apparatus to study a range of ion/molecule reactions. Specifically, we have carried out a detailed study at 300K of the reactions of the phosphorus-bearing ions PH_n^+(n=0 to 4) with many molecular gases. Many reaction processes are observed, but especially interesting are the phosphorus atom insertion reactions which produce ions such as H_nPN^+, H_nPO^+, H_nPS^+ and $H_nC_mP^+$. A considerable amount of kinetic data and information has been obtained from this study. For example, upper limits to the heats of formation of HPO^+, H_2PO^+, $PC_2H_2^+$ and HCP have been obtained. The details are given in the research paper included as Appendix 7 to this report.

We have also carried out a detailed study at 300K of the reactions of the spin states ($^2P_{\frac{1}{2}}$, $^2P_{\frac{3}{2}}$) of Kr^+ and Xe^+ and the reactions of Kr_2^+ and Xe_2^+ using our SIFT apparatus. Again, a

great deal of information has been obtained from this substantial study, including the dissociation energies of the molecular ions Kr_2^+ and Xe_2^+ . Full details are presented in the research paper included as Appendix 8 to this report.

III CONCLUSIONS

Our studies of electron attachment reactions, ion/neutral reactions and especially the products of dissociative recombination reactions have continued apace during the last year. Some seven research papers (included as appendices) summarise the results obtained. Our determination of the neutral products of the dissociative recombination reactions of ground state polyatomic ions are the first ever obtained. The LIF and VUV spectroscopic techniques that we have developed, together with optical spectroscopy, will be exploited further in the coming years to determine the neutral products of a greater range of dissociative recombination reactions. Optical emissions are to be expected from certain positive ion/electron recombination reactions and also from some positive ion/negative ion neutralization reactions. A concerted effort will be made to look for such emissions using the FALP in the near future. Our programme of electron attachment studies will also be continued using the FALP., Using the SIFT, we will soon initiate a detailed survey of the reactions of ions observed from silane (SiH_n^+ reactions), germane (GeH_n^+ reactions), and diborane (BH_2^+ and $B_2H_n^+$ reactions).

APPENDIX 1

IONIC REACTIONS IN ATMOSPHERIC, INTERSTELLAR AND LABORATORY PLASMAS

N.G. ADAMS AND D. SMITH

Contemp.Phys., 29, 559 (1988)

CONTEMP. PHYS., 1988, VOL. 29, NO. 6, 559-578

Ionic reactions in atmospheric, interstellar and laboratory plasmas

Nigel G. Adams and David Smith, Department of Space Research, University of Birmingham, Birmingham B15 2TT, England

ABSTRACT. The ionic reactions that can occur in ionized gases, and especially those in naturally-occurring low-temperature gaseous plasmas, are discussed. These reactions include several types of positive ion and negative ion reactions with molecules, ion–electron dissociative recombination reactions, electron attachment reactions and ion–ion mutual neutralization reactions. The laboratory techniques used to study and to determine the rate coefficients for these reactions are briefly described. Three case studies are presented which illustrate how the various types of ionic reactions modify the ionic and neutral composition of ionized media. These case studies describe the reactions which (1) lead to the observed ions in the terrestrial atmosphere; (2) produce the neutral molecules and molecular ions that are detected in interstellar gas clouds; and (3) can occur in the laboratory discharge plasmas that are used to etch the surfaces of semiconductors in the preparation of microprocessors.

1. Introduction

Mixtures of many gases are quite stable and unreactive at normal temperatures. For example, the terrestrial atmosphere near sea level is fortunately very stable since no reaction occurs between N_2 and O_2 and so toxic gases such as NO_2 are not produced in significant amounts. Also the problem of atmospheric pollution would be much worse if common atmospheric pollutants were reactive with atmospheric gases. However, when gases are exposed to a source of radiation, intense electric fields, and such like, so that the molecules are dissociated to atoms or especially when the neutral species become ionized, their reactivity increases enormously. Thus, when ionization is created in a gas mixture, complex ionic reaction processes are initiated which may greatly modify the molecular species within the ionized gas. For each positive, singly-charged atom or molecule produced in the ionization process, a free electron must also be produced so that the ionized gas remains electrically neutral overall. Then the medium may be termed a gaseous plasma, although this term has to be applied carefully since other criteria must be obeyed for ionized gases to be properly termed gaseous plasmas (McDaniel 1964). In this article, we will be concerned largely with weakly ionized gases at relatively low temperatures, many of which can be correctly termed low-temperature gaseous plasmas. These include the terrestrial ionosphere ($200\ \mathrm{K} \leqslant T \leqslant 2000\ \mathrm{K}$), some interstellar gas clouds ($10\ \mathrm{K} \leqslant T \leqslant 200\ \mathrm{K}$) and laboratory etchant plasmas. In some plasmas, the temperatures of the component particles are not equal (for example, the electron temperature in the F-region of the terrestrial ionosphere exceeds the ion and neutral temperatures by about a factor of three; see Smith and Adams (1980)) and it is important to appreciate this fact when attempting to understand the complex reaction processes that occur. The electrons that are generated in the initial ionization process may remain free for a period or become 'attached' to neutral species to form negative ions. Free electrons and negative ions can react with positive ions, thus neutralizing the plasma and acting to return the medium to the neutral gaseous state. It is these 'recombination' reactions together with the numerous ion–neutral reactions which combine to produce the rich ion physics and chemistry of low-temperature plasmas which we describe in this article.

When gaseous plasmas are only weakly ionized, the collision frequencies between ions and neutrals will greatly exceed those between charged particles (positive ions, negative ions and electrons) and so ion–neutral reactions and electron–neutral (attachment) reactions will generally precede recombination reactions. Hence a great variety of ionic species can be synthesised in the plasma before recombination reactions can occur to produce new neutral species.

Why do ion–neutral reactions and recombination reactions proceed so much more rapidly than neutral–neutral reactions? Why do ion–neutral reactions proceed more rapidly as the temperature of the plasma is reduced contrary to the behaviour of most neutral–neutral reactions? The simple answer lies in the nature of the forces that come into play during the collisional process. The force between two neutral molecules acts over a relatively short range. This limits the collision frequency and thus the so-called collisional rate coefficient, which is an indicator of the maximum efficiency of the reaction. Moreover, most neutral–neutral reactions are inhibited by activation-energy barriers, which can be thought of as potential barriers which the reactants must overcome to achieve new bonding arrangements. The presence of such barriers implies that neutral–neutral reactions should proceed more rapidly as the temperature of the reactants is increased and this is often observed to be the case. So, neutral–neutral reactions will generally proceed only slowly in low-temperature plasmas but there are well known exceptions; notably some reactions involving neutral radical species (Howard and Smith 1983).

The forces between charged (ions) and neutral species are clearly different. When an ion approaches a non-polar molecule the electric field associated with the ion distorts the charge distribution within the molecule, thus inducing an electric dipole. This results in an *attractive* force between the ion and the molecule described by an interaction potential, $V(r)$, proportional to r^{-4}, where r is the ion–molecule separation. This force is relatively long-range compared to that between neutral molecules and thus ensures that the corresponding capture cross-sections exceed those for neutral–neutral interactions by about an order of magnitude at room temperature. An expression for the collisional rate coefficient, k_c, can be readily derived, which shows it to be dependent only on the polarizability of the molecule, α, and the reduced mass of the reactants, μ, ($k_c = 2\pi q(\alpha/\mu)^{1/2}$, where q is the ionic charge, and is typically 10^{-9} cm^3 s^{-1}) and, significantly, is independent of temperature T (although the capture cross-section, which is inversely proportional to the relative velocity of the reactants, varies as $T^{-1/2}$). This simple expression for k_c has been vindicated by numerous experimental measurements of the rate coefficients, k, for ion–molecule reactions (for the experimental methods see the next section). If the reactant molecule possesses a permanent dipole moment then $V(r)$ includes an additional term. This results in an increase in k_c by a factor dependent on the dipole moment of the molecule, μ_D, and, significantly, renders k_c dependent on temperature:

$$k_c = 2\pi q/\mu^{1/2}[\alpha^{1/2} + C\mu_D(2/\pi kT)^{1/2}],$$

where C is a constant (Su and Bowers 1979). Thus for a typical polar molecule (e.g. H_2O or NH_3), k_c for the reaction with a given ion exceeds that for the reaction of the same ion with a non-polar molecule of similar mass and polarizability by about a factor of two at room temperature. However, k_c values for reactions between ions and polar molecules exceed those for reactions between ions and non-polar molecules by a factor of about ten at the low temperatures of interstellar clouds. It is interesting to note that if any

intrinsic energy barrier to molecular rearrangement exists in the ion–molecule interaction, then these energy barriers can be overcome by the energy gained by the reactants in the attractive field. This energy cannot, however, be used to promote endothermic reactions since as the ion–neutral products of the reaction separate the reactive system must 're-absorb' this energy.

When the two reacting species are both charged, as is the case for the dissociative recombination reaction of a molecular positive ion with an electron and for the mutual neutralization reaction of a positive ion with a negative ion, the attractive force is Coulombic and long-range with $V(r)$ proportional to r^{-1} (Bardsley and Biondi 1970, Moseley *et al.* 1975). It is therefore expected that the capture cross-sections, and hence the rate coefficients for such reactions, will exceed those for ion–neutral reactions, and this is observed experimentally. Indeed, dissociative recombination coefficients, α_e, and mutual neutralization coefficients, α_i, exceed ion–molecule collisional rate coefficients by typically two to three orders of magnitude at room temperature. Also, theory predicts, and experiments confirm, that both α_e and α_i should increase with decreasing temperature. This fact, and the fact that many ion–neutral reactions also proceed more rapidly at low temperatures, is important to the proper understanding of the reactions occurring in low-temperature plasmas such as some terrestrial atmospheric regions and interstellar gas clouds, to which we give special attention below.

2. Ionic reaction processes in gaseous plasmas—a brief overview

For simplicity, we consider first the ionization of an unreactive mixture of two diatomic molecular gases, A_2 and B_2. Later, in sections 4–6, we consider real situations as case studies. Even in such a relatively simple A_2/B_2 mixture many different reactive species can be generated by subjecting the gas mixture to an electrical discharge or irradiating it with energetic particles or photons. In the primary processes, positive ions and free electrons (*direct ionization*), atomic and molecular radicals (dissociation) and negative ions (electron attachment) may be formed. Negative-ion formation requires that electronegative gases (such as O_2, halogens, chlorofluorocarbons) be present. A multitude of excited states of A_2 and B_2 and of the newly created charged and neutral

Table 1. A list of the primary processes that occur when a mixture of two molecular gases (A_2 and B_2) is subjected to a source of ionization, such as a gas discharge or energetic photons, and the subsequent reaction processes that can occur between the ions, electrons and neutral species which generate new ionic and neutral species in the gas.

No.	Process	Description	Comments
Primary processes			
(i)	$A_2 \rightarrow A + A$ $B_2 \rightarrow B + B$	Dissociation	The energies of the electrons and photons which cause dissociation and ionization must exceed the threshold energies for these processes
(ii)	$A_2 \rightarrow A_2^+ + e$ $B_2 \rightarrow B_2^+ + e$	Direct ionization	
(iii)	$A_2 \rightarrow A^+ + A + e$ $B_2 \rightarrow B^+ + B + e$	Dissociative ionization	

The dissociative attachment and direct attachment processes given in (5 a) and (5 b) below may also be primary processes.

Table 1. (*Continued*).

Reactions following ionization		
1(*a*). $A^{\pm} + B_2 \rightarrow B_2^{\pm} + A$	Charge transfer (exchange)	Which process dominates is determined by the energetics of the reactions. The rate equation for A^* would, for example, be $d[A^*]/dt = -k_1[A^*][B_2]$, where [ ] denote concentrations. When $[B_2] \gg [A^*]$, as is common, $[A^*]$ decays exponentially.
1(*b*). $\rightarrow B^{\pm} + B + A$	Dissociation charge transfer	
1(*c*). $\rightarrow AB^{\pm} + B$	Ion–atom interchange (or atom abstraction)	
2. $A^- + B \rightarrow AB + e$	Associative detachment	Important in plasmas with negative ions and large concentrations of atomic radicals (such as H or O).
3. $A^{\pm} + B_2 + M \rightarrow A^{\pm}B_2 + M$	Ion–molecule association or clustering (M is the third body which removes energy released in forming the $A^{\pm}B_2$ molecule)	In atmospheric air, M would surely be either N_2 or O_2. This type of reaction is very likely in high-pressure low-temperature media.
4. $A_2^+ + e \rightarrow A + A$	Dissociative recombination	An efficient process; very fast compared to radiative recombination, namely $A^+ + e \rightarrow A + h\nu$. Rate equation for $[A_2^+]$ is $d[A_2^+]/dt = -\alpha_e[A_2^+][e]$. When $[A_2^+] = [e]$, the solution is: $[A_2^+]_t^{-1} = [A_2^+]_0^{-1} + \alpha_e t$. This condition can be realized in some laboratory plasmas.
5(*a*). $A_2 + e \rightarrow A^- + A$	Dissociative electron attachment	For the dissociative process, the electron affinity of A must exceed the bond dissociation energy of A_2. The direct process can occur if A_2 has a finite electron affinity. The rate equation for 5(*a*), for example, is $d[e]/dt = -\beta[A_2][e]$. When $[A_2] \gg [e]$, the solution is exponential.
5(*b*). $A_2 + e + M \rightarrow A_2^- + M$	Direct electron attachment	
6(*a*). $A^+ + B_2^- \rightarrow A + B_2$	Mutual neutralization	The ternary process 6(*b*) could result in the formation of AB_2 molecules. The rate equations are similar to that for the dissociative recombination process (4).
6(*b*). $A^+ + B_2^- + M \rightarrow A + B_2 + M$	Ternary ionic recombination	

species may be present and this constitutes a very reactive mixture. Many sequential and parallel reactions can occur between the positive and negative ions and neutrals which generate different, often polyatomic, ions. Also, recombination (neutralization) reactions between positive ions and electrons and between positive ions and negative ions can occur which act to return the ionized gas to the neutral state (generating other neutral species in the gas). The various reaction processes are summarised in table 1. Limitations are placed on the reactions by the energetics; reactions cannot occur in low-temperature plasmas if they are significantly endothermic. Nevertheless, even under the extremely low temperatures of some interstellar gas clouds, many ionic reactions occur which greatly modify the composition of the clouds. Specific examples of the generalized reaction processes listed in table 1 are presented in sections 4–6.

It is clear that a great deal of laboratory data is required before a quantitative understanding of the overall reaction kinetics and ion chemistry of low-temperature plasmas can be obtained. In response to this, several important experimental techniques have been developed in recent years including those described below.

3. Laboratory techniques for studying ionic reactions at thermal energies

There are two basic methods for the study of ionic reactions: beam methods which yield cross-sections from which rate coefficients must be obtained indirectly; and swarm methods which yield rate coefficients directly.

Beam techniques involve the generation of well collimated beams of the reactive species—ions, electrons or neutrals—which cross at some well defined angle under very low ambient pressure conditions. At the region of interaction the species may react, and from the reduction of intensity of one (or both) of the beams, the cross-section for the reaction is determined as a function of the centre-of-mass interaction energy E_{cm}. Ion beams of a given mass-to-charge ratio, m/q, are usually prepared using mass filters (magnetic sectors instruments are the most common), and the ionic products of the reactions are usually detected using mass spectrometers. Pulse-modulation techniques are often used to determine more accurately the often very small fractional attenuation of the beams and to discriminate against reactions with background gas. By varying the interaction angle and determining the distribution of the products of the reactions as a function of the scattering angle (differential scattering methods), a great deal of information about the dynamics and mechanisms of the reactions as well as the differential scattering cross-sections, σ, can be obtained (McDaniel *et al.* 1970). The disadvantage of conventional beam methods for the provision of kinetic data of relevance to real low-temperature plasmas is that the experiments cannot be performed to sufficient accuracy at sufficiently low E_{cm} (that is, at E_{cm} equivalent to room temperature and below) to give rate coefficients k of acceptable accuracy. (Note that k is related to σ by the relation

$$k = \int_0^\infty f(E_{cm})\sigma(E_{cm})\,dE_{cm},$$

where $f(E_{cm})$ is the Maxwell–Boltzmann thermal energy distribution function. Thus since to determine formation and loss rates in real media we need k as a function of the temperature, T, we have to measure σ as a function of E_{cm} and then take a thermal average.) To alleviate this disadvantage, merged beam experiments have been developed to study binary ion–electron and ion–ion neutralization reactions (see

table 1) in which the reactive species are formed in beams which are merged to overlap collinearly (Moseley *et al.* 1975, Brouillard and McGowan 1983). Thus, by adjusting the laboratory velocities of the two beams to be similar, the E_{cm} can in principle be made very small, that is, similar to those E_{cm} appropriate to low temperatures. These merged beam methods have had some success, although uncertainty still surrounds the data obtained at low E_{cm}, principally because of the extreme difficulty of ensuring that the beams are precisely collinear and are not interacting at a small angle or diverging. Some doubt also exists concerning the internal energy states of the reactant ions generated for such single collision experiments, a very important point when it is considered that the reactivity of positive ions with electrons and with negative ions can be very dependent on the internal energy of the ions. It is for these reasons that kinetic data obtained from swarm experiments are strongly favoured for modelling the ion chemistry of the terrestrial atmosphere (see section 4) and interstellar clouds (section 5).

Swarm methods involve an ensemble of reactive particles, ideally possessing a Maxwellian distribution of velocities which interact with another ensemble of particles which ideally also possess a Maxwellian velocity distribution at the same temperature. The experiment then reduces to the determination of the rate of loss of one or both of the reactants, and then a rate coefficient for the reaction can be determined directly at a fixed temperature (or as a function of temperature in many experiments). Using these methods, kinetic data have been obtained at temperatures as high as 10^3 K and below 10 K (see Adams and Smith (1983) for example).

Perhaps the most successful techniques for the study of ion–neutral reactions in the thermal energy regime are the ion cyclotron resonance (ICR) technique and the fast-flow tube techniques. In the ICR technique (McIver 1978), a swarm of ions of a given m/q is trapped in a cell under low-pressure conditions ($< 10^{-4}$ torr) by a combination of mutually perpendicular static electric and magnetic fields. The trapped ions are detected and their m/q established by matching the frequency of a probing radio frequency (r.f.) field impressed on to the cell to the cyclotron frequency of the ions. Reactive gases are introduced into the cell at (known) low pressures and the change in the r.f. signal strength (resonance absorption) due to the trapped reactant ions is monitored as a function of time at a fixed pressure of the reactant gas. Hence the rate coefficient for the ion–neutral reaction is determined directly at a particular interaction energy which is usually equated to the temperature of the cell walls. Ionic products of the reaction are identified by sweeping the r.f. probing field and recognising resonance absorption at the different frequencies appropriate to the m/q of the product ions. Valuable data have been obtained for ion–neutral reactions using ICR methods, which have been used both to determine the mechanisms of reactions and to establish relative thermochemical quantities such as proton affinities. They have also been valuable in the elucidation of interstellar ion chemistry. The major criticism of such data lies in the uncertainty in the energies of the interacting ions (which it has been suggested may be in excess of that appropriate to the cell temperature by about 0·1–0·2 eV). The internal energy of some ionic species in ICR cells is also uncertain since these ions are produced directly in the low-pressure ICR cell and therefore may not be thermalized to the cell wall temperature.

The most reliable kinetic data for modelling low-temperature ionic reactions are obtained by using higher-pressure, collision-dominated media included in which are the so-called afterglow techniques, in particular the flowing afterglow technique, and the similar (but subtly different) selected-ion flow-tube technique (see Adams and Smith (1987, 1988) for example). The first of the afterglow plasma techniques to be developed

was the stationary afterglow in which ionization is created in a pure gas or a gas mixture by a short ionizing pulse (both r.f. and d.c. voltage pulses have been used). The reactions of the ions are then studied in the afterglow plasma following the cessation of the pulse when the ion (and electron) energies have relaxed to those appropriate to the gas temperature. Ion identification and the temporal decay of the ion density are usually monitored by observing the ion currents diffusing to the sampling orifice of a mass spectrometer located in the walls of the vessel containing the afterglow plasma (McDaniel and Mason 1973). Such experiments are usually performed at a relatively high pressure of an inert (unreactive) gas such as helium (to inhibit diffusive loss of ions and electrons from the plasma) containing small admixtures of reactive gases. The time constant for the loss of a given reactive ion is measured at several pressures of the reactant neutral gas and the truly thermal rate coefficient for the ion–neutral reaction is then readily obtained. A few ion–neutral reactions of importance in the terrestrial ionosphere were studied using this technique more than twenty years ago, some over a significant temperature range (200–600 K). The flowing afterglow and selected-ion flow tube techniques have been used much more widely for the study of ion neutral reactions (see below).

The stationary afterglow has been used to greater effect to determine positive ion–electron dissociative recombination coefficients, α_e (process (4) in table 1). For these measurements, the afterglow plasma is created in a small (dimensions ~1 cm) microwave resonator and the decrease in the electron number density with time resulting from the recombination process is obtained by monitoring the temporal change in the resonant frequency of the cavity. If only a single positive ion species is present in the afterglow (this objective is not always easy to achieve) as determined by a wall-sampling mass spectrometer and if the pressure in the cavity is sufficiently high to inhibit diffusive loss of ionization then, since the ion and electron densities are equal, the α_e value is readily determined (Bardsley and Biondi 1970). Prior to the inception of the flowing afterglow/Langmuir probe technique (see below), the majority of the available thermal energy α_e data were obtained using the stationary afterglow technique and this established the order of magnitude of α_e for dissociative recombination reactions.

With the advent of fast-flow tube techniques, initially the flowing afterglow in 1964 followed by the selected-ion flow tube about a decade later, the study of ion–neutral reactions was transformed, because the types of reactions that could be studied and the rate of provision of reliable kinetic data increased dramatically. The enormous advantage of the flowing afterglow over the stationary afterglow technique is directly attributable to the transformation of the time domain of the latter to the steady-state distance domain (via gas flow) of the former (Ferguson *et al.* 1969). In the flowing afterglow, ionization is created in the upstream region of a fast-flowing inert carrier gas (usually pure helium at a pressure of about 1 torr) by some form of electrical discharge or ion source. Plasma ions and electrons are convected away from the ionization source and thus an afterglow plasma is created in the downstream region of the flow tube (typical dimensions of which are 1–10 cm long by 8 cm diameter) in which the ion and electron temperatures are equal to the carrier-gas temperature. The ions arrive at a small orifice where they are sampled, analysed and detected by a differentially-pumped quadrupole mass spectrometer detection system. In a pure helium carrier gas the only ions detected are He^+ and He_2^+. Reactant gases can then be added to the thermalized afterglow and the mass spectrometer detector registers a reduction in the He^+ and He_2^+ ion signals and the appearance of product ions.

Although the flowing afterglow is an extremely versatile apparatus in that a wide range of ionic species can be generated in the plasma by sequential gas additions along the flow tube, often more than one ion species is generated following the addition of a given gas (for example, when CH_4 is added to a helium afterglow then CH^+, CH_2^+, CH_3^+ and CH_4^+ are all produced and these ions also react rapidly with CH_4) and this can greatly complicate the identification of the ion products of the reactions and the elucidation of reaction mechanisms. This problem has been overcome by the development of the selected-ion flow tube (SIFT) technique (Smith and Adams 1979, 1987) in which ions are generated in an ion source external to the flow tube (see figure 1) and after mass selection (according to m/q) by a quadrupole mass filter, a single ion type is injected through an orifice into the relatively high-pressure carrier gas in which the ions thermalize in collisions with carrier gas atoms as they are convected along the flow tube. By introducing reactant gases into the ion swarm (which is not a plasma!) reaction rate coefficients can be determined and product ions identified in the same way as in flowing afterglow experiments. Note that in the SIFT, ion product distributions can also be determined. The secret of the operation of the SIFT is in the introduction of the carrier gas via a venturi inlet which surrounds the ion-injection orifice (see figure 1). This inhibits back-diffusion of carrier gas through the ion-injection aperture, which allows a relatively large aperture to be used without raising the pressure in the injection mass filter to prohibitively high values. This simple device has enormously increased the versatility of fast-flow tube techniques. It is now possible to study reactions of virtually any ionic species that can be prepared in an ion source with a wide range of reactant gases and vapours. Hence the rate coefficients for several thousands of reactions have been measured using SIFT apparatuses in several laboratories around the world (Albritton 1978), a significant fraction of which have been obtained over the temperature range 80–600 K (currently some twenty SIFT apparatuses are being exploited). A notable success of such experiments is the contribution they have made to the understanding of the reactions occurring in interstellar gas clouds (see section 5).

Another valuable experimental technique which has been developed recently to study ion–neutral reactions is the CRESU technique ('Cinetique de Reaction en Ecoulement Supersonique Uniforme', that is 'Reaction Kinetics in Uniform Supersonic Flow') by which reactions can be studied at temperatures down to 8 K. This is achieved by producing ionization upstream in the very low-temperature isentropic core formed by the expansion of gas via a de Laval nozzle (Rowe *et al.* 1984). Rate coefficients are then determined in a similar manner to the fast-flow tube techniques. A similar experiment in which ions are created in a free jet expansion is providing kinetic data on ion–neutral reactions at temperatures below 1 K (Mazely and Smith 1988)! Both these very low-temperature experiments offer much for the understanding of the reactions which are thought to occur in cold interstellar clouds.

In contrast to the above, the development of the selected-ion flow-*drift* tube has allowed the ion energy to be elevated above that appropriate to the carrier-gas temperature by impressing an electric field along the axis of a selected-ion flow tube (see fig. 1). This allows reactions to be studied at suprathermal energies approaching a few electron volts in the centre-of-mass frame and bridges the energy gap between the truly thermal data obtained from flowing afterglow and SIFT experiments and the data obtained using the beam techniques referred to earlier. The data obtained from selected-ion flow-*drift* tube experiments is also contributing to the understanding of ion–neutral reactions occurring in shocked regions of interstellar gas.

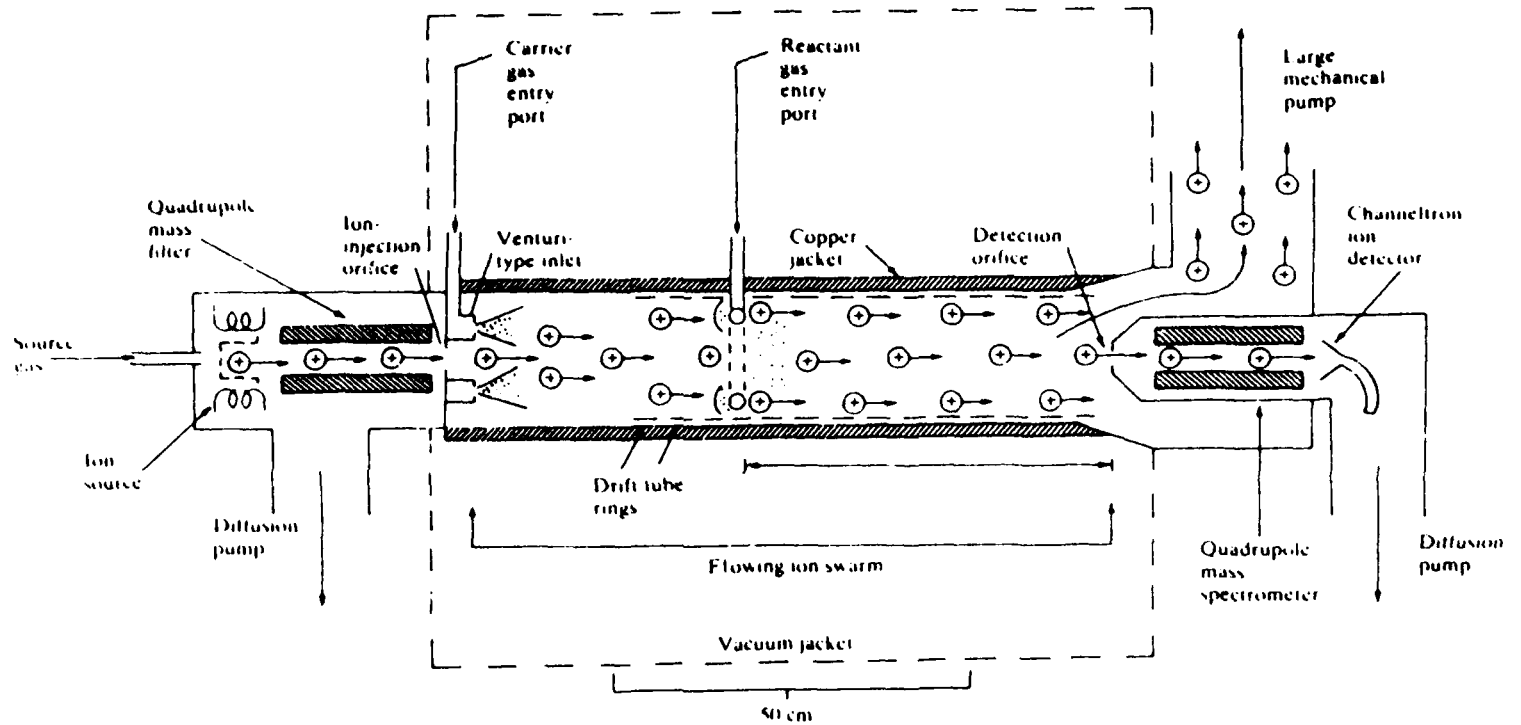

Figure 1. A schematic representation of a selected-ion flow tube, SIFT (and a selected-ion flow-drift tube, SIFDT) apparatus. In this apparatus, ions are created in a remote ion source, selected according to their charge to mass ratio by a quadrupole mass filter and injected into a fast flowing carrier gas whence they are convected along the flow tube and detected by a downstream mass spectrometer/channeltron detection system. Both of the quadrupoles are differentially-pumped against carrier gas flow through the injection and detection orifices. Reactions of the ions are studied by adding controlled amounts of reactant gases via the gas entry port. The series of metal rings illustrated form an electrostatic drift tube (converting the SIFT into a SIFDT) via which the drift energy of the ions can be increased, and thus their reactions can be studied as a function of ion/neutral centre-of-mass energy. A copper jacket to which copper pipes have been brazed surrounds the flow tube. Refrigerant liquids such as liquid nitrogen can be flowed through the pipes to cool the flow tube. Ohmic heaters are also connected to the copper jacket to facilitate experiments at high temperatures. Only an outline is shown of the vacuum jacket which encloses the flow tube.

Fast-flow tube techniques have recently been applied to the study of plasma processes other than ion-neutral reactions, notably dissociative recombination, electron attachment and ion-ion mutual neutralization (see table 1). To achieve this, the flowing afterglow/Langmuir probe apparatus was conceived (described in Brouillard and McGowan (1983)). Essentially the flowing afterglow/Langmuir probe apparatus is a conventional flowing afterglow to which has been added the Langmuir probe diagnostic technique with which the plasma electron and ion number densities can be measured at all positions along the axis of the flow tube. Knowledge of ion neutral reactions is required in order to create plasmas comprising ions of the desired type. Under conditions of high pressure and high ionization density the ions are lost by dissociative recombination, whence the measurement of the gradient of the electron or ion density along the flow tube provides a measurement of the recombination coefficient, α_e, for the reaction. Similarly, the addition of electron attaching gases to the afterglow initiates attachment reactions which result in a loss of electrons and this is readily recorded by the Langmuir probe. The attachment coefficients β are also readily derived (at low ionization density to inhibit recombination) as are rate coefficients for mutual neutralization reactions. These flowing afterglow/Langmuir probe studies have provided much of the available data on mutual neutralization reactions of atmospheric importance (see section 4) and on dissociative recombination reactions of importance in interstellar clouds (see section 5).

Some of the important advances made in the understanding of the fundamentals of ionic reaction processes are described in some recent review papers (Bowers 1979, Adams and Smith 1983). In the following sections, the basic elements of the ionic reactions occurring in the terrestrial atmosphere, in interstellar gas clouds and laboratory etchant plasmas will be outlined as illustrations of the utility of the kinetic data relating to thermal-energy ionic reactions.

4. Ionic reactions in the terrestrial atmosphere

Were it not for the presence of ionizing radiations, the atmosphere of the Earth would be chemically very stable since, at normal temperatures, the dominant gaseous constituents are unreactive. In practice, the action of solar radiation, galactic cosmic rays and radioactive emanations from rocks ensures that the atmosphere is partially ionized at all altitudes and thus that a wide variety of ionic reactions occur.

Owing to gravity, the density of the atmosphere decreases roughly exponentially with altitude. Thus, the incoming intense solar radiation first interacts with a relatively low-density atmosphere of N_2 and O_2 enriched in the lighter gases hydrogen and helium owing to gravitational separation. The destructive short wavelength (extreme ultraviolet and soft X-ray) components of the solar radiation efficiently dissociate and ionize the molecules creating the upper ionosphere (the F-region) in which the primary ions are largely the single-charged species H^+, He^+, N^+ and O^+ (balanced by an equal number of electrons thus creating a quasi-neutral electron–ion plasma medium). The shorter wavelength radiations do not penetrate to the lower altitudes and there the less energetic species O^+, O_2^+ and N_2^+ are produced as the primary ions (in the so-called E-region of the ionosphere). At lower altitudes still (in the so-called D-region, see figure 2) ionization is mainly caused by the solar Lyman-α and Lyman-β line radiations which are able to penetrate into this region of the atmosphere through 'absorption windows' in the O_2 spectrum and thus to selectively ionize NO molecules (1_g) and metastable O_2 ($^1\Delta_g$) molecules (1_g) thus creating NO^+ and O_2^+ ions in the D-region (Wayne 1985). At altitudes below ~ 50 km, solar radiations do not ionize the atmosphere but do

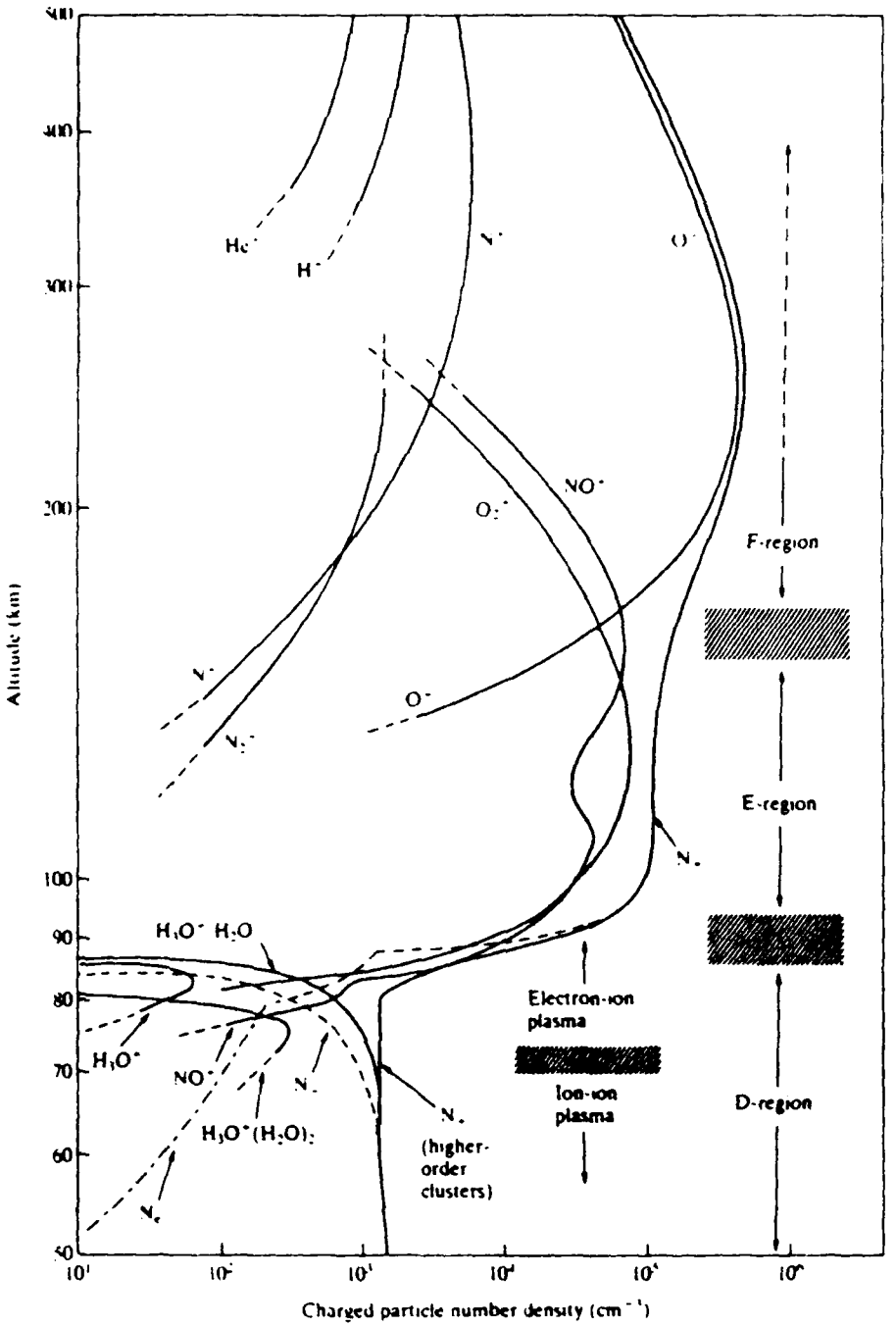

Figure 2. The ionized regions of the Earth's atmosphere. The F, E and D regions of the ionosphere are designated according to the 'ledges' observed in the electron density. Typical altitudinal profiles of the various positive ion number densities in the positive ion–electron plasma are also shown. The negative ion types in the positive ion–negative ion plasma of the lower D-region are known but the detailed altitudinal profiles of density are not well characterised and so only the approximate total negative ion number density, N_-, (dashed line) is indicated. The profiles of the electron density, N_e, and the total positive ion density, N_+, are also included. It is assumed that quasi-neutrality exists throughout the atmosphere, that is $N_e \approx N_+$ in the electron–ion plasma and $N_- \approx N_+$ in the ion–ion plasma (from Smith and Adams 1980).

dissociate molecular oxygen producing oxygen atoms which react to form the ozone (O_3) layer in the stratosphere. Other molecules from natural sources (such as CH_4 and NH_3) and from man-made sources (such as chlorofluorocarbons, CFCs) are also dissociated and the atomic (e.g. Cl) and molecular (e.g. CH_3) fragments initiate a rich, even damaging and dangerous neutral chemistry (the CFCs are strongly implicated in the destruction of the ozone layer and in causing the 'ozone hole' over the antarctic; McElroy (1987)). Ionization in the lower atmosphere (the lower stratosphere and troposphere) is created by penetrating galactic cosmic rays and radioactive emanations from rocks. These energetic radiations ionize the medium non-selectively and thus the major ions produced at low altitudes are N^+, N_2^+, O^+ and O_2^+ (see figure 2 for approximate ion number densities in the various atmospheric regions). Negative ions are also efficiently formed in the lower atmospheric regions, by the attachment processes given in table 1.

What are the actual ion types observed in the various atmospheric regions? The first *in situ* measurements of atmospheric ions were carried out almost thirty years ago in the E- and F-regions of the ionosphere using rocket-borne mass spectrometers. O^+, N^+ and N_2^+ ions were detected as expected, but surprisingly NO^+ ions were seen to be a major component (see fig. 2). NO^+ ions result from the reactions of O^+ ions with N_2 and N^+ ions with O_2, for example

$$O^+ + N_2 \rightarrow NO^+ + N. \tag{1}$$

In this reaction, ions of lower recombination energy, RE (which for NO^+ is 9·25 eV) are formed from ions of higher RE (for O^+, 13·6 eV). This is an important general principle in ionic reactions and leads to so-called terminating ions (it is clear that O^+ ions cannot be formed from NO^+ ions at low interaction energies). Note also that the N^+ and O^+ ions are formed in the ionosphere by photo-ionization of N and O atoms and by the reactions of He^+ with N_2 molecules and O_2 molecules. As summarised in figure 3, it can be seen that the ion chemistry of these ionospheric regions involves the conversion of atomic ions to molecular ions. This is important in controlling the degree of ionization of the plasma because the neutralization of an atomic positive ion by an electron is a slow (inefficient) process whereas, in general, dissociative recombination of molecular ions is very efficient. Thus the production of and recombination of N_2^+, O_2^+ and NO^+ limits the build-up of ionization in the upper ionosphere. The good agreement obtained between model predictions and *in situ* observations has demonstrated that the reactions occurring in these regions are properly understood.

At low altitudes where the gas pressure is much larger, and especially in the troposphere where a number of reactive trace impurities exist and where electron attachment proceeds by converting free electrons to negative ions, a greater variety of ionic reactions occurs. In the D-region, the primary positive ions are NO^+ and O_2^+ and the primary negative ions are O^- and O_2^-, and these undergo clustering reactions (see process (3), table 1), exemplified by the important reaction

$$NO^+ + N_2 + N_2 \rightarrow NO^+.N_2 + N_2 \tag{2}$$

in which the weakly-bonded species $NO^+.N_2$ is formed. Such a species can undergo so-called switching reactions with minority neutral species such as H_2O:

$$NO^+.N_2 + H_2O \rightarrow NO^+.H_2O + N_2 \tag{3}$$

forming the more strongly bonded cluster ion $NO^+.H_2O$. Further reactions of this ion with water molecules occur (see Thomas (1974)). The primary negative ions O^- and O_2^- are converted to the more stable (less reactive) species NO_3^- and CO_3^- in reactions with

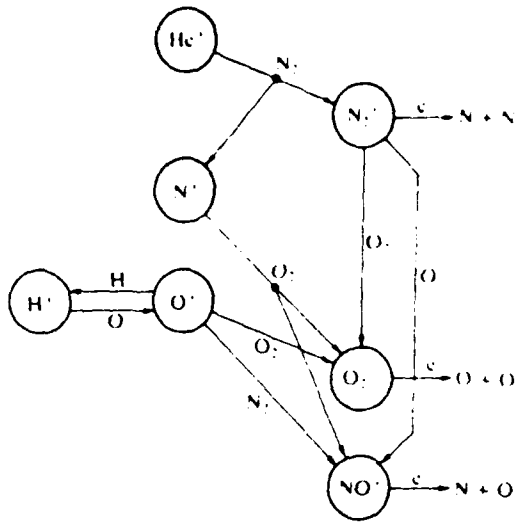

Figure 3. A limited scheme describing the ion chemistry of the upper ionosphere. The ionic species are arranged from top to bottom of the diagram in order of reducing recombination energy. The major primary ions produced by the action of solar photons on the ambient gas are H^+, He^+, N^+ and O^+ in the upper part of the region and O^+, N_2^+ and O_2^+ in the lower part of the region. The major terminating ions throughout the region are NO^+ and O_2^+ (see text), and these ions and also N_2^+ ions can be destroyed by dissociative recombination forming neutral atoms as shown.

NO and CO_2 and then clustering reactions occur. In the D-region, neutralization of charged species results from both dissociative recombination of the cluster positive ions with electrons and also mutual neutralization reactions between the ambient positive ions and negative ions.

In the lower stratosphere and troposphere, the ambient positive ions and negative ions are complex cluster ions of the type $H^+(H_2O)_nX_m$ and $HSO_4^-.Y_n$ respectively, where X are pollutant molecules having basic properties, such as CH_3CN and NH_3, and Y are acidic molecules, including H_2SO_4 and NHO_3, and m and n are small integers. The balance between production of ionization and its loss by neutralization reactions results in a steady-state number density of positive and negative ions of about $2 \times 10^3\ cm^{-3}$ in air at sea level. It is interesting to note that an excess of negative ions (over positive ions) is considered by some to give individuals a feeling of well being!

5. Ionic reactions in interstellar clouds: The formation of interstellar molecules

Diatomic molecules (such as CH and CN) were first detected in diffuse interstellar clouds some fifty years ago by their characteristic absorption spectra in the visible region. More recently, other simple molecules (such as CO and OH) have been detected in these clouds via their characteristic absorption spectra in the vacuum ultraviolet region by using spectrometers borne on satellites, a necessary procedure to avoid absorption by the atmosphere. With the advent of radio- and millimetre-wave astronomy, many complex molecular species have been detected in the denser and colder clouds of gas and dust in the galaxy (of which the Orion Molecular Cloud is the best known example) (Rydbeck and Hjalmarson 1985). The gas in these clouds is very

largely H_2, with CO being the next most abundant molecule with a relative number density some 10^4 times less than that of H_2. Many polyatomic species have been detected (see table 2 and Smith (1987)). The most complex species detected to date is the linear $HC_{10}CN$, although there is no doubt that even more complex molecular species exist in dense interstellar clouds.

The question arises as to how these molecules are formed in these harsh regions of space in which the temperatures are as low as 10 K (in dense clouds) and gas number densities are typically only 10^3-10^4 cm^{-3}. Gas-phase reactions between neutral molecules cannot be important because, as mentioned in section 1, such reactions are generally prohibitively slow at low temperatures. The condensation of neutral atoms on to the very cold surfaces of the micrometre-sized dust grains which pervade dense clouds (the Horsehead Nebula in Orion is the best known manifestation of a dust and gas cloud) can result in the production of molecules by heterogeneous catalysis, but there is no satisfactory explanation of how these molecules could be released into the gas phase. In the early 1970s, it was proposed that the gas-phase reactions of positive ions with neutrals, many of which proceed more rapidly as the temperature is decreased, result in the synthesis of polyatomic molecular ions which then undergo dissociative recombination with electrons producing the observed neutral interstellar molecules (Herbst and Klemperer 1973). In recent years, detailed models have been constructed of the gas-phase ion chemistry of interstellar clouds, which predict the relative abundances of many interstellar molecular species which are in reasonable agreement with astronomical observations. Thus it is now generally believed that the synthesis of most interstellar molecules occurs via ionic reactions in the gas phase. Detailed discussions are given by Dalgarno and Black (1976) and Smith and Adams (1981). Here we briefly describe some of the basic reactions.

Diffuse clouds, as the name implies, are partially transparent to visible radiations and ultraviolet radiations of longer wavelengths than the threshold wavelength for ionization of H atoms (radiations with wavelengths shorter than this are strongly absorbed). Since the ionization energy of carbon atoms (11·26 eV) is less than that of H atoms (13·59 eV) then C^+ ions and electrons can be generated by photo-ionization of C atoms by stellar vacuum ultraviolet radiation. Galactic cosmic rays can also penetrate diffuse clouds and, of course, are non-selective in the species they ionize. Since H, H_2 and He are the major constituents of these clouds then H^+, H_2^+ and He^+ are generated in the cosmic ray ionization process. Dense clouds of gas and dust are opaque to vacuum ultraviolet radiation and the only major source of ionization is penetrating galactic cosmic rays, which in these clouds composed of principally H_2 and He also generate H^+, H_2^+ and He^+ as the primary ions. Two very rapid reactions then occur in both diffuse and dense clouds:

$$H_2^+ + H_2 \rightarrow H_3^+ + H, \tag{4}$$

$$He^+ + CO \rightarrow C^+ + O + He. \tag{5}$$

Both reactions occur on every collision between the reactants as numerous laboratory experiments have shown. Thus both C^+ and H_3^+ ions are the important precursor ions to most other ions formed in interstellar clouds.

As can be seen in table 2, several hydrocarbon molecular species have been detected in interstellar clouds, but not the simplest hydrocarbons CH_4, C_2H_2 and C_2H_4. These species and also H_2, N_2 and O_2 must be present but, unfortunately, because of their

Table 2. Molecules observed in interstellar clouds, and in circumstellar envelopes (indicated by an asterisk). Molecules of a given atomicity are ordered from left to right in increasing molecular weight. Note that several singly-charged molecular-ion species have been detected (CH^+, SO^+, HCO^+, N_2H^+, HCS^+, H_3O^+, H_2CN^+ and HCO_2^+). Both linear (l-) and cyclic (c-) isomers of C_3H have been detected. The cyclic molecules c-C_3H, c-C_3H_2 and c-SiC_2 are essentially triangular in structure.

Number of atoms	Chemical species
2	H_2, CH, CH^+, OH, C_2, CN, CO, NO, HCl, CS, SiO, PN, SN, SO, SO^+, SiS.
3	H_2O, C_2H, HCN, HNC, HCO, HCO^+, N_2H^+, HNO, H_2S, HCS^+, SiC_2^*, C_3S, OCS, SO_2.
4	NH_3, H_3O^+, $C_2H_2^*$, H_2CN^+, H_2CO, l-C_3H, c-C_3H, HNCO, HCO_2^+, H_2CS, C_2CN, C_3O, HNCS, C_3S.
5	CH_4^*, CH_2NH, SiH_4^*, c-C_3H_2, CH_2CO, NH_2CN, HCO_2H, C_4H, HC_2CN.
6	$C_2H_4^*$ CH_3OH, CH_3CN, CH_3NC, NH_2CHO, CH_3SH, C_5H.
7	CH_3NH_2, CH_3C_2H, CH_3CHO, C_2H_3CN, C_6H, HC_5N.
8	CH_3C_2CN, CH_3CO_2H.
9	C_2H_5OH, CH_3OCH_3, C_2H_5CN, CH_3C_4H, HC_6CN.
10	CH_3COCH_3, CH_3C_4CN.
11	HC_9CN.
12	—
13	$HC_{10}CN$.

symmetry (no permanent dipole moment) they do not radiate via rotational transitions in their ground vibronic states. Such molecules have been detected by infrared absorption spectroscopy in the warm, denser atmospheres of evolved stars (i.e. in circumstellar shells). Methane (CH_4) and smaller one-carbon hydrocarbons can be synthesised by the following reaction sequence:

$$\begin{array}{ccccccc} H_3^+ & \xrightarrow{C} & CH^+ & \xrightarrow{H_2} & CH_2^+ & \xrightarrow{H_2} & CH_3^+ \xrightarrow{H_2} CH_5^+ \\ & & \downarrow e & & \downarrow e & & \downarrow e \\ & & CH & & CH, CH_2 & & CH_3, CH_4 \end{array} \qquad (6)$$

CH_2^+ can also be formed directly from H_2 and C^+ via the process of radiative association $C^+ + H_2 \rightarrow CH_2^+ + h\nu$. Reactions of the hydrocarbon ions in sequence (6) with neutral hydrocarbons can then form larger species, e.g.

$$CH_3^+ \xrightarrow{CH_4} C_2H_5^+ \xrightarrow{e} C_2H_2, C_2H_3, C_2H_4. \qquad (7)$$

Further reactions then lead to the observed polyatomic hydrocarbons (see table 2).

The most abundant interstellar molecular species containing nitrogen and hydrogen is ammonia, NH_3. It can be formed by the following reaction sequence starting from N^+ ions:

$$N^+ \xrightarrow{H_2} NH^+ \xrightarrow{H_2} NH_2^+ \xrightarrow{H_2} NH_3^+ \xrightarrow{H_2} NH_4^+ \xrightarrow{e} NH_3. \qquad (8)$$

The NH_3 can then react with C^+ thus:

$$C^+ \xrightarrow{NH_3} HCN^+, H_2CN^+ \xrightarrow{e} CN, HCN \qquad (9)$$

producing both HCN^+ and H_2CN^+ which can then dissociatively recombine to form the cyano compounds CN and HCN that are observed in interstellar clouds. Although the recombination coefficients, α_e, for many of the ions involved in these schemes have been determined (mostly using the FALP apparatus described in section 3), the identities of the neutral products are not yet certain. Other CN-bearing molecules (such as the cyanopolyynes) can be formed by reactions of HCN with hydrocarbon ions. The reactions of hydrocarbon ions with NH_3 form the amino group of interstellar molecules, including CH_2NH and CH_3NH_2:

$$CH_3^+ \xrightarrow{NH_3} CH_2NH_2^+, CH_3NH_3^+ \xrightarrow{e} CH_2NH, CH_3NH_2. \quad (10)$$

Interstellar molecules are of great utility in astrophysics. In particular, the characteristic radiation emissions from CO molecules are used extensively to detect interstellar matter in the Milky Way and indeed in other galaxies. Such emissions are also used as unique probes of the interiors of giant molecular clouds (such as the Orion and Sagittarius clouds) in which star formation is occurring as is indicated by the 'clumping' of the gas due to gravitational collapse. Also the frequency resolution of radio telescopes is such that they can easily distinguish between emissions due to CO in all combinations of the ^{12}C, ^{13}C, ^{16}O, ^{17}O and ^{18}O isotopic variants (Winnewisser *et al.* 1979). Via such observations, it has been observed that the $^{13}C:^{12}C$ ratio in interstellar CO is typically 1:40 and thus exceeds the ratio in solar terrestrial material which is 1:89. This was initially thought by astrophysicists to be due to the greater production of ^{13}C (by the process of nuclear burning in the interiors of stars) in other regions of the galaxy compared to production in the pre-solar nebula from which the Sun and the planets were formed. However, it has been shown by SIFT experiments that ionic reactions of the type involving isotope fractionation are responsible for enriching the stable heavy isotopes of elements into interstellar molecules. Thus the reaction:

$$^{13}C^+ + {}^{12}CO \rightleftharpoons {}^{12}C^+ + {}^{13}CO + 0{\cdot}003\,eV \quad (11)$$

'fractionates' the ^{13}C into CO by virtue of the smaller vibrational zero-point-energy of ^{13}CO compared to ^{12}CO. Since this energy difference is small, this phenomenon is only efficient at low temperatures such as those pertaining to dense interstellar clouds. Isotope exchange reactions are particularly efficient in fractionating deuterium, D, into many interstellar molecules; indeed, the reaction:

$$D^+ + H_2 \rightleftharpoons H^+ + HD + 0{\cdot}04\,eV \quad (12)$$

ensures that most of the D in dense interstellar clouds is locked into HD molecules. Many similar ionic reactions result in the fractionation of deuterium into many other interstellar molecules (Smith and Adams 1984 b).

Also worthy of note in this section is another example of how interstellar molecules (together with a knowledge of ionic reactions) can provide the astrophysicist with valuable information. Since ionization plays a part in inhibiting the rate of gas cloud collapse to form stars, it is important to know the degree of ionization, $x(e)$, in the dense molecular clouds where protostars form. This is an erudite topic but, in essence, the ions and electrons in the clouds are coupled hydromagnetically to the ambient magnetic field and the ions are coupled to the neutral gas by viscous forces i.e. by collisions. Thus, since the motions (in-fall) of the ions and electrons are inhibited by the magnetic field so are the neutral molecules and in this way gravitational collapse is

inhibited. An estimate of the degree of ionization $x(e) = [e]/[H_2]$ can be obtained by considering the rate of formation and rate of loss of HCO^+ ions which are observed in all dense molecular clouds. $x(e)$ turns out to be $\sim 10^{-7}$ for most dense interstellar clouds.

6. Ionic reactions in laboratory discharge plasmas

As was mentioned at the start of section 1, when an electrical discharge is passed through a gas mixture a wide variety of reactions can occur between the new species generated (namely electrons, ions and radicals) and these new species can also react with the ambient gas. These reactions may generate radiation at specific wavelengths (line radiations) and in broad bands (continuum radiations). Radiation can also be generated most efficiently by the direct excitation of the ambient gas by electrons which have been accelerated to sufficiently high energies in the discharge. Thus electrical discharges have been used for decades as sources of line radiations (for example, low-pressure mercury and sodium lamps) and broad-band radiations (for example, high-pressure mercury and xenon lamps). More recent applications of electrical discharges through gases are as flash lamps for the optical pumping of lasers, in the direct generation of laser radiations (intracavity excitation) and in the etching of semiconductor surfaces (commonly silicon) for the preparation of microprocessors. In the early stages of the development of these techniques a 'trial and error' approach was usually taken to optimize the desired light intensity, etching rate, etc. Thus the total pressure, partial pressures of the component gases in mixtures, discharge power, and so on were varied, largely in ignorance of the processes which were occurring.

With advances in the understanding of atomic and molecular physics, of ionic and radical reactions in gases, and in the techniques to study these individual processes, more attention has been given to the processes occurring in laboratory discharge devices. This has, of course, been greatly stimulated by the commercial, industrial and social importance of devices such as microprocessors and lasers.

Plasma etching of the surface of silicon wafers usually involves exposing the surface to an electrical discharge through a gas mixture containing a fluorine- or chlorine-bearing molecule. Halogens (F_2 or Cl_2) can be used but these (particularly F_2) are difficult and dangerous gases to deal with and so fluoro- or chloro-carbons are usually preferred. The important point is that the plasma ions sensitize the surface and then the neutral radical species generated in the discharge, particularly F and Cl atoms but also molecular radicals such as CF_x, actually etch the surface (removing Si as volatile halides). Thus the production of reactive radicals in the discharge must be made efficient (Smith and Adams 1984a). Various mixtures are commonly used, for example, O_2/CCl_4 and O_2/CF_4. Radicals can be produced directly in the discharge by dissociative electron collisions with the halogen-bearing molecules (for example, $CCl_4 + e \rightarrow CCl_3 + Cl + e$) but electron collisions also result in dissociative attachment which generates a negative ion and a neutral radical, for example

$$CCl_4 + e \rightarrow Cl^- + CCl_3, \tag{13}$$

Positive ions formed in the discharge can undergo reactions with negative ions thus:

$$O_2^+ + Cl^- \rightarrow O_2 + Cl \tag{14}$$

again generating radicals. Dissociative recombination can also produce radicals, for example

$$CCl_3^+ + e \rightarrow CCl_2 + Cl. \quad (15)$$

Radical neutrals can also be destroyed in reactions with ions such as via the process of associative detachment (see table 1): for example

$$Cl^- + Cl \rightarrow Cl_2 + e \quad (16)$$

and also in reactions with other neutral radical species (such neutral–neutral reactions are undoubtedly important but are beyond the scope of this review). Reactions (13) to (16) are included with other reactions in figure 4 which indicates some of the many reactions that can occur following a discharge through an O_2/CCl_4 mixture

It is evident that a detailed knowledge of the basic reaction processes which can occur in these discharge plasmas assists in the optimization of discharge conditions, namely the choice of appropriate gas mixtures, partial pressures of the components, current through the discharge, and so on, to obtain the desired etch rate. The already large and growing amount of data available on gas-phase reactions of ions, electrons

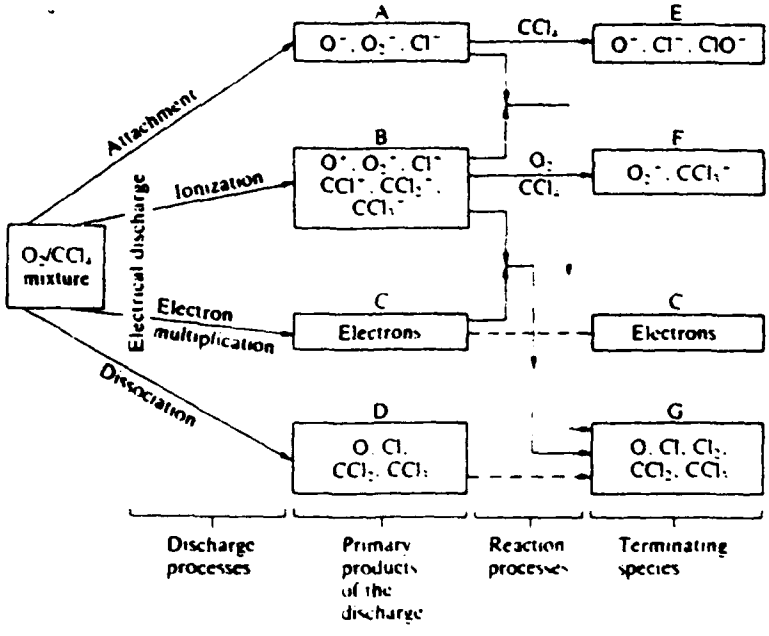

Figure 4. Some reactions which can occur in an etchant plasma created by passing an electrical discharge through a mixture of O_2 and CCl_4. These reactions include positive-ion/negative-ion mutual neutralization (Box A + Box B), positive-ion/electron dissociative recombination (Box B + Box C), negative ion reactions with O_2 and CCl_4 (Box A → Box E) and positive-ion reactions with O_2 and CCl_4 (Box B → Box F). The so-called terminating species indicated include some of the primary species created in the discharge and some formed in subsequent reactions.

and neutral species, obtained by techniques such as those described in section 3, is being used to model the reactions occurring in etchant plasmas and gradually developing semiconductor etching into something better than a 'black art'.

Throughout this brief review we have concentrated on the reactions of charged species in gaseous plasmas but have occasionally alluded to the importance of the reactions of neutral radicals. Mention must also be made, in concluding, that excited neutral species, in particular electronically excited neutrals which can possess many electron volts of energy, can also be involved in the complex reaction schemes which collectively describe the physical and chemical evolution of gaseous plasmas. Excited neutrals can collide with other neutrals transferring their excitation energy and in some cases causing dissociation and ionization. For example, a discharge through helium or a gas mixture containing helium undoubtedly results in the production of helium metastable atoms (both $He(2^1S)$ and $He(2^3S)$ are metastable and long-lived since radiative relaxation to the ground state is forbidden). The electronic excitation energy of $He(2^3S)$ is 19·8 eV and, in collision with most atoms or molecules, Penning ionization occurs, for example

$$He(2^3S) + N_2 \rightarrow N_2^+ + e + He(1^1S_0). \tag{17}$$

This process can therefore represent a significant source of ionization in a gas. Also, if a mixture of helium and neon is discharged then $He(2^1S)$ (the electronic excitation energy is 20·61 eV) can excite the Ne atoms to a specific radiating state:

$$He(2^1S) + Ne(^1S) \rightarrow Ne(3s_2) + He(^1S) \tag{18}$$
$$\hookrightarrow Ne(2p_4) + 632{\cdot}8\text{ nm radiation.}$$

This causes a population inversion between two states of Ne atoms and it is this phenomenon that has been exploited in the helium/neon laser. Other lasers also rely on this phenomenon, as discussed in several reviews (see Nighan (1982), for example).

7. Concluding remarks

In this review we have indicated how the creation of ionization in a gas mixture initiates a variety of ionic reactions that can rapidly change the chemical composition of the medium. Laboratory experiments have been described which can be used to determine the rate coefficients for individual ionic reaction processes. Following this, we have discussed the ways in which data relating to many ionic reactions are being used to successfully explain how the ions observed in the terrestrial atmosphere are formed, how the observed interstellar molecules are synthesised and how the reactive radical species are produced in laboratory etchant plasmas. The study of ionic reactions in gases remains an exciting and interesting interdisciplinary research topic which demands a knowledge of atomic and molecular physics, spectroscopy, mass spectrometry and gas-phase chemistry. It is an ideal discipline for training research scientists both in the fundamentals of theory and experiment, and thus for providing versatile scientists to meet the requirements of modern industrial research and development.

Acknowledgments

Our work in the many aspects of ionic physics referred to in this paper has been generously funded over many years by the Science and Engineering Research Council and the United States Air Force.

References

ADAMS, N. G., and SMITH, D., 1983, *Reactions of Small Transient Species*, edited by A. Fontijn and M. A. A. Clyne (London: Academic Press), pp. 311–385; 1987, *Science Progress*, **71**, 91; 1988, *Techniques for the Study of Gas-Phase Ion–Molecule Reactions*, edited by J. M. Farrar and W. H. Saunders Jr (New York: Wiley) pp. 165–220.

ALBRITTON, D. L., 1978, *Atomic Data. nucl. Data Tables*, **22**, 1.

BARDSLEY, J. N., and BIONDI, M. A., 1970, *Adv. atomic molec. Phys.*, **6**, 1.

BOWERS, M. T. (editor), 1979, *Gas Phase Ion Chemistry*, Vols 1 and 2 (New York: Academic Press).

BROUILLARD, F., and MCGOWAN, J. W. (editors), 1983, *Physics of Ion–Ion and Electron–Ion Collisions* (New York: Plenum Press).

DALGARNO, A., and BLACK, J. H., 1976, *Rep. Prog. Phys.*, **1**, 271.

FERGUSON, E. E., FEHSENFELD, F. C., and SCHMELTEKOPF, A. L., 1969, *Adv. atomic molec. Phys.*, **5**, 1.

HERBST, E., and KLEMPERER, W., 1973, *Astrophys. J.*, **185**, 505.

HOWARD, M. J., and SMITH, I. W. M., 1983, *Prog. Reaction Kinetics*, **12**, 55.

MAZELY, T. L., and SMITH, M. A., 1988, *Chem. Phys. Lett.*, **144**, 563.

MCDANIEL, E. W., 1964, *Collision Phenomena in Ionized Gases* (New York: Wiley).

MCDANIEL, E. W., CERMAK, V., DALGARNO, A., FERGUSON, E. E., and FRIEDMAN, L., 1970, *Ion–Molecule Reactions* (New York: Wiley), pp. 107–158.

MCDANIEL, E. W., and MASON, E. A., 1973, *The Mobility and Diffusion of Ions in Gases* (New York: Wiley), p. 99.

MCELROY, M. B., 1987, *Recent Studies of Atomic and Molecular Processes*, edited by A. E. Kingston (New York: Plenum), pp. 63–78.

MCIVER, R. T. JR, 1978, *Rev. scient. Instrum.*, **49**, 111.

MOSELEY, J. T., OLSON, R. E., and PETERSON, J. R., 1975, *Case Studies in Atomic Physics*, **5**, 1.

NIGHAN, W. L. (editor), 1982, *Applied Atomic Collision Physics, Vol. III, Gas Lasers* (New York: Academic Press).

ROWE, B. R., DUPEYRAT, G., MARQUETTE, J. B., and GAUCHEREL, P., 1984, *J. chem. Phys.*, **80**, 4915.

RYDBECK, O. E. H., and HJALMARSON, A., 1985, *Molecular Astrophysics*, edited by G. H. F. Diercksen, W. F. Huebner and P. W. Langhoff (Dordrecht: Reidel), pp. 45–175.

SMITH, D., 1987, *Phil. Trans. R. Soc., Lond.* A, **323**, 269.

SMITH, D., and ADAMS, N. G., 1979, *Gas Phase Ion Chemistry*, Vol. 1, edited by M. T. Bowers (New York: Academic Press), pp. 1–44; 1980, *Topics in Current Chemistry*, **89**, Plasma Chemistry I, 1; 1981, *Int. Rev. phys. Chem.*, **1**, 271; 1984 a, *Pure appl. Chem.*, **56**, 175; 1984 b, *Ionic Processes in the Gas Phase*, edited by M. A. Almoster Ferreira (Dordrecht: Reidel), pp. 41–66; 1987, *Adv. atomic molec. Phys.*, **24**, 1.

SU, T., and BOWERS, M. T., 1979, *Gas Phase Ion Chemistry*, Vol. 1, edited by M. T. Bowers (New York: Academic Press), pp. 83–118.

THOMAS, L., 1974, *Radio Sci.*, **9**, 121.

WAYNE, R. P., 1985, *Chemistry of Atmospheres* (Oxford: Clarendon Press).

WINNEWISSER, G., CHURCHWELL, E., and WALMSLEY, C. M., 1979, *Modern Aspects of Microwave Spectroscopy*, edited by G. W. Chantry (New York: Academic Press), pp. 313–501.

APPENDIX 2

FALP STUDIES OF ELECTRON ATTACHMENT REACTIONS OF C_6F_5Cl, C_6F_5Br AND C_6F_5I

C.R. HERD, N.G. ADAMS AND D. SMITH

Int.J.Mass Spectrom. Ion Proc., 87, 331 (1989)

International Journal of Mass Spectrometry and Ion Processes, 87 (1989) 331–342
Elsevier Science Publishers B.V., Amsterdam – Printed in The Netherlands

FALP STUDIES OF ELECTRON ATTACHMENT REACTIONS OF C_6F_5Cl, C_6F_5Br AND C_6F_5I

CHARLES R. HERD, NIGEL G. ADAMS and DAVID SMITH

Department of Space Research, University of Birmingham, Birmingham B15 2TT (Gt. Britain)

(First received 5 July 1988; in final form 12 August 1988)

ABSTRACT

Electron attachment reactions of thermal electrons with C_6F_5Cl, C_6F_5Br and C_6F_5I molecules have been studied at 300 and 450 K using the flowing afterglow/Langmuir probe (FALP) technique. The rate coefficients at both temperatures are large and increase with increasing temperature. Different ionic products are obtained in the reactions; $C_6F_5Cl^-$ only for C_6F_5Cl, predominantly $C_6F_5^-$ for C_6F_5I, and predominantly $C_6F_5Br^-$ at 300 K for C_6F_5Br with the percentage of Br^- increasing with increasing temperature and constituting ca. 40% of the total products at 450 K. Comparison of these "high pressure" FALP data with previous "low pressure" data obtained from an ion beam time-of-flight experiment, has enabled the autodetachment lifetime of the excited intermediate ion $(C_6F_5I^-)^*$ to be bracketed between 10^{-7} and 10^{-6} s. Also an upper limit to the C–Br bond dissociation energy in C_6F_5Br of ca. 84 kcal mol^{-1} has been determined from a consideration of the kinetics of the C_6F_5Br reaction. In a parallel study, the reactions of $C_6F_5^-$ ions with several molecular gases have been studied using a SIFT apparatus and these results are reported in an Appendix.

INTRODUCTION

Electron attachment reactions have been studied using a variety of techniques which fall into two distinct categories: (i) low pressure techniques in which electrons interact with molecules, M, forming an excited negative ion $(M^-)^*$ which does not suffer collisions with ambient molecules during its lifetime, and (ii) high pressure techniques in which collisions of $(M^-)^*$ can occur which can modify the internal energy of $(M^-)^*$. The first category includes ion beam (time-of-flight, TOF) [1], ICR [2] and photoionization cell [3] techniques, and the second category includes drift tube [4], Cavalleri [5] and FALP [6,7] techniques. Attachment reactions are classified according to the observed products; when the negative ion products are the parent molecular negative ions (e.g., SF_6^- from SF_6 and $C_7F_{14}^-$ from C_7F_{14}) then the process is termed non-dissociative attachment, but when the

0168-1176/89/$03.50

product ions are fragments of the molecules (e.g., Cl^- from CCl_4, Br^- from CH_3Br) then the process is called dissociative attachment. In some electron/molecule reactions both dissociative and non-dissociative product channels are evident (e.g., SF_5^- and SF_6^- from SF_6 at temperatures ≥ 400 K, and Br^- and $C_6F_5Br^-$ from C_6F_5Br, see below).

The capture of an electron by a molecule may result in the rapid and spontaneous dissociation to the fragment negative ion and a neutral atom or molecule (e.g., $CCl_4 + e \rightarrow Cl^- + CCl_3$). The rate coefficient (or cross section) for the process then depends on the efficiency of the electron capture step which is usually dependent on the interaction temperature and energy of the reactants but not on the pressure of the ambient gas, since the dissociative attachment will usually occur on a timescale much shorter than the collision time, τ_c, of $(M^-)^*$ with an ambient atom or molecule (except at very large ambient gas pressures). However, when $(M^-)^*$ has an appreciable lifetime against autodetachment, τ_a, such that $\tau_a > \tau_c$, then superelastic collisions with ambient molecules can reduce the internal energy of $(M^-)^*$ and prevent autodetachment thus leading to the stable parent negative ion, M^-, or modify the product ion distribution (i.e., as between parent ions or fragment ions, see below). For such reactions it is to be expected that differences will be evident between the rate coefficients and product ion distributions determined using low pressure and high pressure methods and this is a major point to be drawn by comparing the results of the collision-dominated FALP experiments reported in this paper with those obtained from earlier low pressure experiments. It is worthy of note here that when τ_a is long (but necessarily $\ll \tau_c$) then the excited ion $(M^-)^*$ may be stabilised by the emission of an infrared photon. Several such $(M^-)^*$ have been identified in ICR experiments [2] and the radiative lifetimes, τ_r, have been determined.

During the last few years, we have developed the flowing afterglow/Langmuir probe (FALP) technique to study electron attachment reactions and to determine attachment rate coefficients, β, and product ion ratios [6,7]. Thus the β values have been determined for a number of dissociative and non-dissociative attachment reactions over a temperature range of about 200–600 K in helium carrier gas at a pressure of about 1 torr. In all the reactions studied, except that of hexafluorobenzene, C_6F_6, the β value for each reaction was either sensibly independent of temperature over the available range, or increased with temperature and then "activation energies" were determined for the reactions. The β value for the reaction of electrons with C_6F_6 (in which only the parent ion $C_6F_6^-$ was formed) very surprisingly was observed to decrease dramatically with increasing temperature [8]. This anomalous behaviour was subsequently verified using different techniques [9,10]. However, no totally convincing explanation for this behaviour has yet

been given [11]. In pursuit of a better understanding of this unusual phenomenon, we chose to study electron attachment to the monosubstituted perfluorobenzenes C_6F_5Cl, C_6F_5Br, and C_6F_5I using the FALP apparatus.

Naff et al. [1] studied these reactions some years ago using their elegant and productive TOF mass spectrometer method. For these C_6F_5X molecules (X = Cl, Br, I), and for ill-defined electron energies < 0.1 eV in their ion source, they observed that X^- and $C_6F_5^-$ ions were formed in all three cases. The ratios of the maximum current levels of X^- to $C_6F_5^-$ were 100 : 1, 3 : 1 and 1 : 3 for X = Cl, Br and I respectively. The parent ions $C_6F_5Cl^-$ and $C_6F_5Br^-$ were also observed and the autodetachment lifetimes, τ_a, were determined to be 17.6 μs and 20 μs respectively for the excited ions $(C_6F_5Cl^-)^*$ and $(C_6F_5Br^-)^*$. $C_6F_5I^-$ was not observed, indicating that τ_a for any $(C_6F_5I^-)^*$ formed was < 1 μs which was the smallest τ_a measurable in the TOF experiment. Conditions in the FALP plasma are, of course, quite different than in the TOF experiment. In the FALP plasma the ion collision time with carrier gas (helium) atoms, τ_c, is about 10^{-7} s which is much smaller than the τ_a given above for the $(C_6F_5Cl^-)^*$ and $(C_6F_5Br^-)^*$ ions. Also, since the temperatures of the reactant electrons and molecules (and hence their interaction energies) are precisely defined in the FALP, then differences in the product ion distributions of X^-, $C_6F_5^-$ and $C_6F_5X^-$ between the FALP and TOF experiments are to be expected.

EXPERIMENTAL

The FALP technique has been described in detail previously [6,7] and its application to the study of electron attachment has been thoroughly described in other papers [6,7,12]. Briefly, a thermalised afterglow plasma is created in helium carrier gas at about 1 torr pressure flowing along a flow tube (which is about 100-cm long and 8 cm in diameter) with a mass spectrometer sampling system located at the downstream end to identify the positive ion and/or negative ion types which, with free electrons, comprise the plasma. Controlled amounts of electron attaching gases are introduced into the thermalised flowing plasma and the modification of the gradient in the electron number density, n_e, along the axis of the flow tube (z-direction) due to the attachment process is determined using a Langmuir probe that can be positioned anywhere along the axis of the flow tube. Attachment coefficients, β, are derived from the analysis of the n_e versus z data obtained at fixed flow rates of the attaching gas into the afterglow [6]. The attachment reactions which are the subject of this paper are very rapid at the two temperatures for which measurements were made (300 K and 450 K, see Table 1) and so only very small number densities ($\sim 10^{10}$ cm^{-3}) of the attaching gases were required to establish workable gradients of n_e along z.

TABLE 1

Rate coefficients and product ion distributions for electron attachment to C_6F_5Cl, C_6F_5Br and C_6F_5I

Reaction	Temperature = 300 K		Temperature = 450 K	
	β ($cm^3\ s^{-1}$)	Ion products	β ($cm^3\ s^{-1}$)	Ion products
$C_6F_5Cl + e$	8.4×10^{-8}	$C_6F_5Cl^-$ (100)	1.3×10^{-7}	$C_6F_5Cl^-$ (100)
$C_6F_5Br + e$	8.3×10^{-8}	$C_6F_5Br^-$ (≥ 97) Br^- (≤ 3)	2.4×10^{-7}	$C_6F_5Br^-$ (~ 60) Br^- (~ 40)
$C_6F_5I + e$	3.1×10^{-8}	$C_6F_5^-$ (≥ 95) $C_6F_5I^-$ (≤ 5)	1.2×10^{-7}	$C_6F_5^-$ (~ 100) I^- (trace)

Thus, dilute (about 1%), accurately known mixes of the C_6F_5X gases with helium were made up to facilitate the accurate determination of the flow rates of C_6F_5X into the afterglow plasma. Since the number densities of the attaching molecules are so small, ion/molecule reactions cannot occur to any significant extent along the axis of the flow tube and so the product ions of the attachment reactions, as determined by the downstream mass spectrometer, are not confused. The values of β determined in this study are considered to be accurate to $\pm 25\%$, although relative values of β for the different reactions are more accurate.

RESULTS AND DISCUSSION

As was previously mentioned, earlier FALP studies showed that β for the attachment of electrons to C_6F_6 decreased dramatically with increasing temperature and that only the parent ion $C_6F_6^-$ was observed as a product of the reaction. Naff et al. [1] have measured the τ_a for $(C_6F_6^-)^*$ to be 12 μs. Longer autodetachment lifetimes of > 30 μs [13] and ca. 50 μs [14] have been measured for $(C_6F_6^-)^*$ formed by electron transfer to C_6F_6 from Rydberg atoms. It is apparent that these τ_a values are much greater than the τ_c values in the FALP plasma so all the $(C_6F_6^-)^*$ formed in the FALP plasma could be collisionally stabilised. Since there are no exothermic dissociative channels in the C_6F_6 attachment reaction then the observation that $C_6F_6^-$ is the only product ion is understandable. This same argument applies to the C_6F_5Cl reaction and therefore only the parent negative ion was observed to be formed in the FALP plasma. However, for both the C_6F_5Br and C_6F_5I reactions, dissociative channels are observed in the FALP experiments; notable is the attachment reaction of C_6F_5I in which the major product ion was $C_6F_5^-$. (In a parallel project, we have studied various ion/molecule reactions of $C_6F_5^-$ using a selected ion flow tube (SIFT) apparatus and the results are presented in the Appendix.)

As expected, some differences are apparent between the FALP data and the TOF data of Naff et al. [1]. Consideration of the FALP and TOF data provides information concerning the thermochemistry of these attachment reactions and the lifetimes of the excited $(C_6F_5X^-)^*$ ions. The reactions of C_6F_5I, C_6F_5Cl and C_6F_5Br are discussed separately below in the order stated.

Electron attachment to C_6F_5I

For this attachment reaction the major product was $C_6F_5^-$ (> 95%) at both 300 and 450 K. The parent ion $C_6F_5I^-$ was a minor product at 300 K and only a trace of I^- was observed at 450 K (see Table 1). A consideration of the thermochemistry for the two dissociative product channels gives

$$C_6F_5I + e \rightarrow I^- + C_6F_5 + (4.3 \pm 1.0) \text{ kcal mol}^{-1} \quad (1a)$$

$$\rightarrow C_6F_5^- + I - (3.0 \pm 1.4) \text{ kcal mol}^{-1} \quad (1b)$$

The reaction ergicities were calculated using the accurately known electron affinity of I atoms, $EA(I) = (70.482 \pm 0.023)$ kcal mol^{-1} [15], and the less certain values of $EA(C_6F_5) = (63.2 \pm 1.0)$ kcal mol^{-1} [16,17] and the bond dissociation energy $D(C_6F_5\text{–}I) = (66.2 \pm 1.0)$ kcal mol^{-1} [18].

It is interesting that the major product ion is $C_6F_5^-$ since this product channel is apparently endothermic whereas the exothermic I^- product is minimal. Similar behaviour has been observed by Compton and Reinhardt [17] for the collisional ionisation of C_6F_6 by fast alkali atoms, i.e., the more endothermic production of $C_6F_5^-$ appeared at a lower centre-of-mass energy than that for the less endothermic production of F^-. The reason for this type of behaviour is not yet understood; however, consideration of the availability of acceptor states for the free electron favours electron attachment to the multi-state polyatomic C_6F_5 radical rather than the singlet ground state I^-. The derived endothermicity of channel (1b) is not inconsistent with the present data if the following argument can be accepted. The β values for the reaction at both temperatures are appreciable fractions of the upper limit (collisional) value, β_{max}, which we estimate to be about $2\text{–}3 \times 10^{-7}$ cm^3 s^{-1} (using the theory of Klots [19]). The β value at 300 K is measured to be 3.1×10^{-8} cm^3 s^{-1} (see Table 1), and if this value is less than the β_{max} value by virtue of the reaction endothermicity or an activation energy barrier, ΔE, then assuming a simple Boltzmann relationship (i.e., $\beta = \beta_{max} \exp - \Delta E/RT$) ΔE is calculated to be about 1.2 kcal mol^{-1}. Also, if the factor-of-four larger value of the measured β at 450 K (see Table 1) is also attributed to the effect of ΔE, then combining the β values at the two temperatures and again assuming the simple Boltzmann law, the ΔE value is calculated to be about 2.4 kcal mol^{-1}. It should be said that from these

measurements it is not possible to distinguish between an activation energy barrier or an endothermicity. However it is notable that if ΔE is assumed to be due to an endothermicity then it is entirely consistent with ΔE calculated above for $C_6F_5^-$ production (reaction 1b). On this basis, the $D(C_6F_5\text{-}I)$ and the $EA(C_6F_5)$ adopted in the calculation of ΔE are seemingly quite accurate (to within about 1 kcal mol^{-1} as indicated above).

As mentioned above, the parent ion $C_6F_5I^-$ was discernible in the product ion spectrum at 300 K in the FALP experiment whereas in the TOF experiments of Naff et al. [1], in which negative ions with lifetimes $\lesssim 1$ μs could not be detected, parent ions were not detected. Hence the implication is that $(C_6F_5I^-)^*$ has $\tau_a < 1$ μs but greater than the τ_c value in the FALP plasma which is about 0.1 μs. This therefore brackets the τ_a of $(C_6F_5I^-)^*$ between 10^{-7} s and 10^{-6} s. The lower limit to τ_a may be somewhat greater than that quoted since helium, in general, inefficiently collisionally stabilizes excited ions and so several collisions may be needed to stabilize the $(C_6F_5I^-)^*$. In view of this, it seems probable that τ_a for $(C_6F_5I^-)^*$ at 300 K is close to 10^{-6} s. Also, because $C_6F_5I^-$ is absent from the product ion spectrum at 450 K a significantly lower τ_a for $(C_6F_5I^-)^*$ at this higher temperature is indicated.

Electron attachment to C_6F_5Cl

The parent negative ion $C_6F_5Cl^-$ was the only significant product ion observed in the FALP experiment at both temperatures, whereas both $C_6F_5Cl^-$ and Cl^- were produced in the ion source of the TOF experiment [1]. Cl^- and $C_6F_5^-$ production are both quite endothermic

$$C_6F_5Cl + e \rightarrow C_6F_5 + Cl^- - (8.8 \pm 2.2) \text{ kcal mol}^{-1} \quad (2a)$$

$$\rightarrow C_6F_5^- + Cl - (29.0 \pm 2.4) \text{ kcal mol}^{-1} \quad (2b)$$

and thus the truly thermal FALP experiment is consistent with these energetics. The reaction ergicities were calculated using $EA(Cl) = (83.336 \pm 0.092)$ kcal mol^{-1} [15], $D(C_6F_5\text{-}Cl) = (92.2 \pm 2.2)$ kcal mol^{-1} [20] and the $EA(C_6F_5)$ as given in sub-section 1. The long τ_a of 17.6 μs for the $(C_6F_5Cl^-)^*$ [1] together with the large β values measured in the FALP experiment (which are appreciable fractions of β_{max} at both temperatures, see Table 1), implies that thermal electrons are efficiently captured by the C_6F_5Cl molecules and that the $(C_6F_5Cl^-)^*$ ions are effectively stabilised in collisions with He atoms. The increase in β with temperature (in this case about a factor of 2 between 300 K and 450 K) is not uncommon for non-dissociative attachment reactions and could be a manifestation of a small activation energy barrier to electron capture (equated to ΔE) which as before, is

estimated from the kinetics to be ca. 0.8 kcal mol^{-1}. It is unlikely to be due to a variation of τ_a with temperature (since $\tau_a \gg \tau_c$) or a variation of the collisional stabilisation efficiency of $(C_6F_5Cl^-)^*$ by He atoms over such a relatively small temperature range. It is worthy of note that the sense of the β dependence on temperature is opposite to that for the β for non-dissociative attachment to C_6F_6 (the C_6F_6 case has been discussed in detail in previous papers [8–11]). A final note worth making here is that the observation of Cl^- as a major product in the TOF experiment implies that a fraction of the electrons in the TOF ion source must be suprathermal by at least 0.3 eV (rather than the upper limit energy of 0.1 eV indicated by Naff et al. [1]) if the energetics given with Eq. 2a are correct. Alternatively, the literature value for $D(C_6F_5-Cl)$ may be too large by a few kcal mol^{-1}.

Electron attachment to C_6F_5Br

The major product ions of this reaction were $C_6F_5Br^-$ ($\geq 97\%$ at 300 K and $\sim 60\%$ at 450 K) and Br^- ($\leq 3\%$ at 300 K and $\sim 40\%$ at 450 K) with the percentage of Br^- and the overall attachment rate coefficient, β, increasing with increasing temperature (see Table 1). The energetics for Br^- and $C_6F_5^-$ production in this reaction are uncertain because an accurate value of $D(C_6F_5-Br)$ is not available. A value of $D(C_6F_5-Br) = 105.9$ kcal mol^{-1} has previously been reported [21] but this must be greatly in error since using this value, an endothermicity of 28.4 kcal mol^{-1} for Br^- production is indicated and this cannot be remotely correct since Br^- production is facile at 450 K in the FALP plasma. However an estimate of $D(C_6F_5-Br) \cong 80$ kcal mol^{-1} can be made by considering the trend in the analogous C_6H_5X compounds (where X = F, Cl, Br, and I) [15] and this value along with the accurately known EA(Br) of 77.530 ± 0.092 kcal mol^{-1} has been used to calculate the ergicities of the reactions

$$C_6F_5Br + e \rightarrow Br^- + C_6F_5 - \sim 3 \text{ kcal mol}^{-1} \text{ (est)} \quad (3a)$$

$$\rightarrow C_6F_5^- + Br - \sim 17 \text{ kcal mol}^{-1} \text{ (est)} \quad (3b)$$

Clearly the production of $C_6F_5^-$ is very endothermic and indeed is not observed in significant quantities in the FALP.

The appearance of $C_6F_5Br^-$ as the major product at 300 K in the FALP experiment is consistent with the long lifetime of the $(C_6F_5Br^-)^*$ ion determined by Naff et al. [1], implying that this excited ion can be stabilized against autodetachment in collision with He atoms ($\tau_a \gg \tau_c$). Notwithstanding the fact that $(C_6F_5Br^-)^*$ ions can undergo collisions with He atoms during their lifetime, which may modify the nascent state distribution of the excited ions, we treat the product channels as separate reactions and, as

before, assume a Boltzmann law to derive a ΔE value for each reaction. Thus ΔE for Br^- production is calculated to be ca. 6 kcal mol^{-1}. As before this may represent a barrier to dissociative electron attachment or the endothermicity of the reaction and again these are indistinguishable. However, large barriers ($\gtrsim$ 3 kcal mol^{-1}) to dissociative electron attachment are not uncommon [6,7] (note that the barrier for $C_6F_5^-$ production from C_6F_5I is not greater than 2 kcal mol^{-1}). However, if ΔE for Br^- production derived from the experiment represents an endothermicity of the reaction, then $D(C_6F_5\text{-}Br) = \Delta E + EA(Br) \equiv 84$ kcal mol^{-1}. In view of the uncertainties as to whether ΔE represents an endothermicity or an activation energy barrier, this value should be viewed as an upper limit to $D(C_6F_5\text{-}Br)$. This upper limit is not inconsistent with the estimate of 80 kcal mol^{-1} obtained from the analogous C_6H_5Br bond dissociation energy.

It is also interesting to note that an energy barrier of ca. 1.0 kcal mol^{-1} can be deduced for $C_6F_5Br^-$ production which is similar to the barrier for $C_6F_5Cl^-$ production mentioned previously. So it appears that the mechanisms for parent ion production for C_6F_5Cl and C_6F_5Br are similar (C_6F_5I forms very little parent ion at 300 K).

CONCLUDING REMARKS

These studies of electron attachment to C_6F_5Cl, C_6F_5Br and C_6F_5I, have clearly shown how different product ions can result from electron attachment studied in a low pressure (beam) experiment in which the electrons are suprathermal in the ion source and in a "high" pressure experiment in which electrons are truly thermal. The production of $(C_6F_5I^-)^*$ in the FALP experiment but not in the TOF experiment has been used to bracket the previously unknown lifetime to autodetachment, τ_a, of $(C_6F_5I^-)^*$ in the range 10^{-7} s $< \tau_a$ $(C_6F_5I^-)^* < 10^{-6}$ s. It has also been shown that thermal electron attachment to C_6F_5Br yields both $C_6F_5Br^-$ and Br^-, from which an upper limit to $D(C_6F_5\text{-}Br)$ of ca. 84 kcal mol^{-1} has been established.

A most important conclusion to be drawn from these studies is that the rate coefficients and product ions resulting from attachment reactions of electrons with a given molecular species can be dependent on the environment in which the reaction occurs. Even where the electron/molecule (M) interaction energies or temperatures are the same in two systems but where the ambient pressures are very different (such that the τ_c value for collisions between the nascent parent negative ion $(M^-)^*$ and ambient gas atoms or molecules vary greatly relative to the autodetachment lifetime of $(M^-)^*$) then different results are to be expected. Thus, for example, it is dangerous to assume that results obtained in very low pressure time-of-flight experiments and in low pressure experiments, including FALP results obtained at

pressures of typically 1 torr, are appropriate to electron capture detectors which generally operate at ambient pressures close to atmospheric pressure. Recently, we observed that the CCl_3 radicals generated from the dissociative attachment reactions of CCl_4 with thermal electrons in the FALP plasma rapidly undergo dissociative attachment with thermal electrons [12]. However, we have been informed by Grimsrud [22] that he sees no evidence for such a phenomenon in his high pressure electron capture detectors. This difference may be a manifestation of the production of vibrationally-excited CCl_3 radicals in the CCl_4 + e dissociative attachment reactions which are not effectively quenched to the ground vibrational state before interacting with an electron in the lower pressure FALP but are quenched at the higher pressure of the capture detector. This would imply a barrier to dissociative attachment to CCl_3 radicals which is effectively overcome by vibrational excitation. More work is necessary to clarify this.

ACKNOWLEDGEMENT

We are grateful to the United States Air Force for financial support of this work.

REFERENCES

1 W.T. Naff, R.N. Compton and C.D. Cooper, J. Chem. Phys., 54 (1971) 212.
2 R.L. Woodin, M.S. Foster and J.L. Beauchamp, J. Chem. Phys., 72 (1980) 4223.
3 A. Chutjian and S.H. Alajajian, Phys. Rev., 131 (1985) 2885.
4 L.M. Chanin, A.V. Phelps and M.A. Biondi, Phys. Rev. Lett., 2 (1959) 344.
5 R.W. Crompton and G.N. Haddad, Aust. J. Phys., 36 (1983) 15.
6 E. Alge, N.G. Adams and D. Smith, J. Phys. B, 16 (1984) 1433.
7 D. Smith, N.G. Adams and E. Alge, J. Phys. B, 17 (1984) 461.
8 N.G. Adams, D. Smith, E. Alge and J. Burdon, Chem. Phys. Lett., 116 (1985) 460.
9 S.M. Spyrou and L.G. Christophorou, J. Chem. Phys., 82 (1985) 1048.
10 N. Herdandez-Gil, W.E. Wentworth, T. Limeru and E.C.M. Chen, J. Chromatogr., 312 (1984) 31.
11 L.G. Christopborou, J. Chem. Phys., 83 (1985) 6543.
12 N.G. Adams, D. Smith and C.R. Herd, Int. J. Mass. Spectrom. Ion Processes, 84 (1988) 231.
13 I. Dimicolli and R. Botter, J. Chem. Phys., 74 (1981) 2355.
14 R.W. Marawar, C.W. Walter, K.A. Smith and F.B. Dunning, J. Chem. Phys., 88 (1988) 2853.
15 T.M. Miller, in R.C. Weast (Ed.), CRC Handbook of Chemistry and Physics, 66th edn., CRC Press, Boca Raton, FL, 1985, E-62.
16 F.M. Page and G.C. Goode, in Negative Ions and the Magnetron, Wiley Interscience, New York, 1969.
17 R.N. Compton and P.W. Reinhardt, Chem. Phys. Lett., 91 (1982) 268.
18 M.J. Kreech, S.J.W. Price and W.F. Yared, Int. J. Chem. Kinet., 6 (1974) 257.

19 C.E. Klots, Chem. Phys. Lett., 38 (1976) 61.
20 K.Y. Choo, O.M. Golden and S.W. Benson, Int. J. Chem. Kinet., 7 (1975) 713.
21 S.J.W. Price and H.J. Sapiano, Can. J. Chem., 52 (1974) 4109.
22 E. Grimsrud, private communication, June 1988.

APPENDIX A

Ion / molecule reactions of $C_6F_5^-$

Little is known about the reactivity of $C_6F_5^-$ ions, so we chose to investigate this in order to gain a more complete understanding of the chemistry of this ionic species. Reactions of $C_6F_5^-$ with CH_3Cl, CH_3Br, CH_3I, HF, HCl, HBr and C_6F_5Cl were studied at 300 K using a selected ion flow tube (SIFT) apparatus which has previously been described in detail [A1]. The carrier gas was pure helium at a pressure of about 0.5 torr. Copious amounts of $C_6F_5^-$ were produced by electron impact on C_6F_5I in a high pressure ion source and injected into the carrier gas. Reactant gas was added downstream and the binary rate coefficients, k_2, were determined in the usual manner [A1]. The k_2 values and the ionic products observed are listed in Table A1.

The k_2 values for the reactions with CH_3Cl and HF (reactions (a) and (d) in Table A1) were immeasurably small, being $< 10^{-13}$ cm^3 s^{-1}. This is not surprising for reaction (d) since it is calculated to be endothermic by about 6 kcal mol^{-1}. The reactions with CH_3Br and CH_3I (reactions (b) and (c)) seemingly occur via a binary nucleophilic substitution mechanism [A2,A3] (an S_N2 displacement mechanism [A4]) giving Br^- and I^- as the product ions, respectively. These reactions have small reaction efficiencies (k_2/k_{ADO}, where k_{ADO} is the collisional limiting rate coefficient calculated using the average dipole orientation theory (ADO) [A5]; see Table A1). Many organic ion/molecule reactions proceed with k_2 well below their collisional limiting values, this being qualitatively ascribed to the effect of a double-well potential surface [A2,A6]. However, it is interesting to note that in reactions (a) to (c) the nucleophile, $C_6F_5^-$, and the substrate, CH_3, are obviously the same and thus the leaving group ability of the halogen ion should be an important factor affecting the efficiency of the reactions. It is known that the leaving group abilities of the halogen ions in the gas phase are the same as in the liquid phase, i.e., $I^- > Br^- > Cl^-$ and, as can be seen from Table A1, the efficiencies of reactions (a)–(c) do indeed increase with the leaving group abilities of the halogen ions. Note also that the reaction efficiency increases with the exothermicity of the reactions.

The reaction with HCl and HBr (reactions (e) and (f) in Table A1) giving Cl^- and Br^- as product ions are proton transfer reactions and proceed with

TABLE A1

Rate coefficients, k_2, at 300 K for the reactions of $C_6F_5^-$ with the molecules indicated as measured using a selected ion flow tube (SIFT). Also listed are the collisional limiting values of the rate coefficients k_{ADO} [a], the reaction efficiences (k_2/k_{ADO}) and the reaction ergicities ΔH_r (calculated from the bond dissociation energies and electron affinities given in ref. 15)

Reaction	k_2 ($cm^3\ s^{-1}$)	k_{ADO} ($cm^3\ s^{-1}$)	k_2/k_{ADO}	ΔH_r ($kcal\ mol^{-1}$)
(a) $C_6F_5^- + CH_3Cl$: no reaction	$<10^{-13}$	1.40×10^{-9}	7.0×10^{-5}	−41
(b) $C_6F_5^- + CH_3Br \rightarrow C_6F_5CH_3 + Br^-$	4.4×10^{-12}	1.14×10^{-9}	3.9×10^{-3}	−49
(c) $C_6F_5^- + CH_3I \rightarrow C_6F_5CH_3 + I^-$	6.5×10^{-11}	1.04×10^{-9}	6.3×10^{-2}	−57
(d) $C_6F_5^- + HF$: no reaction	$<10^{-13}$	1.79×10^{-9}	5.6×10^{-5}	+6
(e) $C_6F_5^- + HCl \rightarrow C_6F_5H + Cl^-$	6.0×10^{-10}	1.05×10^{-9}	5.7×10^{-1}	−41
(f) $C_6F_5^- + HBr \rightarrow C_6F_5H + Br^-$	2.0×10^{-10}	7.44×10^{-10}	2.7×10^{-1}	−41
(g) $C_6F_5^- + C_6F_5Cl \rightarrow (C_6F_5)_2 + Cl^-$	1.9×10^{-10}	-	-	−45

[a] The polarisabilities and dipole moments of the neutral molecules which were required to calculate k_{ADO} were obtained from ref. 15 and the dipole locking constants were determined from data in refs. A9 and A10.

k_2 values which are appreciable fractions of, although significantly smaller than, their collisional limiting values. Proton transfer to negative ions generally occurs at or near the collisional limiting value for localised anions (e.g., O^-, OH^- and C_2H^-) [A7]. However there are many examples of relatively slow proton transfer for delocalised anions, e.g., $C_6H_5O^-$ and $(C_6H_5)CH_2^-$ [A6]. $C_6F_5^-$ is a delocalised anion and thus it is not surprising that the k_2 values for reactions (e) and (f) are significantly smaller than their collisional limiting values.

The reaction with C_6F_5Cl (reaction (g)) proceeds with a k_2 value of $1.9\times10^{-10}\ cm^3\ s^{-1}$ which again is significantly smaller than the collisional value and as before the halogen negative ion is the product. (Since the polarizability of C_6F_5Cl is unknown, k_{ADO} could only be estimated as $5.2\times10^{-10}\ cm^3\ s^{-1}$ (using an estimated polarisability of $5\times10^{-24}\ cm^3$) giving a reaction efficiency of 0.3). This reaction probably proceeds via an addition elimination mechanism [A8], with the strong electron withdrawing F atoms stabilising the resulting carbanion which then eliminates Cl^- to produce $(C_6F_5)_2$. Dissociative charge transfer from $C_6F_5^-$ to C_6F_5Cl to give Cl^- and two C_6F_5 radicals is not possible since this process is ca. 55 kcal

mol^{-1} endothermic. The relative inefficiency of this reaction may be attributed to a barrier on an, as yet, undetermined potential surface.

REFERENCES

A1 (a) D. Smith and N.G. Adams, in M.T. Bowers (Ed.), Gas Phase Ion Chemistry, Vol. 1, Academic Press, New York, 1979, p. 1. (b) D. Smith and N.G. Adams, Adv. At. Mol. Phys., 24 (1988) 1.

A2 W.N. Olmstead and J.I. Brauman, J. Am. Chem. Soc., 99 (1977) 4219.

A3 M. Tanaka, G.I. Mackay, J.D. Payzant and D.K. Bohme, Can. J. Chem., 54 (1976) 1643.

A4 T.H. Lowry and K.S. Richardson, Mechanism and Theory in Organic Chemistry, Harper and Row, New York, 1976.

A5 T. Su and M.T. Bowers, in M.T. Bowers (Ed.), Gas Phase Ion Chemistry, Vol. 1, Academic Press, New York, 1979, p. 83.

A6 W.E. Farneth and J.I. Brauman, J. Am. Chem. Soc., 98 (1976) 7891.

A7 D.K. Bohme, in P. Ausloos (Ed.), Interactions Between Ions and Molecules, Plenum Press, New York, 1975, pp. 489–504.

A8 J.M. Harris and C.S. Wamser, Fundamentals of Organic Reaction Mechanisms, Wiley, New York, 1976.

A9 T. Su and M.T. Bowers, Int. J. Mass Spectrom. Ion Phys., 12 (1973) 347.

A10 T. Su and M.T. Bowers, Int. J. Mass Spectrom. Ion Phys., 17 (1975) 211.

APPENDIX 3

A STUDY OF DISSSOCIATIVE ELECTRON ATTACHMENT TO $CF_3SO_3CH_3$ AND $CF_3SO_3C_2H_5$ TRIFLATE ESTERS USING THE FALP APPARATUS

C.R. HERD, D. SMITH AND N.G. ADAMS

Int.J.Mass Spectrom.Ion Proc., 91, 177 (1989)

International Journal of Mass Spectrometry and Ion Processes, 91 (1989) 177-182
Elsevier Science Publishers B.V., Amsterdam - Printed in The Netherlands

A STUDY OF DISSOCIATIVE ELECTRON ATTACHMENT TO $CF_3SO_3CH_3$ AND $CF_3SO_3C_2H_5$ TRIFLATE ESTERS USING THE FALP APPARATUS

CHARLES R. HERD, DAVID SMITH and NIGEL G. ADAMS

School of Physics and Space Research, University of Birmingham, Birmingham B15 2TT (Gt. Britain)

(Received 16 December 1988)

ABSTRACT

The rate coefficients, β, for dissociative electron attachment to the triflate esters $CF_3SO_3CH_3$ and $CF_3SO_3C_2H_5$, have been determined at 300, 385 and 475 K using the FALP apparatus. The β for both reactions are small ($\sim 10^{-10}$ cm^3 s^{-1}) at 300 K, in contrast to the β for triflic acid, CF_3SO_3H, which is very large ($\sim 10^{-7}$ cm^3 s^{-1}) at 300 K. In a parallel study, the reactions of F^-, Cl^-, Br^- and I^- with the two esters have been studied at 300 K using the SIFT technique. These ion/molecule reactions proceed at or near their collisional rates, again producing the triflate anion $CF_3SO_3^-$, and reveal that the dissociative electron attachment reactions of these esters are exothermic.

INTRODUCTION

The extreme acidity in the liquid phase of the (Brønsted-type) superacid CF_3SO_3H, commonly called triflic acid, has its equivalence in the very efficient gas-phase dissociative attachment it undergoes when reacting with free electrons in a plasma

$$CF_3SO_3H + e \rightarrow CF_3SO_3^- + H \quad (1)$$

This may be viewed as the acid donating a proton to an electron, (the base) generating the triflate anion $CF_3SO_3^-$ [1]. This anion is extremely stable (unreactive) and this implies a large detachment energy or equivalently that the radical CF_3SO_3 has a very large electron affinity. Indeed, from the studies of the ion chemistry of triflic acid, a gas phase electron affinity of 5.5 eV for CF_3SO_3 has been estimated [2] which exceeds that of most other species [3]. The combination of a very large electron capture rate coefficient and the generation of an extraordinarily stable negative ion makes triflic acid a very attractive scavenger of electrons from ionized gases and plasmas.

However, the problem is that it is a very corrosive material. Attractive alternatives as electron scavengers may be the methyl and ethyl esters of triflic acid, $CF_3SO_3CH_3$ and $CF_3SO_3C_2H_5$, which are quite stable, easier to handle and less corrosive. The major question is whether they undergo dissociative attachment with electrons at normal temperatures. We have therefore studied these attachment reactions and the ion chemistry of these triflate esters to determine their suitability as efficient electron scavengers in the gas phase.

EXPERIMENTAL

The electron attachment studies were carried out using the flowing afterglow/Langmuir probe (FALP) apparatus which has been described in detail previously [4]. Measured flow rates of the vapours of the esters were introduced into a thermalized flowing afterglow plasma and the increase in the rate of reduction of the electron density along the axis of the flowing plasma was determined using a movable Langmuir probe. The analysis of the data to determine attachment coefficients, β, is straightforward and is well documented [4–6]. The product ions of the reactions were identified using a downstream mass spectrometer sampling system. The β-values for both esters were measured at three temperatures 300, 385 and 475 K.

In order to better understand the energetics of reactions (2) and (3) below, studies were also made of the gas phase reactions of the halogen atomic negative ions F^-, Cl^-, Br^- and I^- with the $CF_3SO_3CH_3$ and $CF_3SO_3C_2H_5$ at 300 K. These studies were carried out using a selected ion flow tube (SIFT) apparatus which has also been described in detail previously [7] and which is now a commonly-used technique for studying ion/molecule reactions at thermal energies [8].

RESULTS AND DISCUSSION

Since the value of β at 300 K for the triflic acid reaction (1) is very large (1×10^{-7} cm^2 s^{-1}) [1] being close to the predicted upper limit value for attachment reactions ($\beta_{max} \sim 3 \times 10^{-7}$ cm^2 s^{-1}) [9] it was somewhat surprising to find that the β-values for the esters were some three orders-of-magnitude smaller at the same temperature at $\sim 10^{-10}$ cm^3 s^{-1} (see Table 1). However, although slow, these reactions did proceed via dissociative attachment

$$CF_3SO_3CH_3 + e \rightarrow CF_3SO_3^- + CH_3 \quad (2)$$

$$CF_3SO_3C_2H_5 + e \rightarrow CF_3SO_3^- + C_2H_5 \quad (3)$$

TABLE 1

Rate coefficients for electron attachment to $CF_3SO_3CH_3$ and $CF_3SO_3C_2H_5$

Reaction	Electron attachment coefficient $\beta \times 10^{-10}$ ($cm^3\ s^{-1}$)		
	300 K	385 K	475 K
$CF_3SO_3CH_3 + e$	1.8	10	23
$CF_3SO_3C_2H_5 + e$	2.7	6.7	6.5

generating the stable triflate anion in both cases. The β-value for reaction (2) increased dramatically with temperature, at 475 K being some 40 times greater than at 300 K. An additional value of β at 385 K allowed a 3-point Arrhenius plot to be constructed (Fig. 1) and the slope of the line indicates an activation energy barrier or an endothermicity for reaction (2) of about 170 meV (we show below that reactions (2) and (3) are exothermic). However, even if this rapid rise in β with temperature was maintained at higher temperatures, the β-value would not reach β_{max} (i.e. become comparable to triflic acid as an electron scavenger) before the ester thermally decomposed. (The decomposition of these esters is discussed in ref. 10; it occurs only at much higher temperatures and pressures than are used in the present experiments.) The values of β for reaction (3) are also given in Fig. 1 where it can be seen that β appears to be reaching a maximum at the higher temperatures, so no meaningful value for an activation energy or the reaction endothermicity can be obtained.

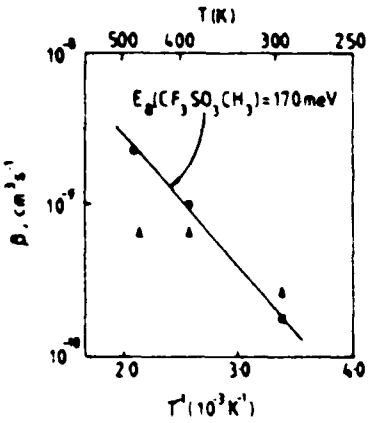

Fig. 1 Plots of the attachment coefficients, β, vs. reciprocal temperature, T^{-1}, (Arrhenius-type plots) for the dissociative attachment reactions of electrons with $CF_3SO_3CH_3$ (●) and $CF_3SO_3C_2H_5$ (▲). The slope of the line for $CF_3SO_3CH_3$ (●) provides an activation energy for the reaction of 170 meV as shown.

TABLE 2

Rate coefficients for the reactions of $CF_3SO_3CH_3$ and $CF_3SO_3C_2H_5$ with F^-, Cl^-, Br^-, and I^- [a]

	k_2 ($cm^3\ s^{-1}$)	$\mu^{-1/2}$
$CF_3SO_3CH_3 + F^-$	2.1×10^{-9}	0.242
$+ Cl^-$	1.7×10^{-9}	0.185
$+ Br^-$	9.6×10^{-10}	0.136
$+ I^-$	8.9×10^{-10}	0.118
$CF_3SO_3C_2H_5 + F^-$	3.2×10^{-9}	0.241
$+ Cl^-$	2.1×10^{-9}	0.184
$+ Br^-$	1.5×10^{-9}	0.135
$+ I^-$	7.8×10^{-10}	0.116

[a] The product ion is $CF_3SO_3^-$ in all cases and it can be seen that k_2 decreases as $\mu^{-1/2}$ (where μ is the reduced mass) as expected if the reactions proceed at the collision rate.

In order to determine whether reactions (2) and (3) were exothermic or endothermic we studied the reactions of the esters with the halide ions

$$X^- + CF_3SO_3R \rightarrow CF_3SO_3^- + RX \qquad (4)$$

where X is F, Cl, Br or I, and R is CH_3 or C_2H_5. All of these reactions proceed very efficiently, essentially on every collision, although the precise efficiencies cannot be determined because the polarizabilities and the dipole moments of the esters, which are needed for calculation of the collisional rate coefficient, are not available. The measured rate coefficients, k_2, are given in Table 2 where it can be seen that the k_2-values decrease roughly in accordance with $\mu^{-1/2}$ (where μ is the reduced mass of the reactants) as predicted by theories for determining collisional rate coefficients [11]. This variation with reduced mass is itself an indicator that the reactions proceed at or near the collisional rate. That the reactions of the halide ions with both esters occur so rapidly indicates that they are exothermic. If a thermodynamic cycle is constructed the enthalpy change, ΔH, for the reactions is given by

$$\Delta H = D(CF_3SO_3\text{-}R) + EA(X) - D(R\text{-}X) - EA(CF_3SO_3) \qquad (5)$$

(note the formation of the neutral product R–X is assumed and this must be so or the reactions would be very endothermic). Because $\Delta H < 0$, an *upper limit* to $D(CF_3SO_3\text{-}R)$ can be determined and it is found that the smallest value for this *upper limit* is obtained for X = I. An upper limit of ~ 5 eV was deduced using the following values: $EA(CF_3SO_3) = 5.5$ eV [2], $EA(I) = 3.0591$ eV, and $D(CH_3\text{-}I) \sim 2.4$ eV ($D(C_2H_5\text{-}I)$ is similar and is ~ 2.3 eV) [3]. Thus the dissociative electron attachment reactions (2) and (3) are exothermic by at least 0.5 eV, i.e., $EA(CF_3SO_3) - D(CF_3SO_3\text{-}R)$, and there-

fore the slope of the Arrhenius plot in Fig. 1 yields an activation energy and not an endothermicity for reaction (2).

It is worthy of note that the reactions between the halide ions and the triflate esters occur essentially on every collision generating the $CF_3SO_3^-$ ion whereas significant energy barriers exist to the formation of this anion via dissociative electron attachment. Barriers to binary ion/molecule reactions are the exception rather than the rule and when they are exothermic they usually (but not always) proceed rapidly [12]. However, there are many examples of activation energy barriers to dissociative electron attachment [4,5] and these are usually rationalized in terms of the need for vibrational energy in the reactant molecule and/or electron energy in order to access a repulsive potential curve along which the product negative ion and fragment neutral can separate [13].

Note that these results again indicate that it is usually incorrect to make the assumption that dissociative attachment will proceed efficiently even if exothermic channels are available.

Finally, as we stated in the Introduction, the detachment energy of $CF_3SO_3^-$ is large and it is worthy of mention here that we have obtained independent information that this is indeed the case. Using a tunable laser system, we have been unable to photodetach electrons from $CF_3SO_3^-$ with photons of wavelength 226 nm = 5.3 eV (photodetachment from I^- has been achieved with 226 nm photons), suggesting (but not proving) that the $EA(CF_3SO_3)$ exceeds 5.3 eV, in accordance with the ion-chemical data [1].

ACKNOWLEDGEMENT

The authors are grateful to the United States Air Force for financial support of this work.

REFERENCES

1 N.G. Adams, D. Smith, A.A. Viggiano, J.F. Paulson and M.J. Henchman, J. Chem. Phys., 84 (1986) 6728.
2 J.F. Paulson, A.A. Viggiano, M. Henchman and F. Dale, Proc. Symposium on Atomic and Surface Physics, Obertraun, Austria, 9-15 Feb. 1986, p. 7.
3 T.M. Miller, in R.C. Weast (Ed.), CRC Handbook of Chemistry and Physics, 66th edn., CRC Press, Boca Raton, FL, p. E-62.
4 D. Smith, N.G. Adams and E. Alge, J. Phys. B, 17 (1984) 461.
5 E. Alge, N.G. Adams and D. Smith, J. Phys. B, 17 (1984) 3827.
6 N.G. Adams, D. Smith and C.R. Herd, Int. J. Mass Spectrom. Ion Processes, 84 (1988) 243.
7 N.G. Adams and D. Smith, Int. J. Mass Spectrom. Ion Phys., 21 (1976) 349.
8 D. Smith and N.G. Adams, Adv. At. Mol. Phys., 24 (1987) 1.
9 C.E. Klots, Chem. Phys. Lett., 38 (1976) 61.

10 T. Gramstad and R.N. Haszeldine, J. Chem. Soc., (1957) 4069.
11 T. Su and M.T. Bowers, in M.T. Bowers (Ed.), Gas Phase Ion Chemistry, Vol. 1, Academic Press, New York, 1979, p. 83.
12 N.G. Adams and D. Smith, in A. Fontijn and M.A.A. Clyne (eds.), Reactions of Small Transient Species, Academic Press, New York, 1983, p. 311.
13 L.G. Christophorou, D.L. McCorkle and A.A. Christodoulide, in L.G. Christophorou (Ed.), Electron-Molecule Interactions and their Applications, Vol. 1, Academic Press, 1984, Chap. 6.

APPENDIX 4

STUDIES OF DISSOCIATIVE ELECTRON ATTACHMENT TO SOME HALOETHANES USING THE FALP APPARATUS: COMPARISON WITH DATA OBTAINED USING NON-THERMAL TECHNIQUES

D. SMITH, C.R. HERD AND N.G. ADAMS

Int.J.Mass Spectrom.Ion Proc. (1989), in press

STUDIES OF DISSOCIATIVE ELECTRON ATTACHMENT TO SOME HALOETHANES USING THE FALP APPARATUS: COMPARISONS WITH DATA OBTAINED USING NON-THERMAL TECHNIQUES

D. Smith, C.R. Herd and N.G. Adams

School of Physics and Space Research

University of Birmingham

P.O. Box 363

Birmingham, B15 2TT

England

ABSTRACT

Measurements are reported of the rate coefficients, β, for the dissociative attachment reactions with electrons of the four haloethanes CH_3CCl_3, $CH_2ClCHCl_2$, CF_3CCl_3 and $CF_2ClCFCl_2$, obtained under truly thermal equilibrium conditions at 298, 385 and 470K using the flowing afterglow/Langmuir probe (FALP) technique. In all four reactions the only product ion observed was Cl^-. These values of β are compared with the equivalent β obtained by the non-thermal swarm and krypton photoionization techniques for which β values were deduced as a function of mean electron/molecule interaction energy, $\dot{E}$, at a fixed reactant molecule temperature of ~298K. The different senses of the variations of β with temperature and with $\dot{E}$ are discussed and are rationalized in terms of the thermal and non-thermal nature of the different experiments and not as 'discrepancies' as described previously.

INTRODUCTION

During the past few years, we have developed our flowing afterglow/Langmuir probe (FALP) technique to determine electron attachment rate coefficients, β, under truly thermal conditions for a number of molecular species over the approximate range of temperature from 200 to 600K (i.e. mean interaction energies, ~25 to ~77 meV (= (3/2)kT) [1]). Several examples are seen of both direct attachment, in which negative ions MX^- of the parent molecules MX are formed, and dissociative attachment, in which fragment ions X^- and fragment radicals M are formed [2,3]. An obvious feature of the collected data is that when dissociative attachment is inefficient at room temperature, i.e., when the measured β is much less than β_{max}, the upper-limit value for the process [4,5,6], then an approximately exponential increase of β with increasing temperature, T, is observed and then 'activation energies', E_a, can be derived for exothermic dissociative attachment [2,3]. The increase in β with T is often very marked; for example, the β for dissociative electron attachment to CH_3Br (producing Br^- and CH_3) increases by about a factor of 100 between 300K and 500K, which is equivalent to an E_a of some 300 meV [3]. It is just as obvious from published data obtained from swarm experiments [7] and by the krypton photoionization technique [8] in the low energy (thermal) regime, that when the gas temperature is held constant and the mean electron energy $\dot{E}$ is increased then the β for the same dissociative attachment reaction often decreases, sometimes quite dramatically. Thus, increasing the internal temperature (energy) of the molecule tends to increases the β while increasing the electron/molecule interaction energy $\dot{E}$ (and thus, equivalently, the translational temperature of the reactants) in general tends to decrease the β, the latter being in accordance with theoretical

predictions (see ref.9 and references therein). In the truly thermalised plasma medium of the FALP experiment, where both the internal energy and the interaction energy are changed, the β is therefore a convolution of these two opposing effects.

In this paper, we report the results of a FALP study of the β for four haloethanes CH_3CCl_3, $CH_2ClCHCl_2$, CF_3CCl_3 and $CF_2ClCFCl_2$ which have previously been studied using the krypton photoionization technique and/or the (electron) swarm techninque for which the opposite trends in the true temperature and electron energy variations of the β are again very evident.

EXPERIMENTAL

The FALP apparatus and the method for determining β have been discussed in detail previously [2,3]. Basically, a flowing thermalized plasma is created in helium carrier gas (at a pressure of ~ 1 torr) by using a microwave discharge located in the upstream region of a flow tube which is ~100 cm long and 8 cm in diameter. The carrier gas/plasma is convected along the flow tube by means of a large Roots pump creating a thermalised afterglow plasma in the downstream region. A mass spectrometer sampling system is located downstream for identification of the positive and negative ions in the afterglow plasma as well as to identify the negative ions of the electron attachment reactions. Reactant (attaching) gases are introduced into the flow tube in controlled amounts and the resulting increase in the gradient of the electron density, n_e, along the flow tube (z - direction) is determined by a Langmuir probe which can be positioned at any point on the flow tube axis. The straightforward analysis [2,3] of the n_e versus z data provides a value for the attachment rate coefficient, β. Because the β

for CF_3CCl_3 was quite large ($\sim 2\times10^{-7}$ cm^3 s^{-1} at 298K) a dilute (~1%), accurately known mix of CF_3CCl_3 with helium was made to facilitate the accurate measurement of the very small flow rates which were required of this reactant gas into the thermalised afterglow plasma. Measurements of β were made at temperatures of 298, 385 and 470K.

RESULTS

The β values obtained in this study are given in Table 1 together with those previously determined using the swarm method at a fixed buffer gas temperature, T, of 298K and at a mean electron energy $\dot{E}$(~39 meV) equivalent to this temperature [7]. It can be seen that there is reasonably good agreement between the β obtained from the FALP and from the swarm experiments under comparable conditions (i.e. at T ~298K, equivalent to ~39meV), particularly when sensible uncertainties in both experiments are considered (the present β values are considered to be accurate to ± 20%). The only product ion observed in all cases in the FALP was Cl^-.

It is interesting to note the trends in β between the different isomeric forms of these ethanes as well as the effect on β of substitution of F atoms for H atoms. It can be seen from Table 1 that for a given temperature, in going from $CX_2ClCXCl_2$ to CX_3CCl_3 (where X=H or F) that there is an increase in β of more than one order of magnitude. Also, in going from the H atom substituted ethanes to the F atom substituted ethanes there is an increase in β of slightly more than one order of magnitude (i.e. in going from CH_3CCl_3 to CF_3CCl_3 or $CH_2ClCHCl_2$ to $CF_2ClCFCl_2$). The exact reasons for these two phenomena is not yet understood fully, but these trends have been observed previously by McCorkle et al, [7]. They suggest that the increase in β in going from $CX_2ClCXCl_2$ to CX_3CCl_3 results from a smaller bond dissociation energy of

the C-Cl bond in CX_3CCl_3 as compared to $CX_2ClCXCl_2$, which lowers the asymptotic limit of the negative ion potential energy curve and in effect increases the probability of separating to give the product negative ion and radical.

As mentioned above, the only product ion observed in all cases was Cl^-, but it has previously been reported by Alajajian and Chutjian [10] that in the reaction of CF_3CCl_3 with near thermal electrons another product ion besides Cl^- was formed (they assumed parent ion formation although this ion was not observed). However, for a 0 to 250 amu mass scan of the quadrupole mass filter on the FALP, the parent ion $CF_3CCl_3^-$ was not observed, indicating that if it is formed it is not stabilized against autodetactment in the FALP plasma.

The major point to which we wish to draw attention is the comparison between the changes which occur in the β with increasing T, as determined in the FALP experiment, and with increasing $\dot{E}$, as determined in the swarm experiment. The data for both experiments are presented in Fig. 1 (filled symbols are FALP data; open symbols refer to swarm data). The rapid increase in the β with increasing T for CH_3CCl_3 and $CF_2ClCFCl_2$ is not mirrored for a changing $\dot{E}$ in the swarm experiment, but rather only a very small, if any, increase in β occurs for $\dot{E}$ within the thermal range. For CF_3CCl_3, the FALP data indicate that β does not increase with T; but it is clear that the β at 298K is close to the upper- limit value for this process, β_{max}, and so β cannot increase by much as T is increased. Note, though, that the β decreases with increasing $\dot{E}$ for this reaction. For the much slower reaction of $CH_2ClCHCl_2$ the FALP data again indicates a rapid increase of β with T but the β increases only slowly with increasing $\dot{E}$ in the swarm experiment.

Before commenting further on the FALP data vis-a-vis the swarm data, it is pertinent to consider the data obtained for the CH_3CCl_3 reaction in comparison to that obtained using the krypton photoionization method [10] and these are presented in Fig. 2. Also included in this figure are the data obtained previously from both the FALP and the krypton photoionization experiments for the dissociation attachment reactions of CH_2Br_2 [3,10]. It is clear from these data that again the β for these reactions increase with increasing T and decrease slowly with increasing $\dot{E}$ in the thermal energy regime. Thus a pattern emerges for dissociative attachment reactions in the thermal energy (temperature) regime as studied by the truly thermal FALP experiment and the non-thermal swarm and krypton photoionization methods. How can the obvious differences be explained ?

DISCUSSION

The maximum electron capture cross section by a molecule, σ, is predicted theoretically to vary as E^{-1} (according to s-wave capture theory [6]) and this has been substantiated by many experimental measurements of the cross sections for rapid dissociative attachment [9]. Thus it is to be expected that the β for fast dissociative attachment reactions will also reduce with increasing $\dot{E}$ (since $\dot{\beta} \simeq \dot{\sigma}\,\dot{v}$ and $\dot{v} \sim \dot{E}^{1/2}$ then $\beta \sim \dot{E}^{-1/2}$). Also, if a β measured at 298K in the truly thermal FALP experiment or in the low energy limit of the swarm experiment is found to be large and close to β_{max}, then it is reasonable to assume that no energy barrier exists to inhibit dissociative attachment. If, however, a β is small ($<<\beta_{max}$) at 298K and the reaction is exothermic, then, as previously mentioned, an energy barrier is assumed to be reponsible and an 'activation energy', E_a, can be derived [2,3]. The origin of this energy barrier has been discussed by Wentworth [11] who

suggests that it results from an unfavourable crossing of the bound M-X potential curve with a repulsive curve of the $M\text{-}X^{\cdot}$ system. Vibrational excitation of the M-X bond, which can result from an increase in temperature, accesses the repulsive curve allowing more facile separation to M and X^- to occur. Thus β will increase with increasing T and this will be dramatic when E_a is large.

Using these ideas the differences between the T and $\dot{E}$ dependences of β can be qualitatively explained. When β is large and close to β_{max} (i.e. when there is no energy barrier and the repulsive curve passes through the minimum of the M-X potential well) then increasing T cannot produce an increasing β but an increasing $\dot{E}$ can result in a decreasing β (since the electron capture rate decreases with increasing $\dot{E}$). However when β is small ($<<\beta_{max}$, i.e. an energy barrier exists due to unfavourable curve crossings) then β will invariably increase with T in the FALP experiment but how will it vary with $\dot{E}$? Inspection of the data in Figs. 1 and 2 indicates that when β increases rapidly with T (i.e. when E_a is large) then β does not decrease rapidly with $\dot{E}$ and can even increase somewhat as is the case for $CH_2ClCHCl_2$.

We suggest that (i) this may be because in collision of the attaching electron with the molecule in the swarm experiments, partial internal (vibrational) excitation of the reactant molecule (or equivalently of the transient molecular negative ion) results [12] which tends to enhance β by more readily accessing the repulsive $M\text{-}X^{\cdot}$ curve and therefore mitigates the inhibiting effect an increasing $\dot{E}$ has on the capture rate. Alternatively, (ii) an increase in σ with $\dot{E}$ may also result from an unfavourable curve crossing which then requires an increase in electron energy for a favourable Franck- Condon transition to occur from low lying vibrational states to the repulsive $M\text{-}X^{\cdot}$ curve [9].

Independent of whether explanation (i) or (ii) is appropriate, this phenomenon will be more evident when E_a is large. When the E_a is relatively small (and β only increases slowly with T) then the β would be expected to decrease, albeit slowly, with increasing $\dot{E}$. This reasoning satisfactorily explains the different trends in the variation of β with T and with $\dot{E}$. So, rather than these differences being 'discrepancies' as has been suggested by others [8], differences are actually to be expected. It should be noted again that increasing the temperature of the FALP plasma, of course, results in both an increased rovibrational temperature of the reactant molecules and an increase in the electron/molecule interaction energy. Thus the influence of T on β is a convolution of these two opposing effects. Following these ideas, inferences may be drawn as to the $\dot{E}$ dependence of β when the T dependence is known and vice versa. Further investigations are continuing in our laboratory into this phenomenon.

Finally, it should be noted that these conclusions do not relate to direct attachment (referred to in the Introduction) but only to dissociative attachment. The direct attachment process appears to be much more complex and capture resonances appear to be involved [9]. The β for this process may even decrease rapidly from very high values close to β_{max} as is the case for SF_6^- formation with increasing $\dot{E}$ [9] and for $C_6F_6^-$ formation with increasing T [13].

ACKNOWLEDGEMENT

We would like to thank the United States Air Force for financial support of this work.

REFERENCES

1. P.W. Atkins, Physical Chemistry, Third Edition, W.H. Freeman and Company, New York, 1986, p.8.

2. D. Smith, N.G. Adams and E. Alge, *J. Phys. B: At. Mol. Phys.*, 17 (1984) 461-472.

3. E. Alge, N.G. Adams and D. Smith, *J. Phys. B: At. Mol. Phys.*, 17 (1984) 3827-3833.

4. C.E. Klots, *Chem. Phys. Lett.*, 38 (1976) 61.

5. J.M. Warman and M.C. Sauer Jr., *Intern. J. Radiat. Phys. Chem.*, 3 (1971) 273.

6. A.A. Christodoulides, L.G. Christophorou, R.Y. Pai and C.M. Tung, *J. Chem. Phys.*, 70 (1979) 1156.

7. D.M. McCorkle, I. Szamrej, and L.G. Christophorou, *J. Chem. Phys.*, 77 (1982) 5542.

8. S.H. Alajajian and A. Chutjian, *J. Phys. B: At. Mol. Phys.*, 20, (1987) 5567.

9. L.G. Christoporou, D.L. McCorkle and A.A. Christodoulides in Electron-Molecule Interactions and their Applications. Vol.1., Academic Press, 1984, Chapter 6, pp. 556-557.

10. S.H. Alajajian and A. Chutjian, *J. Phys. B: At. Mol. Phys.*, 20 (1987) 5567.

11. W.E Wentworth, R. George and H.Keith, *J. Chem. Phys.*, 51 (1969) 1791.

12. H.S.W. Massey, Negative Ions, Third Edition, Cambridge University Press, London, 1976, p. 169.

13. D. Smith, N.G. Adams, E. Alge and J. Burdon, *Chem. Phys. Lett.*, 116 (1985) 460.

14. H. Shimamori and Y. Nakatani, *Chem. Phys. Lett.*, 150 (1988) 109.

TABLE 1. Rate coefficients, β, determined on the FALP apparatus for electron attachment to CH_3CCl_3, $CH_2ClCHCl_2$, CF_3CCl_3 and $CF_2ClCFCl_2$ at the temperature indicated. The product ion in all cases was Cl^-. Also given are the data obtained in a swarm experiment [7] at a gas temperature of ~298K and a mean electron energy of 39meV.

	FALP β, cm^3s^{-1}			SWARM β, cm^3s^{-1}
	298K	385K	470K	
Reaction	(39meV)	(50meV)	(63meV)	39meV
CH_3CCl_3 + e	1.5×10^{-8}	3.9×10^{-8}	9.3×10^{-8}	1.5×10^{-8}
$CH_2ClCHCl_2$ + e	3.1×10^{-10}	9.5×10^{-10}	5.0×10^{-9}	1.8×10^{-10}
CF_3CCl_3 + e	2.4×10^{-7}	2.4×10^{-7}	---	2.8×10^{-7}
$CF_2ClCFCl_2$ + e	1.1×10^{-8}	2.0×10^{-8}	5.5×10^{-8}	1.1×10^{-8}

Figure 1

The rate coefficients, β, as a function of $\dot{E}$ obtained from the present FALP studies (filled symbols) and from previous swarm studies [7] (open symbols) for the dissociative attachment reactions of electrons with CH_3CCl_3(●,o), $CH_2ClCHCl_2$(▲, Δ), CF_3CCl_3(■,□) and $CF_2ClCFCl_2$ (◆,◇). FALP data were obtained under truly thermal equilibrium conditions at three temperatures (298, 385, and 470K). The swarm data were obtained at a fixed temperature of the attaching gas molecules of ~298K and at elevated mean electron energies, $\dot{E}$ as plotted. To facilitate comparison of the FALP and the swarm data, the temperatures of the FALP measurements are converted to mean energies according to $\dot{E} = (3/2)\ kT$. The upper solid line is the theoretical maximum value of β, i.e. β_{max} as a function of $\dot{E}$ obtained from s-wave capture theory [14].

Figure 2

The rate coefficients, β, as a function of $\dot{E}$ obtained from FALP studies (filled symbols) and those obtained using the krypton photoionization technique (open symbols) for the dissociation attachment reactions of CH_3CCl_3 (●, o) and CH_2Br_2 (★,☆) with electrons. The CH_2Br_2 data were obtained from previous studies (FALP, ref [3], Kr photoionization method, ref [10]). The FALP data were obtained under truly thermal equilibrium conditions at three temperatures (298, 385 and 470K). The Kr photoionization data were obtained at a fixed temperature of the attaching gas molecules of ~298K and at elevated mean electron energies, $\dot{E}$ as plotted. To facilitate comparison of the FALP and Kr photoionization data the temperatures of the FALP measurements are converted to mean energies according to $\dot{E} = (3/2)\ kT$. The upper solid line is the theoretical maximum value of β, i.e. β_{max}, as a function of $\dot{E}$ obtained from s-wave capture theory [14].

Fig. 1

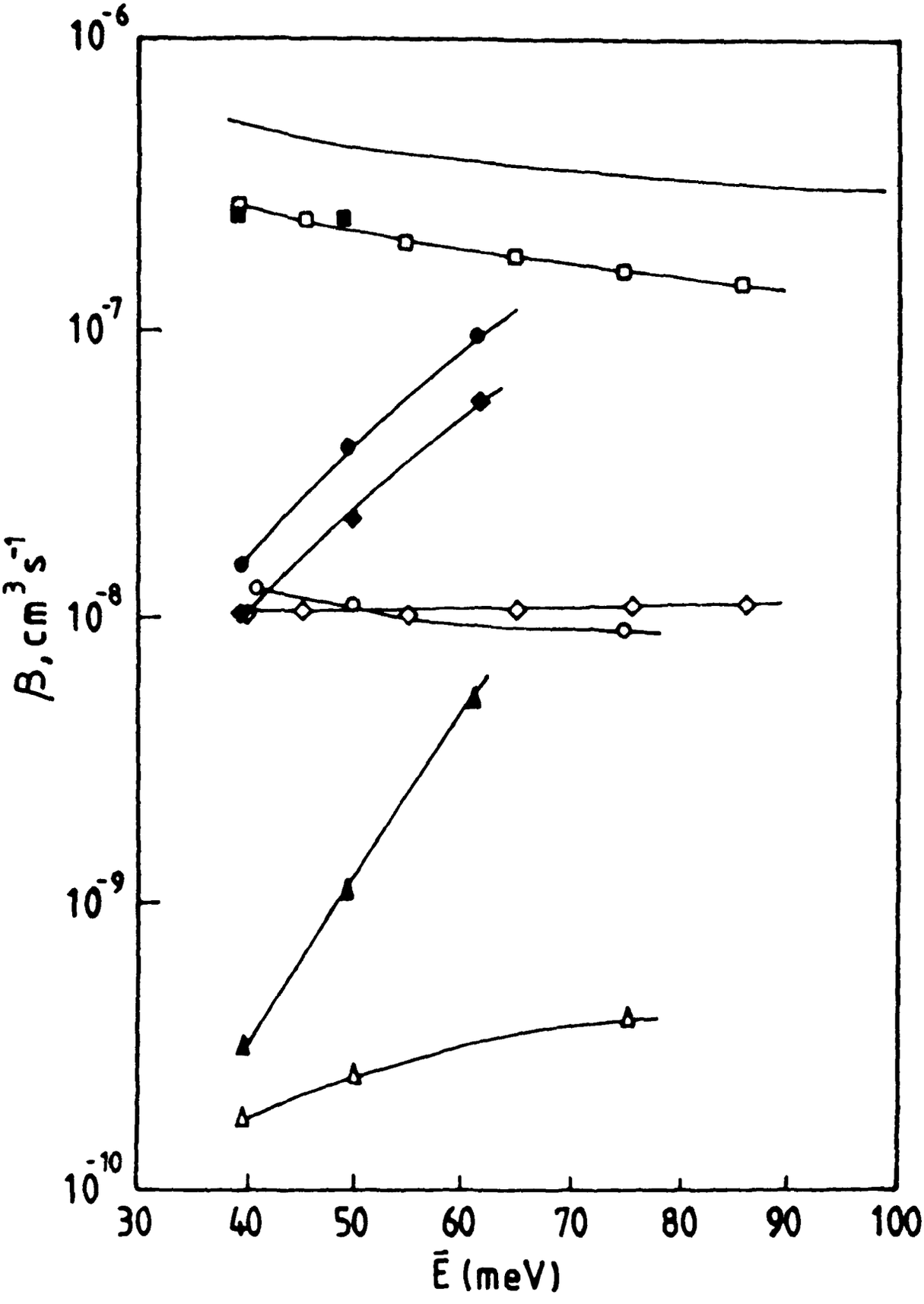

Fig. 2

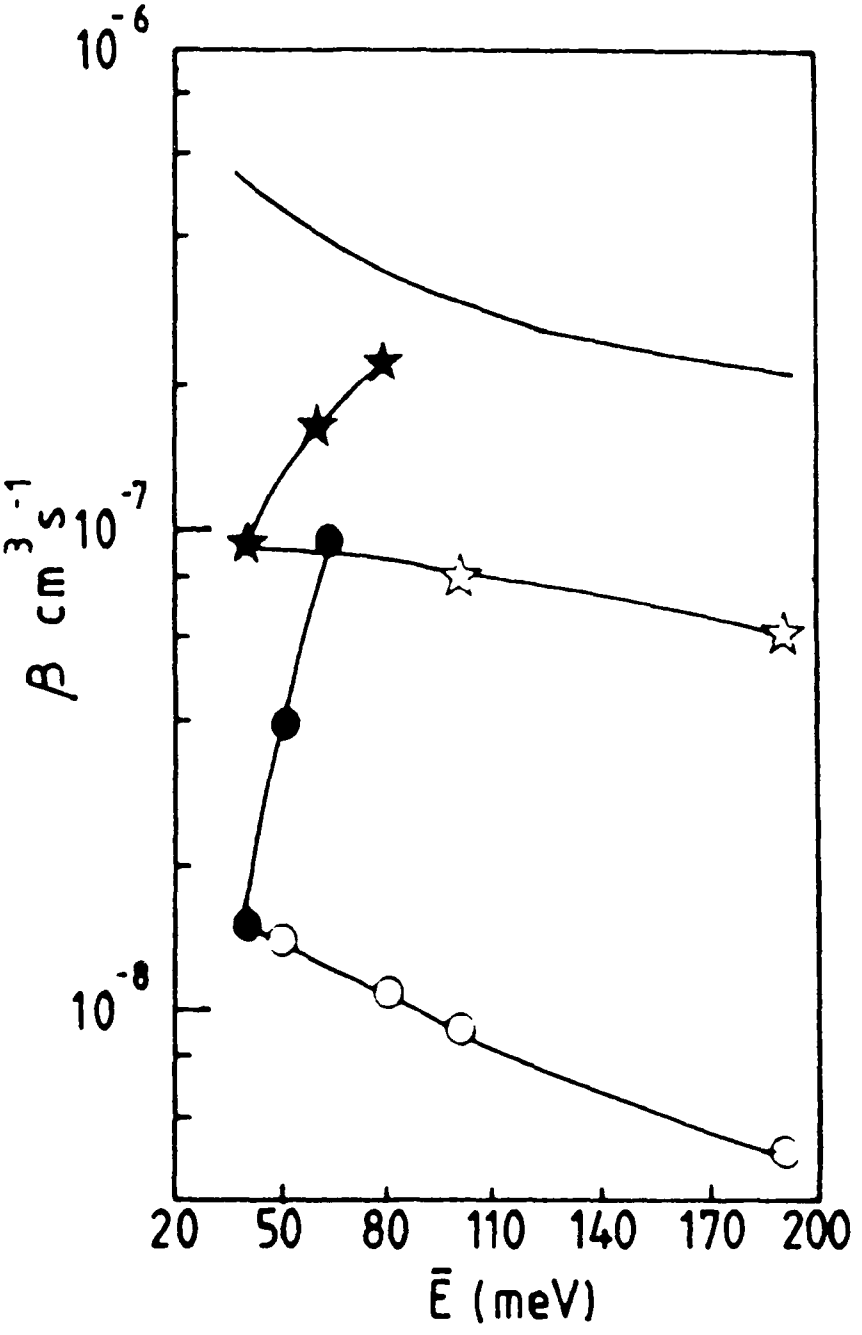

APPENDIX 5

DEVELOPMENT OF THE FLOWING AFTERGLOW/LANGMUIR PROBE TECHNIQUE FOR STUDYING THE NEUTRAL PRODUCTS OF DISSOCIATIVE RECOMBINATION USING SPECTROSCOPIC TECHNIQUES: OH PRODUCTION IN THE HCO_2^+ + e REACTION

N.G. ADAMS, C.R. HERD AND D. SMITH

J.Chem.Phys., 91, 963 (1989)

Development of the flowing afterglow/Langmuir probe technique for studying the neutral products of dissociative recombination using spectroscopic techniques: OH production in the $HCO_2^+ + e$ reaction

Nigel G. Adams, Charles R. Herd, and David Smith
School of Physics and Space Research, University of Birmingham, P. O. Box 363, Birmingham B15 2TT, England

(Received 2 March 1989; accepted 31 March 1989)

The flowing afterglow/Langmuir probe (FALP) technique has been extended to enable the neutral products of electron–ion dissociative recombination in thermalized afterglows to be identified by spectroscopic methods. Absolute number densities of H atoms in the afterglow have been determined using vacuum ultraviolet (VUV) absorption at the L_α wavelength. By exploiting the reaction $H + NO_2 \rightarrow OH + NO$, all of the H atoms can be incorporated into OH molecules and thus observation of the intensity of laser induced fluorescence (LIF) I_f, obtained by exciting the (1,0) band of $OH(A\,^2\Sigma \leftarrow X\,^2\Pi)$, allows a calibration to be obtained of I_f against the known number density of OH $X\,^2\Pi(v'' = 0)$ in the afterglow. Following this procedure, a recombining HCO_2^+/electron afterglow was probed for production of ground state OH $X\,^2\Pi(v'' = 0)$ using LIF and it was established that $OH(v'' = 0)$ resulted from 17% of the recombining ground state HCO_2^+ ions. It was also established that a further 17% of the recombinations resulted in $OH(v'' > 0)$, i.e., that, in total, (34 ± 6)% of the HCO_2^+ ions recombine to produce OH $X\,^2\Pi$ radicals, either directly or via the electronically excited $A\,^2\Sigma$ state. Details of the calibration procedure for H and OH number densities, of the ion chemistry involved in the production of the HCO_2^+ afterglow plasmas and of the checks carried out to establish that the fluorescence observed was from OH produced in the recombination reaction are presented. During these experiments, the rate coefficient at 300 K for the $H + NO_2$ reaction was determined to be 1.3×10^{-10} cm^3 s^{-1} from observations of the H-atom decay as a function of NO_2 number density in the afterglow (in good agreement with previous determinations). Also the rate coefficient for the quenching reaction of $OH(v'' > 0)$ with NO to produce $OH(v'' = 0)$ was determined to be 6×10^{-11}cm^3 s^{-1}.

I. INTRODUCTION

Electron–ion dissociative recombination is an important ionization loss process in natural plasmas such as interstellar gas clouds[1-3] and planetary ionospheres.[4,5] Over the years, the rate coefficients α_e for the dissociative recombination of many molecular ion species have been measured mainly at room temperature using stationary[6] and flowing afterglow[7] techniques and deduced from cross-section measurements made using the merged beam technique.[8] Subsequently several reviews have appeared in the literature which describe the theoretical and experimental aspects of this process and give tables of α_e values.[9-11] However, very little information is available concerning the identity of the neutral products of dissociative recombination reactions and that available relates only to excited ions.[11] Atomic products have been identified for the recombination of O_2^+,[12] NO^+,[13] CO_2^+,[14,15] and H_2O^+,[16] but the ions were internally excited to unknown degrees; only in the case of N_2^+ $(v = 1)$ was the state of excitation known.[17]

Some theoretical effort also has been directed to predicting the products of dissociative recombination reactions. Detailed calculations have been made of the ion and neutral potential energy curves implicated in the dissociative recombination of O_2^+,[18] H_3^+,[19] and HCO^+,[20] while Herbst[21] and Green and Herbst[22] have used a statistical phase space model to predict the products of the dissociative recombination of H_2CN^+, H_3O^+, CH_3^+ and NH_4^+ with electrons. Bates[23-25] has used a more intuitive approach to predict the recombination products of many ions; he argues that the neutral products which involve the least rearrangement will be favored. The approach of Bates has recently been extended by including quantum chemical calculations of the electron density distributions[3] and by considering the likelihood of favorable curve crossings of the bound ionic potential curve with repulsive curves to products.[26]

However, for specific recombination reactions these theoretical approaches predict very different products for the same reaction.[3,21,24,25] Some of these theoretical findings have been discussed in a recent review.[27] Because of the paucity and uncertainty of the available information on the products of dissociative recombination and because of the desperate need for such data to include in models of molecular synthesis in interstellar clouds,[25] we have extended the flowing afterglow/Langmuir probe (FALP) technique[7] (which we have previously used to determine dissociative recombination coefficients[7,11]) to permit the quantitative determination of the neutral products of the dissociative recombination of some ground state ions. To this end, laser

induced fluorescence (LIF) and vacuum ultraviolet (VUV) spectroscopic diagnostic techniques have been applied to recombining plasmas created in the FALP apparatus. This is the first study in which the molecular products of dissociative recombination have been identified and it is the extension of the FALP technique and its application to the study of the recombination of HCO_2^+ ions with electrons that are the subject of this paper.

Only three product channels are energetically possible in the HCO_2^+ recombination reaction viz.

$$HCO_2^+ + e \rightarrow H + CO_2, \quad \Delta H = -185 \text{ kcal mol}^{-1}, \quad (1a)$$

$$\rightarrow OH + CO, \quad \Delta H = -160 \text{ kcal mol}^{-1}, \quad (1b)$$

$$\rightarrow O + H + CO, \quad \Delta H = -58 \text{ kcal mol}^{-1}. \quad (1c)$$

The recombination coefficient α_e for the overall process has recently been measured to be 3.4×10^{-7} cm^3 s^{-1} at 300 K.[28] In the present study, the fractions of the reactions leading to OH in both the ground and excited vibrational states of the electronic ground state have been determined from absolute intensity measurements using LIF. The fluorescence intensity from laser excitation of rovibronic transitions in $OH[A\,^2\Sigma(v'=1) \leftarrow X\,^2\Pi(v''=0)]$ was related to the absolute OH $X\,^2\Pi(v''=0)$ number density using the calibration reaction

$$H + NO_2 \rightarrow OH + NO, \quad \Delta H = -29.5 \text{ kcal mol}^{-1}. \quad (2)$$

This reaction has been has been widely studied [the rate coefficient at 300 K, $k(300) = 1.3 \times 10^{-10}$ cm^3 s^{-1}][29] and is known to produce OH in a variety of vibrational states.[30] However, $OH(v'' > 0)$ is expected to be rapidly quenched to the $v'' = 0$ vibrational level by further reaction with NO_2 since this is facilitated by the deep potential well in the $(HNO_3)^*$ intermediate complex.[31] The rate coefficient k for quenching of $OH(v''=1)$ by NO_2 at 298 K is large $[k(298) = 4.8 \times 10^{-11}$ cm^3 s$^{-1}]$.[32]

II. EXPERIMENTAL

The FALP technique, without spectroscopic diagnostics, has been described previously in some detail in the literature.[7,33] Therefore we discuss the basic FALP apparatus only briefly and concentrate more fully on the spectroscopic aspects of the present experiments. A diagram of the apparatus is given in Fig. 1. Ionization is created in a microwave discharge through flowing He carrier gas which convects the ion/electron plasma along a stainless steel flow tube (8 cm diameter; 1 m length). The ion types in the thermalized afterglow plasma so formed are identified in the downstream region by a mass spectrometer/channeltron detection system. At a He pressure of 1.6 Torr (typical of the pressures used in these studies), the He^+ ions formed in the discharge are rapidly converted to He_2^+ viz.

$$He^+ + He + He \rightarrow He_2^+ + He \quad (3)$$

(note that He_2^+ can also be produced in the discharge by the Hornbeck-Molnar process which involves collisions between highly excited He^* atoms and He, i.e., $He^* + He \rightarrow He_2^+ + e$). Helium metastable atoms, which

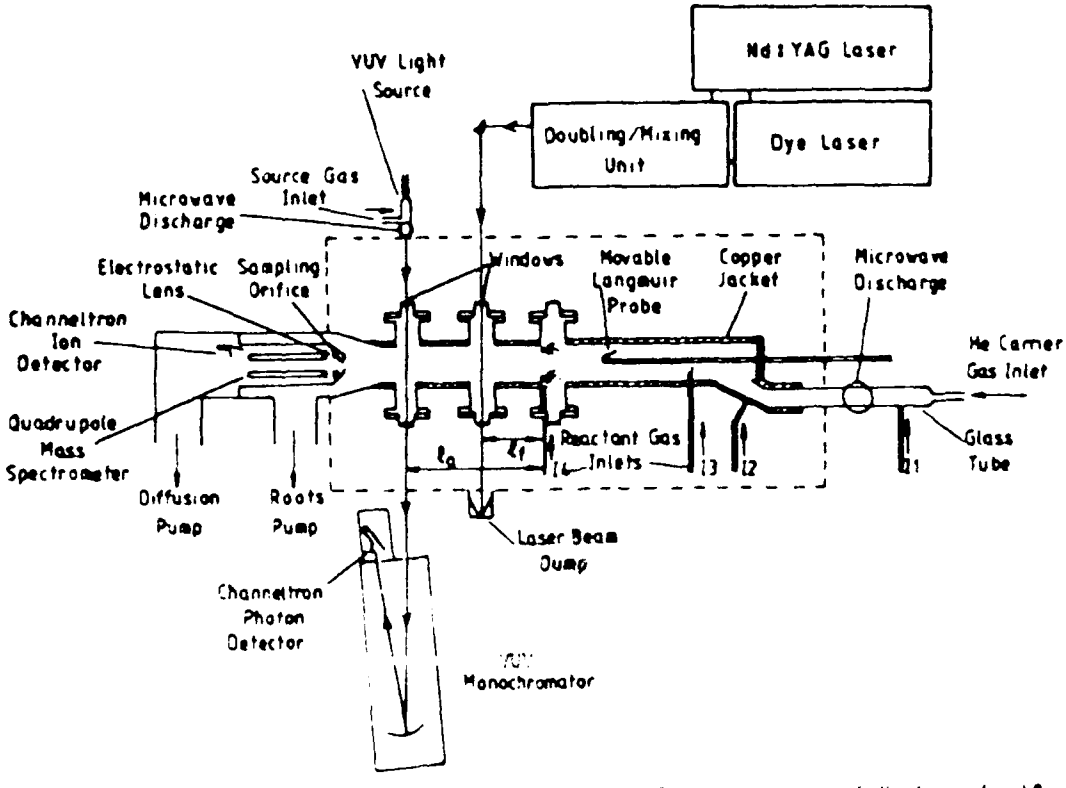

FIG. 1. A schematic diagram of the flowing afterglow/Langmuir probe (FALP) apparatus, now including laser induced fluorescence (LIF) spectroscopy (for the detection of molecular radicals, e.g., OH and CN) and vacuum-ultraviolet (VUV) absorption spectroscopy (for the detection of atoms, e.g., H, N, and O). All of the optical components in the LIF section are UV-grade fused quartz or sapphire, and the windows in the VUV section are nonfluorescent magnesium fluoride. Also shown is the movable Langmuir probe and the downstream mass spectrometer/detection system. The various gases are added to the afterglow through reactant gas inlet ports 11 to 14. The distances l_f and l_a are those between inlet port 14 and the respective axial positions at which LIF and VUV absorption spectroscopy were carried out. The dashed line represents the outline of the vacuum jacket which surrounds the flow tube and which facilitates operation at temperatures other than room temperature.

are also produced in the discharge and which, if allowed to, would result in a distributed source of ionization in the afterglow due to Penning reactions, are completely removed from the afterglow by adding Ar (at a partial pressure of ~3 mTorr) just downstream of the discharge (at inlet port I2; see Fig. 1) viz.;

$$He^m(2\,^1S, 2\,^3S) + Ar \rightarrow Ar^+ + He + e. \quad (4)$$

Ar also reacts with He_2^+ [$k(200) = 2.0\times10^{-10}$ cm^3 s^{-1}][34] viz.

$$He_2^+ + Ar \rightarrow Ar^+ + 2He. \quad (5)$$

Thus an Ar^+/e afterglow plasma is created. The presence of Ar in the flow tube was also observed to reduce the amount of short wavelength radiation which was transmitted from the microwave discharge to the downstream spectroscopic diagnostics (this is especially important for the absorption measurements at the hydrogen L_α wavelength, see Sec. III A). The addition of H_2 (at inlet port I3) to the Ar^+/e plasma then rapidly converts it to an H_3^+/e plasma via the reactions

$$Ar^+ + H_2 \rightarrow ArH^+ + H$$
$$\rightarrow H_2^+ + Ar, \quad (6)$$
$$ArH^+(H_2^+) + H_2 \rightarrow H_3^+ + Ar(H). \quad (7)$$

This afterglow plasma is a *unique* polyatomic molecular ion/electron plasma because H_3^+ ions in their ground vibrational state ($v = 0$) do not dissociatively recombine with electrons at a significant rate.[11,35] $H_3^+(v)$ can dissociatively recombine[35] but, in the presence of sufficient H_2 it is rapidly quenched via the reaction[36]

$$H_3^+(v) + H_2 \rightarrow H_3^+ + H_2^*. \quad (8)$$

Thus the ionization density in the H_3^+/e (and Ar^+/e) plasma decays only by the process of ambipolar diffusion which is quite slow at the pressures used in these experiments.

Since H_3^+ has a small proton affinity [PA(H_2) = 101.3 kcal mol^{-1}] it can transfer a proton to many other species which can be added to the flow tube (at inlet port I4) thus creating a plasma, which can recombine,[28] e.g.,

$$H_3^+ + CO_2 \rightarrow HCO_2^+ + H_2, \quad \Delta H = -27.7 \text{ kcal mol}^{-1}. \quad (9)$$

This approach to the production of plasmas consisting of particular protonated species has been used previously in the determination of the recombination coefficients for many protonated species.[28] The exothermicity of reaction (9) is such that the product HCO_2^+ can be produced in vibrationally (and perhaps electronically) excited states, however any excitation of this ion will be rapidly quenched by the proton transfer reaction:

$$(HCO_2^+)^* + CO_2 \rightarrow HCO_2^+ + (CO_2)^*. \quad (10)$$

The electron (and thus the ion) densities on the axis of the afterglow plasma can be measured readily using a Langmuir probe which can be moved along the whole length of the flow tube.[7,37] Also, by adjusting the position of the microwave discharge on the glass tube (see Fig. 1) to change the diffusive loss of ionization along that tube, the ionization density can be varied at the upstream end of the recombination region (i.e., port I4) from a maximum of $\sim 1\times10^{10}$ cm^{-3} at which recombination is the dominant ionization loss process, down to densities for which recombination loss is insignificant, so that the plasma ion composition and the ion–molecule chemistry can be determined using the downstream mass spectrometer.

As previously mentioned, in these studies of the neutral products of dissociative recombination, the OH product of the recombination of HCO_2^+ [reaction (1)] has been monitored using LIF. The LIF technique has been widely used to monitor radical species and in particular the OH radical has been thoroughly studied.[38–41] However, to our knowledge, the LIF technique has not been used previously to determine *absolute* densities of OH radicals produced in ionic reactions and therefore this requires some discussion. The experimental arrangement is shown in Fig. 2. A laser beam at a wavelength of ~281 nm is produced by frequency doubling the output of a pulsed dye laser (Spectron SL400B operating with a Rhodamine 6G dye) which is pumped by the doubled output of a Nd:YAG laser (Spectron SL803). This laser beam is passed across the diameter of the flow tube 17.5 cm downstream of the CO_2 addition point (see Fig. 1), and when spacially filtered provides an energy of typically 1 mJ in a 4 mm diameter laser beam of 10 ns pulse duration. The fluorescence from the OH in the plasma is detected at right angles to the laser beam (see Fig. 2). Collection of the fluorescence is via a quartz lens (focal length 3.8 cm) situated in a side arm of the flow tube which images the fluorescence production region (i.e., part of the volume occupied by the laser beam) onto a slit and thence through an interference filter to a photomultiplier (EMI 9813QB) which is cooled to about −30 °C to minimise noise counts. After amplification, the output pulses are accumulated by a gated photon counter (Stanford Research Systems, model 400) and then transferred via an IEEE interface to a microcomputer which is used for data analysis.

Throughout these studies, the laser was used to excite the $A\,^2\Sigma(v' = 1)$ to $X\,^2\Pi(v'' = 0)$ transition of OH (at

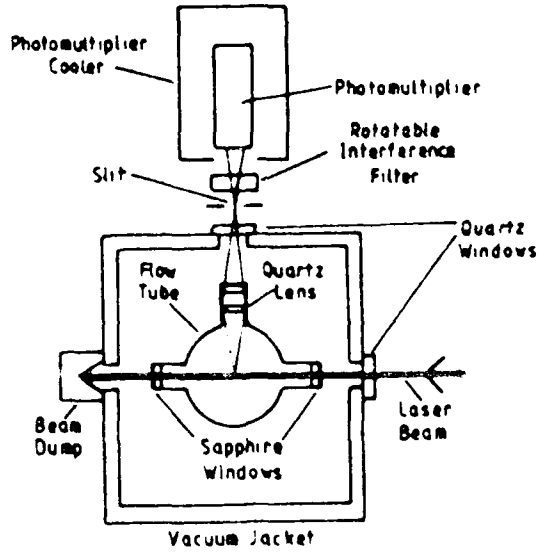

FIG. 2. A schematic diagram of the LIF fluorescence detection system viewed at right angles to the axis of the flow tube.

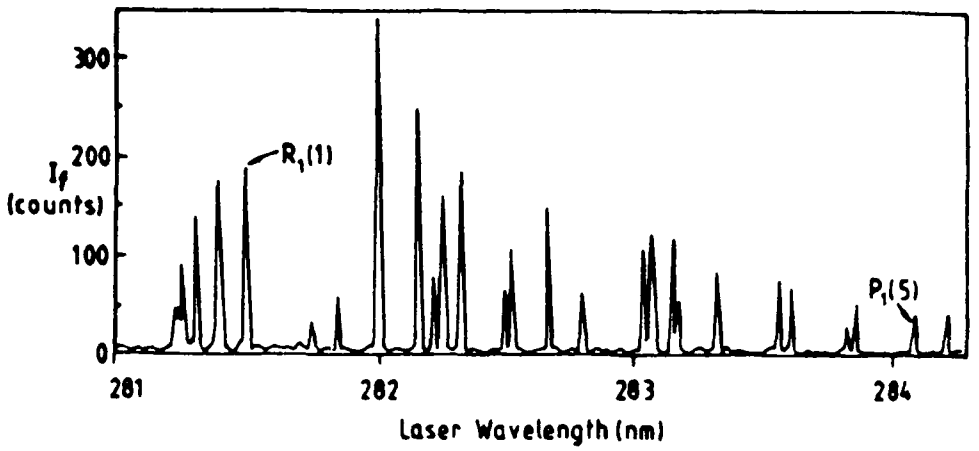

FIG. 3. A laser excitation spectrum of OH $X\,^2\Pi(v'' = 0)$ radicals produced in the dissociative recombination of HCO_2^+ with electrons. This spectrum was obtained by scanning the *laser* wavelength through the rotational structure of the vibronic transition $A\,^2\Sigma(v' = 1) - X\,^2\Pi(v'' = 0)$ (~281–284nm) and detecting the fluorescence intensity I_f (counts per 50 laser shots) in the $A\,^2\Sigma(v' = 1) - X\,^2\Pi(v'' = 1)$ band (~312 nm). Note the small background count level and the correspondingly large signal-to-noise levels on the most intense lines. The two identified rovibronic lines, $R_1(1)$ and $P_1(5)$, are those which were used in the present studies (see the text).

~281 nm) and the nonresonance fluorescence was observed in the $A\,^2\Sigma(v' = 1) \rightarrow X\,^2\Pi(v'' = 1)$ transition using a 10 nm bandpass interference filter with a central wavelength of 312 nm. This filter prevents scattered laser light from reaching the photomultiplier and results in practically zero background noise counts. Contributions to the signal from background sources were further minimized by gating the photon counter to count only for a period of 3 μs following a delay of ~50 ns from each laser pulse (the trigger pulse for the photon counter was provided by a photodiode on to which a small fraction of the laser beam was deflected) thus allowing photon counting only during the time period in which the majority of the OH $A\,^2\Sigma$ states spontaneously radiatively decay.[42,43] To enable the photon counter to count rapidly during the gated period without significant pulse pile-up, a fast photomultiplier (3 ns FWHM) and electronics with > 100 MHz bandwidth were used.

An example of part of the excitation spectrum of OH $X\,^2\Pi(v'' = 0)$ [which was produced in the $HCO_2^+ + e$ recombination, reaction (1b)] obtained by scanning the laser over the wavelength range from ~281 to ~284 nm is shown in Fig. 3. All of the rotational lines are identified as originating from the OH(A–X) transition[44] and the signal to noise is seen to be excellent (~100:1 on the most intense line). Following Guyer *et al.*,[45] and assuming that the laser transition is saturated (as is expected for the laser beam intensity employed in this study), then the relative intensities of the lines can be shown to be consistent with a rotational level population distribution of OH $X\,^2\Pi(v'' = 0)$ which is Boltzmann at a temperature of 310 K i.e., essentially at the temperature of the experiment (~300 K). Thus the OH rotational modes, as expected,[40] are thermalized in multiple collisions with the He carrier gas atoms prior to laser excitation. This is not the case for the vibrational modes and so detailed information is potentially available concerning the OH product vibrational distribution.

III. CALIBRATION PROCEDURE: LIF INTENSITY VS OH NUMBER DENSITY

In order to determine the fraction of the HCO_2^+ ions that recombine to produce OH $X\,^2\Pi(v'' = 0)$ it is necessary to relate the fluorescence intensity in a given rovibronic line to the OH number density in the flow tube. To attempt to obtain this relationship by calculation is fraught with difficulty since, in addition to having to depend on Einstein coefficients, Franck–Condon factors and Höln–London factors, it also depends on various inaccurately known instrumental factors. Thus, it is more accurate to calibrate by using a reaction such as reaction (2), $H + NO_2 \rightarrow OH + NO$, to relate observed OH fluorescence intensity to a known OH number density which can be obtained by first determining the H-atom number density.

A. Determination of the H-atom number density

It is straightforward to obtain the H-atom column density across the flow tube using VUV absorption spectroscopy at the H-atom resonance line (L_α at 121.57 nm).[46,47] Thus, knowing the radial profile of H atoms (see Sec. IV C) then the H-atom number density can be determined. The technique used, as illustrated in Fig. 1, is fairly standard[46] and is as follows. L_α radiation is produced in a microwave discharge source (with a 50 W power dissipation in these experiments) through nominally pure He at a pressure of ~0.05 Torr in a 1 cm diameter Pyrex tube terminated with a MgF_2 window. Since the oscillator strength of the transition f is so large, such lines are often self-reversed. However, detailed experimental studies[48] of the profiles of L_α lines from discharges similar to that used in the present work have shown that significant self-reversal only occurs with > 0.01% H_2 mixed with He at a pressure of ~2 Torr. This is a much greater H_2 partial pressure than that in the present source (which is $< 10^{-6}$ Torr) when "pure helium" is used.

In addition, the present source is thoroughly degassed by heating under vacuum and with a continuous flow of helium passing through it to remove water and any volatile hydrocarbons from which H atoms can be generated. Also the microwave discharge is operated as close as possible to the MgF_2 window to minimise the column density of H atoms that the L_α radiation must pass through, thus minimizing any self-reversal. Note that it was not possible to check directly for self-reversal in the L_α line from the source because of the limited dispersion of the VUV monochromator used in these experiments (see below). However, for the O-atom resonance line triplet, which was also emitted by the source, the individual components could be resolved and their intensities were in the ratios $^3P_2$: $^3P_1$: $^3P_0$ = 5:3:1 which are the ratios of the statistical weights thus showing that no self-reversal occurred for this line. We are therefore confident that there is no significant self-reversal for the L_α line.

The L_α radiation is directed across the diameter of the flow tube at a distance 35.5 cm downstream of port I4 (see Fig. 1) and onto the entrance slit of a 1 m vacuum monochromator equipped with a 1200 lines mm^{-1} grating to disperse other interfering radiations originating in the L_α source and in the discharge which produces the flowing afterglow plasma. It is then detected at the exit slit of the monochromator by a channeltron multiplier which, because of its large work function, is only sensitive to VUV radiation (wavelength < 150 nm) and thus has a low background count rate. The He II line at 121.52 nm, which is close in wavelength to L_α is a possible source of interference in these studies. Fortunately, however, spectral scans at maximum resolution over the L_α region showed that there was no significant contribution due to this line from the L_α source.

The fractional absorption A of the L_α radiation which occurs in its passage through the flow tube is related to the H-atom column density by the expression (see, for example, Mitchell and Zemansky[46])

$$A = \frac{I_t - I_t}{I_t} = \frac{\int_0^\infty I_\nu \exp(-k_\nu L)d\nu}{\int_0^\infty I_\nu\, d\nu} \tag{11}$$

$$= \sum_{p=1}^{\infty} (-1)^{p+1} \frac{(k_0 L)^p}{p!(1+\alpha^2 p)^{1/2}}, \tag{12}$$

where the frequency dependent absorption coefficient k_ν in the case of Doppler broadening (see below) is given by

$$k_\nu = k_0 \exp\left[-\frac{2(\nu - \nu_0)(\ln 2)^{1/2}}{\Delta\nu_a} \right]^2, \tag{13}$$

where

$$k_0 = \frac{1}{\Delta\nu_a}\left(\frac{\ln 2}{\pi}\right)^{1/2} \frac{e^2 Nf}{2mc\epsilon_0 c}. \tag{14}$$

I_t and I_t are the incident and transmitted intensities, I_ν is the frequency dependent emission line profile, p is an integer, ν_0 is the frequency at the line centre, α is the ratio $(\Delta\nu_e/\Delta\nu_a)$ where $\Delta\nu_e$ is the full width at half-maximum (FWHM) of the L_α line emitted by the source, and $\Delta\nu_a$ is the FWHM of the absorption line, L is path length through the absorbing medium, N is number density of H atoms, f is the oscillator strength for the transition and m is the electron mass. If both the emission and absorption line profiles are determined by thermal Doppler broadening (as has been shown to be the case for microwave discharge sources of the type used in this work[46]) then $\alpha = (T_t/T_a)^{1/2}$ where T_t and T_a are the source and afterglow temperatures, respectively. Thus the deduced column density is not a sensitive function of the source temperature. For this type of source T_t has been previously measured to range from 305 to 900 K depending on the microwave power level.[46] These data suggest a T_t of 650 K for the power level of 50 W used in the present experiment. That this T_t was an appropriate value was confirmed by adding a trace of N_2 to the lamp and observing the rotationally resolved emission from the $B\,^2\Sigma_u^+$ $(v' = 0) \rightarrow X\,^1\Sigma_g^+$ $(v'' = 1)$ transition in N_2^+. Analysis of the relative intensities of the rotational lines[49] gives a value for the temperature of 650 K. It is known that the $B\,^2\Sigma_u^+$ state of N_2^+ is populated by Penning reactions with He metastable atoms[50] (reaction with He^+ produces N_2^+ in the $C\,^2\Sigma_u^+$ state) and that the N_2^+ rotational populations reflect those of the N_2 precursor. Thus since the rotational population of the N_2 will be equilibrated by collisions at the kinetic temperature of the He and H atoms, then the kinetic temperature of the H atoms is expected to be ~ 650 K. Note that any error in this temperature will contribute to some degree to the error in the H-atom density determination (typically, an error in T_t of 100 K results in an error in N of $\sim 6\%$). Taking all known sources of error into account, we estimate that the deduced H-atom densities are accurate to within $\pm 15\%$.

B. The calibration reaction: $H + NO_2 \rightarrow OH + NO$

For this calibration, the H-atom density in the flow tube was maximised by passing H_2 through the microwave discharge and by adding N_2 at inlet port I2 (see Fig. 1). By passing H_2 through the discharge the H_2 was partially dissociated to produce H atoms with the accompanying production of an H_3^+/e plasma. The introduction of N_2 to this plasma resulted in a rapid loss of H_3^+ and the conversion to an N_2H^+/e plasma (following proton transfer from H_3^+ to N_2) which at high electron densities produces additional H atoms via the recombination reaction

$$N_2H^+ + e \rightarrow N_2 + H. \tag{15}$$

This reaction also resulted in a large reduction in the electron density in the region of the afterglow just upstream of inlet port I4 from 1×10^{10} to 5×10^8 cm^{-3}. NO_2 was then added at inlet port I4 and the OH LIF fluorescence and H-atom absorption were monitored further downstream at distances l_f of 17.5 cm and l_a of 35.5 cm, respectively (see Fig. 1). Since the electron density and the H_3^+ density were so small, the calibration via reaction (2) was not significantly influenced ($\sim 0.5\%$) by production of OH in the reaction

$$\begin{aligned} H_3^+ + NO_2 &\rightarrow HNO_2^{+\,*} + H_2 \\ &\quad\hookrightarrow NO^+ + OH \\ &\rightarrow HNO^+ + H_2O \end{aligned} \tag{16}$$

even though the rate coefficient for this reaction is large.[51]

Figure 4 shows semilogarithmic plots of the H-atom absorption, $I_t - I_t$, [see Eq. (11)] and the OH LIF intensity

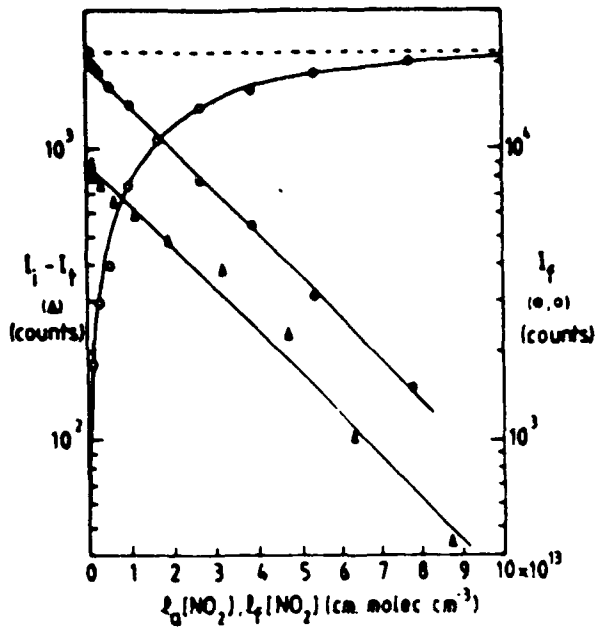

FIG. 4. Decrease in the absorption $I_i - I_f$ (counts per 50 s) of L_α radiation by H atoms (triangles) as a function of the product $l_a[NO_2]$ due to the calibration reaction $H + NO_2 \rightarrow OH + NO$ [reaction (2)]. $[NO_2]$ is the number density of NO_2 molecules introduced into the afterglow at port I4 and l_a is the reaction length between this port and the position at which the H atoms are monitored (see Fig. 1). Also given is the related increase in the LIF intensity of OH I_f (open circles) (fluorescence photon counts per 500 laser shots) for the $P_1(5)$ line in the $A\,^2\Sigma(v' = 1) - X\,^2\Pi(v'' = 0)$ excitation spectrum (see Fig. 3) with increasing $l_f[NO_2]$ where l_f is the reaction length between port I4 and the laser beam. Both l_a and l_f are included since these reaction lengths for H atom and OH radical detection are different (35.5 and 17.5 cm, respectively). The filled circles were obtained by subtracting the OH fluorescence intensities from the asymptotic value at large $l_f[NO_2]$ (as given by the dashed line). This line and that for the L_α absorption give values of the rate coefficient for the $H + NO_2$ reaction which are in good agreement with the literature value (see the text).

for the $P_1(5)$ line against $l_a[NO_2]$ and $l_f[NO_2]$, respectively, where $[NO_2]$ is the NO_2 number density in the flow tube (determined from the NO_2 flow rate which was measured in the conventional manner for flow tube experiments) and l_a and l_f are the appropriate reaction lengths. The linear decrease in the H-atom absorption with $[NO_2]$ gives a rate coefficient for reaction (2) of $(1.3 \pm 0.3) \times 10^{-10}$ cm^3 s^{-1}, in excellent agreement with the literature value at 300 K of 1.3×10^{-10} cm^3 s^{-1} as obtained from several studies.[10] The rate coefficient for this reaction can also be deduced from the increase in the OH LIF intensity by subtracting the measured intensities at various $[NO_2]$ from the constant value at large $[NO_2]$ (the dashed line in Fig. 4). This again provides a linear decrease from which the same rate coefficient is again obtained. Thus the H-atom column density and the OH LIF intensity for the $P_1(5)$ line are related via reaction (2) and a calibration can be obtained for [OH] using [H] deduced from L_α absorption measurements. In addition, the relative intensities of the $P_1(5)$ line and the more intense $R_1(1)$ line were measured at a lower [OH] in order to obtain a calibration of the OH LIF intensity for the $R_1(1)$ line which was unaffected by pulse pile-up in the detection system (see Sec. II). This extends to lower values the range of [OH] which can be measured and is useful since the [OH] produced in the HCO_2^+ recombination reaction was smaller than for the $H + NO_2$ reaction.

IV. RESULTS: OH FROM THE $HCO_2^+ + e$ RECOMBINATION

A. OH($v'' \simeq 0$) production

In order to ensure that the observed LIF fluorescence intensity I_f, following laser excitation of the $A\,^2\Sigma(v' = 1) - X\,^2\Pi(v'' = 0)$ transition in OH, was originating from OH produced in the dissociative recombination of HCO_2^+ with electrons [reaction (1)], two experimental checks were made. These checks proved conclusively that the observed fluorescence originated from the HCO_2^+ recombination. First, the fluorescence was monitored as a function of the flow of CO_2 introduced at inlet port I4 and thus as a function of the CO_2 number density in the flow tube, $[CO_2]$. This varies the amount of HCO_2^+ produced by proton transfer from H_3^+ [reaction (9)] and consequently the amount of OH($v'' = 0$) which can be produced in the recombination reaction (1). A sample of the data obtained is given in Fig. 5 where it can be seen that I_f increases smoothly with $[CO_2]$, reaching a maximum at large $[CO_2]$, in the manner expected for production via reaction (9) followed by reaction (1). The form of this increase is not simply related only to $[CO_2]$ since the HCO_2^+ and electron densities are also involved in the reaction sequence. The form of this curve has been modeled taking into account the production of HCO_2^+ in reaction (9) and its loss by recombination to produce OH [reaction (1)] and is consistent with the known rate coefficients for these reactions.[2a,5,2]

The second experimental check was to monitor I_f as a function of the initial HCO_2^+ density (i.e., before recombination had occurred). For these measurements, a $[CO_2]$ was established in the flow tube which was sufficient to produce the maximum I_f (see Fig. 5). For this situation,

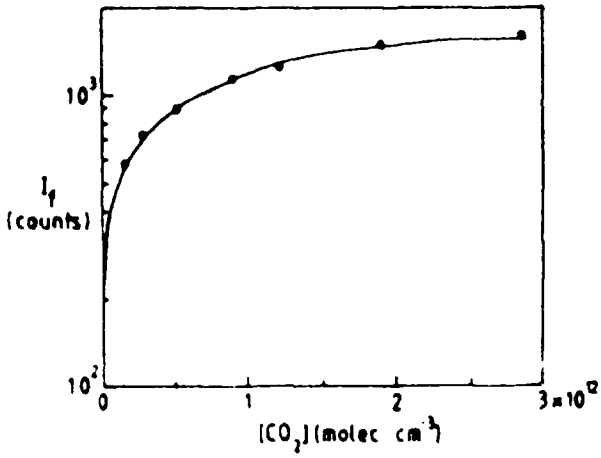

FIG. 5. Increase in the LIF intensity from OH I_f (photon counts per 250 laser shots) with increasing CO_2 number density $[CO_2]$ in the afterglow for the $R_1(1)$ line in the $A\,^2\Sigma(v' = 1) - X\,^2\Pi(v'' = 0)$ excitation spectrum (see Fig. 3). The increase results from OH($v'' = 0$) production in the HCO_2^+ dissociative recombination with electrons [reaction (1)], the HCO_2^+ being produced by proton transfer from H_3^+ to CO_2 [reaction (9)]. For further discussion, see the text.

HCO_2^+ is rapidly produced by reaction (9) and any excited HCO_2^+ is rapidly quenched by reaction (10) before recombination can occur. Thus the initial HCO_2^+ density was equal to the H_3^+ density just upstream of the port through which the CO_2 was added and therefore equal to the electron density $n_e(0)$ at that axial position. The electron density can of course be determined very easily using the Langmuir probe. The $n_e(0)$ was then varied as described in Sec. II.

The way in which I_f is expected to vary with n_e (and hence [OH]) requires some discussion. When recombination of HCO_2^+ with electrons is the dominant loss mechanism, the variation of the HCO_2^+ number density $[HCO_2^+]$ with distance z along the flow tube is given by

$$v_p \frac{d[HCO_2^+]}{dz} = -\alpha_e [HCO_2^+]_z n_e(z), \tag{17}$$

where v_p is the plasma flow velocity (this is readily determined, see Ref. 53) and α_e is the ion–electron recombination coefficient. For $[HCO_2^+]_z = n_e(z)$, as in the present situation, this has the solution

$$[HCO_2^+]_z = \left(\frac{\alpha_e z}{v_p} + \frac{1}{[HCO_2^+]_0}\right)^{-1}, \tag{18}$$

where the subscripts 0 and z identify the initial number density and that at position z, respectively. As for Eq. (17), the rate of production of OH can be represented as

$$v_p \frac{d[OH]_z}{dz} = f\alpha_e [HCO_2^+]_z n_e(z), \tag{19}$$

where f is the fraction of the recombinating HCO_2^+ ions that result in the production of OH. Substitution for $[HCO_2^+]_z$ from Eq. (18) and integration yields

$$\frac{[HCO_2^+]_0^2}{[OH]_z} = \frac{[HCO_2^+]_0}{f} + \frac{v_p}{\alpha_e f z}. \tag{20}$$

Thus since $[HCO_2^+]_0 = n_e(0)$ and, $[OH]_z$ is related to I_f, then a plot of $n_e(0)^2/I_f$ vs $n_e(0)$ should be linear. Such a plot is given in Fig. 6. Note that it is linear as predicted and if the relationship between I_f and $[OH]_z$ is known (see Sec. III A), then f and α_e can be determined from the slope and intercept, respectively. Since it is the relationship between I_f and $[OH(v'' = 0)]$ that is actually determined, then f represents the fraction of recombinations that produce $OH(v'' = 0)$. The above experimental checks confirm that the fluorescence I_f and thus the $OH(v'' = 0)$ is originating from the HCO_2^+ recombination.

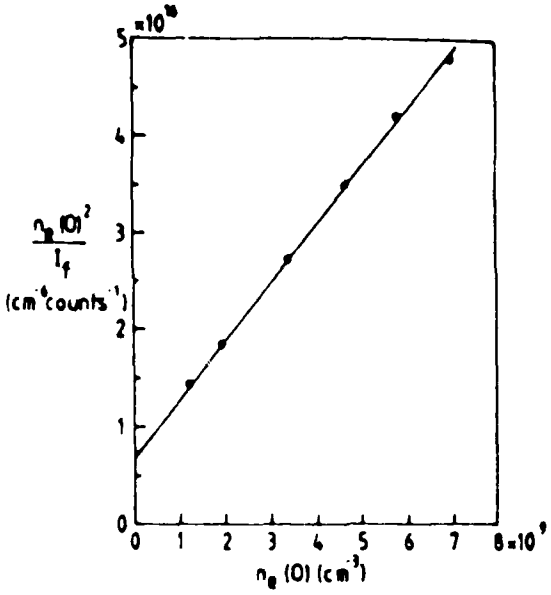

FIG. 6. A sample plot of $n_e(0)^2/I_f$ against $n_e(0)$ for the dissociative recombination of HCO_2^+ with electrons [reaction (1)]. $n_e(0)$ is the electron density just upstream of the point at which CO_2 is added into the H_3^+/e afterglow plasma, and I_f is the LIF intensity from OH (photon counts per 500 laser shots) for the $R_1(1)$ line in the $A\,^2\Sigma(v' = 1) \leftarrow X\,^2\Pi(v'' = 0)$ excitation spectrum (see Fig. 3) at a distance l_f of 17.5 cm downstream from the CO_2 addition point. This plot is linear as expected from Eq. (20). From calibration data, such as given in Fig. 4, I_f can be related to the $OH(v'' = 0)$ number density and then the fraction of the HCO_2^+ ions that recombine to produce $OH(v'' = 0)$ can be obtained from the slope of this linear plot. The overall recombination coefficient can be obtained from the intercept of the line on the ordinate [see the text and Eq. (20)].

B. $OH(v'' > 0)$ production

Examination of the energetics quoted in reaction (1) shows that, in this recombination, it is also possible to produce highly vibrationally excited OH [it is also energetically possible to produce OH in the electronically excited $A\,^2\Sigma$ state, see Eq. (22d), however, this would have rapidly radiatively relaxed to the ground state before the position at which the OH was monitored]. To determine the fraction of OH $(v'' > 0)$ produced in the recombination, NO was added to the flow tube at a position where all of the recombination had occurred but upstream of the point at which I_f was monitored. NO is known to vibrationally quench $OH(v'' > 0)$[31,32] [for $OH(v'' = 1)$ quenching by NO, the rate coefficient at 298 K, i.e., $k(298) = 3.8 \times 10^{-11}$ cm^3 s^{-1} [32]] but unlike NO_2 [reaction (2)], it reacts only very slowly with H-atoms.[29] Thus it is ideal for use in detecting $OH(v'' > 0)$, viz.

$$OH(v'' > 0) + NO \rightarrow OH(v'' = 0) + NO^*. \tag{21}$$

The variation of I_f with [NO] is shown in Fig. 7 for the situation where a large $[CO_2]$ had been added to ensure that an HCO_2^+/e plasma was rapidly produced. It can be seen from the upper curve (filled circles) that as [NO] increases I_f increases showing that additional $OH(v'' = 0)$ is being produced from the quenching of $OH(v'' > 0)$ generated in HCO_2^+ recombination. The increase in $OH(v'' = 0)$ due to the quenching of $OH(v'' > 0)$ can be seen more clearly from the lower curve (open circles) which is obtained by subtracting the constant contribution to I_f due to the $OH(v'' = 0)$ produced directly in the recombination reaction. Comparison of the asymptotic value of I_f from this curve at large [NO] with the value of I_f at zero [NO] gives a ratio of $OH(v'' > 0)$ to $OH(v'' = 0)$ produced in the HCO_2^+ reaction of ~ 1 [this ratio will be unaffected by any nascent rotational excitation in the $OH(v'' = 0)$ product of reaction (20) since this will be rapidly quenched by the He carrier gas]. Note that an overall quenching rate coefficient, i.e., that for reaction (21), can be deduced from the lowest curve (open circles) in Fig. 7. By subtracting the values of I_f on

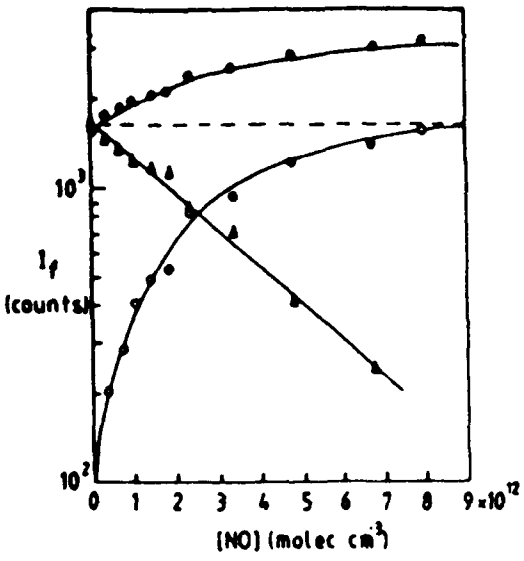

FIG. 7. Variation with NO number density in the afterglow [NO] of the LIF intensity from OH I_f (photon counts per 250 laser shots, filled circles) for the $R_1(1)$ line in the $A^2\Sigma(v'=1)\leftarrow X^2\Pi(v''=0)$ excitation spectrum (see Fig. 3). OH $X^2\Pi(v''>0)$ and $X^2\Pi(v''=0)$ were produced upstream of the NO addition point from the dissociative recombination of HCO_2^+. The increase in I_f with [NO] is due to quenching of $OH(v''>0)$ by NO to produce $OH(v''=0)$ [reaction (21)]. Thus the change in I_f between zero [NO] and the asymptotic value at large [NO], relative to the value of I_f at zero [NO], represents the amount of $OH(v''>0)$ relative to $OH(v''=0)$ which is produced in the HCO_2^+ recombination reaction. The increase in $OH(v''>0)$ can be seen more clearly (open circles) by subtracting the contribution of $OH(v''=0)$ from I_f. The effective rate coefficient for the quenching reaction can be deduced from the slope of the linear plot (triangles) which was obtained by subtracting the values represented by the open circles from the asymptotic value at large [NO], as represented by the dashed line.

this curve from the asymptotic value at large [NO], the decay curve (triangles) can be constructed which provides a rate coefficient of $(6\pm1.5)\times10^{-11}$ cm^3 s^{-1} for the reaction at 300 K. It is interesting to note that this value is similar to the value of $(3.8\pm0.6)\times10^{-11}$ cm^3 s^{-1} recently obtained at 300 K,[32] and within the range of values (1.5×10^{-11} to 7.5×10^{-11} cm^3 s^{-1})[29] previously obtained, for the quenching of $OH(v''=1)$ by NO [a rate coefficient for the quenching of $OH(v''=2)$ by NO of 1.2×10^{-10} cm^3 s^{-1} has also been obtained[29]].

If the ratio $OH(v''>0)/OH(v''=0)$ is to be equated to that resulting from the $HCO_2^+ + e$ recombination reaction, then it is necessary to establish that $OH(v''>0)$ is not significantly radiatively or collisionally quenched in its passage along the flow tube. Radiative lifetimes of $OH(v''>0)$ for $v''=1$ to 15 (for relaxation to all lower v'' levels) have been calculated by Langhoff *et al.*[34] and range from 93 to 8 ms, respectively. Therefore, there is expected to be very little radiative relaxation of $OH(v''>0)$ in the ~4 ms time scale of the present experiments. Also, it is known that collisional quenching of $OH(v''=1)$ by He and Ar is very slow; the rate coefficients for these reactions at 298 K are $\sim5\times10^{-17}$ and $<1\times10^{-15}$ cm^3 s^{-1}, respectively[34] and at the pressures of He and Ar used in the present experiments are equivalent to reaction time constants of 350 ms and 9.4 s, respectively. Thus quenching by He and Ar is insignificant. Experiments were conducted to establish that there were no quenching effects due to the presence of the various other gases in the flow tube. $OH(v''>0)$ was produced via the $HCO_2^+ + e$ recombination in the upstream region of the flow tube and Ar, H_2, and CO_2 were added separately in large concentrations at port I4. Addition of these gases at number densities of $\sim2\times10^{14}$ cm^{-3} (which is equal to or greater than the number densities of these gases used in the recombination experiments) produced no significant increase in the $OH(v''=0)$ fluorescence and thus it is concluded that quenching of $OH(v''>0)$ (produced in the present experiments) by these gases at the number densities used was not significant. The fact that the $OH(v''=0)$ fluorescence did not increase when CO_2 was added also established that the H atoms present in the flow tube reacted only insignificantly with CO_2 to produce OH which is consistent with previous findings.[35]

C. Diffusive and reactive losses of H and OH

It is now only necessary to relate I_f to $[OH(v''=0)]$ to obtain absolute values for the fractions of $OH(v''>0)$ and $OH(v''=0)$ which are produced in reaction (1). The discussion of the calibration procedure given in Sec. III A relates I_f for the $OH(v''=0)$ produced in the $H + NO_2$ reaction to the initial H-atom column density. However, in order to relate I_f to $[OH(v''=0)]$ it is necessary to know the H-atom radial density profile across the flow tube so that [H] can be deduced. From an empirical expression, the diffusion coefficient D for H atoms in He at a pressure of 1.6 Torr and at temperature of 300 K used in these experiments can be calculated to be $\sim(1300\pm200)$ cm^2 s^{-1}.[36] Thus, under the pressure conditions of the present experiments, H atoms can readily diffuse to the walls of the flow tube. In an earlier study of the reactions of H atoms with ions, Howard *et al.* concluded that H atoms are not lost significantly on the walls of stainless steel flow tubes of similar dimensions to that used in the present study.[37] This has been confirmed by Rowe *et al.*[16] who also showed in a flow tube that there is no significant radial variation of H-atom density. So, in the present studies, it is to be expected that the H-atom density is sensibly independent of radial position and based on this, [H] and thus $[OH(v''=0)]$ can be easily deduced from the H-atom column density and $[OH(v''=0)]$ can be related to I_f.

At this point, it is worth considering whether significant radial diffusion and wall recombination loss of OH occurs between its production and detection. This general situation has been analyzed by Kaufman[38] who showed that, in the steady state for loss only by wall recombination, the fractional difference between the number density on axis, $[OH]_a$, and that at the walls, $[OH]_w$, (in terms of the average number density $[\overline{OH}]$) is

$$\frac{[OH]_a - [OH]_w}{[\overline{OH}]} = \frac{3k_w r^2}{8D}, \tag{22}$$

where k_w is the wall recombination coefficient, r is the flow tube radius, and D is the diffusion coefficient for OH radicals at the pressure of the experiment. The value of D for OH radicals in helium can be estimated from the D of oxygen

atoms in helium[39] to be $\sim (436 \pm 150)$ cm^2 s^{-1} at a helium pressure of 1.6 Torr. The value of k_w has been found to vary widely, ranging from 8 to 50 s^{-1} (and perhaps even greater) for tubes of diameter 2.5 cm depending on whether the surface is nominally clean Pyrex or is Pyrex coated with H_3PO_4 suitably aged.[40-42] Assuming the largest value of k_w, the worst case situation, correcting it for the difference between previous and present flow tube diameters[38] and using an appropriate value for D in Eq. (22) gives an $[OH]_w = 65\%[OH]_s$, a small radial gradient. Further, from Kaufman[38]

$$[OH]_z = [OH]_0 \exp - \frac{2k_w}{v_0}\left(1 - \frac{4k_w D}{v_0^2}\right)z, \qquad (23)$$

where v_0 is the bulk velocity of the flowing He gas, which predicts only a 13% reduction in [OH] between its production at port I4 and its detection 17.5 cm downstream. In any case, the calibration procedure corrects for such a reduction and thus it should not influence the determination of [OH] from the recombination reaction.

Finally, it is necessary to consider whether there are any reactive loss processes for OH. OH can react with the H, O, and OH present in the flow tube, viz.,

$$OH + H \xrightarrow{M} H_2O + M$$

$$\rightarrow H_2 + O, \qquad (24)$$

$$OH + O \rightarrow O_2 + H, \qquad (25)$$

$$OH + OH \xrightarrow{M} H_2O_2 + M, \qquad (26)$$

however, the small concentrations of these radicals compounded with the small rate coefficients[29] renders these loss processes insignificant.

D. Absolute OH($v^* = 0$) and OH($v^* > 0$) products of the HCO_2^+ recombination reaction

The percentage of OH($v^* = 0$) produced in the HCO_2^+ recombination [reaction (1)] has been deduced using the calibration procedure [reaction (2) and Sec. III B], the data in Fig. 5 together with the measured value of $n_e(0)$, and the slope of Fig. 6 [see Eq. (20)]. In this manner, it was determined that OH($v^* = 0$) is a 17% product and thus from the OH($v^* > 0$)/OH($v^* = 0$) ratio of ~ 1 deduced in Sec. III B that OH($v^* > 0$) is also about a 17% product giving a total OH $X\,^2\Pi$ of (34 ± 6)%.

Once the contribution of OH($v^* = 0$) to the product distribution has been determined, then the data in Fig. 6 together with Eq. (20) can be used to determine the recombination coefficient α_{v^*} for the reaction. Thus α_{v^*} has been determined to be $(2.8 \pm 0.8) \times 10^{-7}$ cm^3 s^{-1} at 300 K in reasonable agreement with the value of $(3.4 \pm 0.85) \times 10^{-7}$ cm^3 s^{-1} previously determined in the usual FALP experiments (from the axial electron density gradient in the flow tube) at the same temperature.[28]

V. DISCUSSION

The energetically allowed product channels for the dissociative recombination of HCO_2^+ with electrons are

	ΔH (kcal mol^{-1})	
$-H(^2S_{1/2}) + CO_2(X\,^1\Sigma_g^+)$	-185.1	(22a)
$-H(^2S_{1/2}) + CO_2[\tilde{A}\,^1B_2(\Delta_u)]$	-53.6	(22b)
$-OH(X\,^2\Pi) + CO(X\,^1\Sigma^+)$	-160.1	(22c)
$-OH(A\,^2\Sigma^+) + CO(X\,^1\Sigma^+)$	-63.6	(22d)
$-O(^3P_J) + H(^2S_{1/2}) + CO(X\,^1\Sigma^+)$	-57.9	(22e)

obtained from Refs. 63–65. Production of CH $X\,^2\Pi$ and $O_2X\,^3\Sigma_g^-$ is close to thermoneutral ($\Delta H \sim +0.4$ kcal mol^{-1}), however, this channel requires a great deal of rearrangement of the $(HCO_2)^*$ after neutralization and before its dissociation and is therefore unlikely. The experimental data obtained so far show that ~ 35% of the recombinations finally result in the production of OH in the electronic ground state. However, at least some of this product could result from the initial production of OH $A\,^2\Sigma$ which would then radiatively decay to the ground state with a lifetime ~ 700 ns.[41,42] Indeed recently, we have detected weak optical emissions from OH $A\,^2\Sigma \rightarrow X\,^2\Pi$ transitions in a recombining HCO_2^+/e plasma (unpublished results). Therefore a fraction of the detected OH $X\,^2\Pi$ ($v^* = 0$ and $v^* > 0$) originated from nascent OH $A\,^2\Sigma$. However, because of the weakness of the emissions, our judgement is that an appreciable fraction of the detected OH $X\,^2\Pi$ ($v^* = 0$ and $v^* > 0$) are nascent species. That such a large fraction of the detected OH $X\,^2\Pi$ are in the lowest vibrational level for such an exothermic process [channel 22(c)] can be explained, at least qualitatively, since the O–H bond length in HCO_2^+ (as determined by structural calculations[66] to be 0.9979 Å) is very similar to that of OH in the $X\,^2\Pi$ state (0.9697 Å).[67] Thus, upon recombination of HCO_2^+ to produce OH $X\,^2\Pi$, there is no significant change in the OH equilibrium bond length, resulting in minimal vibrational excitation of the nascent OH product. The remaining excess energy in the recombination reaction would then appear largely as kinetic energy of the separating products. It should be noted that it is also possible to produce CO_2 in the $\tilde{A}\,^1B_2$ state [reaction (22b)] and radiation from the decay of this state should also be searched for by emission spectroscopy.

To our knowledge, no theoretical effort has been directed towards predicting the products of the recombination of HCO_2^+. However, the theoretical ideas of Bates[23–25] can be used to make some predictions. The structure of HCO_2^+ has been calculated to be HOCO with the positive charge localized on the O atom between the H and the C.[66,68] For this situation, the ideas of Bates suggest that $H + CO_2$ and $OH + CO$ would be the likely product channels. Further, Bates[24] has suggested that the likelihood of a favorable curve crossing to products will be greatest when both products are radical and molecular. Such an effect would be expected to enhance the probability of dissociation to produce $OH + CO$ relative to $H + CO_2$. However, it should be noted that if the OH is produced in the $A\,^2\Sigma^+$ state with $v' > 2$ then rapid predissociation to O and H can occur.[63] Although these qualitative predictions are consistent with the present experimental observations, it is obviously important for quantitative theoretical predictions to be made which include the effects of curve crossings.

V. CONCLUSION

A technique has been described which can be used to quantitatively identify the neutral products of electron–ion dissociative recombination when these are amendable to detection by laser induced fluorescence. In particular, recombination reactions of protonated species can be studied. Data have been presented for the HCO_2^+ recombination reaction which show that OH in its ground electronic state (in both its $v'' = 0$ and vibrationally excited states) is a substantial product being ~35% of the product distribution (note that this percentage may include a contribution due to the $A\ ^2\Sigma^+$ state which rapidly radiatively decays to the ground state). These data have implications to the chemistry of CO_2 in interstellar gas clouds and this, together with data concerning the products of other recombination reactions is the subject of a separate paper.[69] In addition, in the HCO_2^+ recombination it is energetically possible for OH and CO_2 to be produced in their first electronically excited states. The quantitative detection of radiation from these excited species using emission spectroscopy would provide information on energy disposal in the reaction and such observations are planned. Also it is energetically possible for H and O atoms to be produced. Efforts are underway in our laboratory to improve the sensitivity of atomic absorption and atomic fluorescence spectroscopy at the atomic resonance line wavelengths (e.g., L_α) to enable the contributions of O and H to the product distribution to be quantitatively determined. When this is achieved, the total product distribution of this reaction will be specified. This then will give guidance to theorists in the calculation of the product distributions for this type of reaction.

ACKNOWLEDGMENTS

We are grateful to the USAF and the SERC for financial support of this work. We are also grateful to the University of Birmingham for the award of a special grant with which it was possible to purchase the spectroscopic equipment. We wish to thank Professor I.W.M. Smith for useful discussions concerning neutral–neutral reactions. Thanks are also due to Mark Geoghegan for his assistance with the data analysis.

[1] A. Dalgarno and J. H. Black, Rep. Prog. Phys. 39, 573 (1976).
[2] D. Smith and N. G. Adams, Int. Rev. Phys. Chem. 1, 271 (1981).
[3] T. J. Millar, D. J. DeFrees, A. D. McLean, and E. Herbst, Astron. Astrophys. 194, 250 (1988).
[4] G. C. Reid, Adv. At. Mol. Phys. 63, 375 (1976).
[5] D. Smith and N. G. Adams, Top. Curr. Chem. 89, 1 (1980).
[6] F. J. Mehr and M. A. Biondi, Phys. Rev. 181, 264 (1969).
[7] E. Alge, N. G. Adams, and D. Smith, J. Phys. B 16, 1433 (1983).
[8] D. Auerbach, R. Cacak, R. Caudano, T. D. Gaily, C. J. Keyser, J. W. McGowan, J. B. A. Mitchell, and S. F. J. Wilk, J. Phys. B 10, 3797 (1977).
[9] J. N. Bardsley and M. A. Biondi, Adv. At. Mol. Phys. 6, 1 (1970).
[10] J. B. A. Mitchell and J. W. McGowan, in *Physics of Ion–Ion and Electron–Ion Collisions*, edited by F. Brouillard and J. W. McGowan (Plenum, New York, 1983), p. 279.
[11] N. G. Adams and D. Smith, in *Rate Coefficients in Astrochemistry*, edited by T. J. Millar and D. A. Williams (Kluwer, Dordrecht, 1988), p. 173.
[12] F. Vallee, B. R. Rowe, J. L. Queffelec, J. C. Gomet, and M. Morlais, J. Chem. Phys. (to be published).
[13] D. Kley, G. M. Lawrence, and E. J. Stone, J. Chem. Phys. 66, 4157 (1977).
[14] R. A. Gutcheck and E. C. Zipf, J. Geophys. Res. 78, 3429 (1973).
[15] F. Vallee, B. R. Rowe, J. C. Gomet, J. L. Queffelec, and M. Morlais, Chem. Phys. Lett. 124, 317 (1986).
[16] B. R. Rowe, F. Vallee, J. L. Queffelec, J. C. Gomet, and M. Morlais, J. Chem. Phys. 88, 845 (1987).
[17] J. L. Queffelec, B. R. Rowe, M. Morlais, J. C. Gomet, and F. Vallee, Planet. Space Sci. 33, 263 (1985).
[18] S. L. Guberman, in Ref. 10, p. 167.
[19] H. H. Michels and R. H. Hobbs, Astrophys. J. Lett. 286, L27 (1984).
[20] W. P. Kraemer and A. U. Hazi, in *Dissociative Recombination: Theory, Experiment and Applications*, edited by J. B. A. Mitchell and S. L. Guberman (World Scientific, Singapore, 1989), p. 61.
[21] E. Herbst, Astrophys. J. 222, 508 (1978).
[22] S. Green, and E. Herbst, Astrophys. J. 229, 121 (1979).
[23] D. R. Bates, Phys. Rev. 78, 492 (1950).
[24] D. R. Bates, Astrophys. J. Lett. 306, L45 (1986).
[25] D. R. Bates, in *Modern Applications of Atomic and Molecular Processes*, edited by A. E. Kingston (Plenum, London, 1987), p. 1.
[26] D. R. Bates, Astrophys. J. (in press).
[27] D. R. Bates and E. Herbst, in Ref. 11, p. 41.
[28] N. G. Adams and D. Smith, Chem. Phys. Lett. 144, 11 (1988).
[29] M. J. Howard and I. W. M. Smith, Prog. React. Kinet. 12, 55 (1983).
[30] D. Klenerman and I. W. M. Smith, J. Chem. Soc. Farad. Trans. 2 83, 229 (1987).
[31] I. W. M. Smith (private communication).
[32] I. W. M. Smith, and M. D. Williams, J. Chem. Soc. Faraday Trans. 2 81, 1849 (1985).
[33] D. Smith and N. G. Adams, in Ref. 10, p. 501.
[34] D. K. Bohme, N. G. Adams, M. Mosesman, D. B. Dunkin, and E. E. Ferguson, J. Chem. Phys. 52, 5094 (1970).
[35] N. G. Adams, D. Smith, and E. Alge, J. Chem. Phys. 81, 1778 (1984).
[36] J. K. Kim, L. P. Theard, and W. T. Huntress, Jr., Int. J. Mass Spectrom. Ion Phys. 15, 223 (1974).
[37] D. Smith, N. G. Adams, A. G. Dean, and M. J. Church, J. Phys. D 8, 141 (1975).
[38] M. A. A. Clyne and W. S. Nip, in *Reactive Intermediates in the Gas Phase*, edited by D. W. Setser (Academic, New York, 1979), pp. 1–58.
[39] A. C. Eckbreth, P. A. Bonczyk, and J. F. Verdieck, Prog. Energy Combust. Sci. 5, 253 (1979).
[40] V. M. Iberbaum, G. B. Ellison, and S. R. Leone in *Gas Phase Ion Chemistry, Ions and Light*, edited by M. T. Bowers (Academic, New York, 1984), Vol. 3., pp. 1–39.
[41] A. C. Eckbreth, *Laser Diagnostics for Combustion, Temperature and Species* (Abacus, Tunbridge Wells, 1988).
[42] K. R. German, J. Chem. Phys. 63, 5252 (1975).
[43] W. L. Dimpfl and J. L. Kinsey, J. Quant. Spectrosc. Radiat. Transfer 21, 233 (1979); W. H. Smith, B. G. Elmergreen, and N. H. Brooks, J. Chem. Phys. 61, 2793 (1974).
[44] G. H. Dieke and H. M. Crosswhite, J. Quant. Spectrosc. Radiat. Transfer 2, 97 (1962).
[45] D. R. Guyer, L. Huwel, and S. R. Leone, J. Chem. Phys. 79, 1259 (1983).
[46] A. C. G. Mitchell and M. W. Zemansky, *Resonance Radiation and Excited Atoms* (Cambridge University, New York, 1971).
[47] M. Dudeck, G. Poissant, B. R. Rowe, J. L. Queffelec, and M. Morlais, J. Phys. D 16, 995 (1983).
[48] A. Lifshitz, G. B. Skinner, and D. R. Wood, J. Chem. Phys. 70, 5607 (1979).
[49] G. Herzberg, *Molecular Spectra and Molecular Structure I. Spectra of Diatomic Molecules* (Van Nostrand, Princeton, 1950).
[50] A. L. Schmeltekopf, E. E. Ferguson, and F. C. Fehsenfeld, J. Chem. Phys. 48, 2966 (1968).
[51] J. A. Burt, J. L. Dunn, M. J. McEwan, M. M. Sutton, A. E. Roche, and H. I. Schiff, J. Chem. Phys. 52, 6062 (1970).
[52] Y. Ikezoe, S. Matsuoka, M. Takebe, and A. Viggiano, *Gas Phase Ion Molecule Reaction Rate Constants through 1986* (Maruzen, Tokyo, 1987).
[53] N. G. Adams, M. J. Church, and D. Smith, J. Phys. D 8, 1409 (1975).
[54] S. R. Langhoff, R. L. Jaffe, J. H. Lee, and A. Dalgarno, Geophys. Res. Lett. 10, 596 (1983).
[55] I. W. M. Smith, Top. Curr. Chem. 99, 112 (1986).
[56] E. M. Mason and T. R. Marrero, Adv. At. Mol. Phys. 6, 156 (1970).
[57] C. J. Howard, F. C. Fehsenfeld, and M. McFarland, J. Chem. Phys. 60, 5086 (1974).
[58] F. Kaufman, Prog. React. Kinet. 1, 1 (1961).
[59] P. A. Bernhardt, J. Geophys. Res. 84, 793 (1979).

[60]J. O. Anderson, J. J. Margitan, and F. Kaufman, J. Chem. Phys. 60, 3301 (1974).
[61]M. A. A. Clyne and S. Dunn, J. Chem. Soc. Faraday Trans. 2, 70, 253 (1974).
[62]M. A. A. Clyne and P. M. Holt, J. Chem. Soc. Faraday Trans. 2, 75, 582, (1979).
[63]N. G. Adams, D. Smith, M. Tichy, G. Javahery, N. D. Twiddy, and E. E. Ferguson, J. Chem. Phys. (in press).
[64]H. M. Rosenstock, K. Draxel, B. W. Steiner, and J. T. Herron, J. Phys. Chem. Ref. Data. 6, Suppl. 1 (1977).
[65]*CRC Handbook of Chemistry and Physics*, 66th ed. edited by R. C. West (Chemical Rubber, Boca Raton, Florida, 1985), p. F174.
[66]M. J. Frisch, H. F. Schaefer III, and J. S. Binkley, J. Phys. Chem. 89, 2192 (1985).
[67]K. P. Huber and G. Herzberg, *Molecular Spectra and Molecular Structure. IV. Constants of Diatomic Molecules* (Van Nostrand Reinhold, New York, 1979).
[68]H. F. Schaefer III, in *Ion and Cluster Ion Spectroscopy and Structure* edited by J. P. Maier (Elsevier, Amsterdam, 1989) pp. 109–130.
[69]C. R. Herd, N. G. Adams, and D. Smith, Astrophys. J. (submitted).

APPENDIX 6

OH PRODUCTION IN THE DISSOCIATIVE RECOMBINATION OF H_3O^+, HCO_2^+ AND N_2OH^+: COMPARISON WITH THEORY AND INTERSTELLAR IMPLICATIONS

C.R. HERD, N.G. ADAMS AND D. SMITH

Astrophys.J., in press, 20th Jan (1990)

OH PRODUCTION IN THE DISSOCIATIVE RECOMBINATION OF H_3O^+, HCO_2^+ AND N_2OH^+ : COMPARISON WITH THEORY AND INTERSTELLAR IMPLICATIONS

Charles R. Herd, Nigel G. Adams and David Smith

School of Physics and Space Research

University of Birmingham

P.O. Box 363

Birmingham, B15 2TT

England

Short Title: OH Production in Recombination

ABSTRACT

The percentages of OH radicals produced in the dissociative recombination reactions of H_3O^+, HCO_2^+ and N_2OH^+ with electrons at 300K have been determined to be (65 ± 10)%, (34 ± 6)% and (31 ± 5)% respectively. The experiments were conducted using a flowing afterglow/Langmuir probe (FALP) apparatus modified to include spectroscopic diagnostics. In the case of H_3O^+, the amount of OH produced is intermediate between the theoretical predictions of Bates and of Herbst. The importance of this finding in determining the dominant oxygen containing species in dense interstellar clouds is discussed in relation to recent chemical models of these clouds. In the case of HCO_2^+, it is concluded that recombination will be a significant overall loss process for HCO_2^+, and thus CO_2, in dense interstellar clouds for fractional electron abundances $\geq 10^{-8}$.

I. INTRODUCTION

Quantitative gas-phase ion-chemical models of diffuse and dense interstellar clouds have been developed which, for many of the species observed, sensibly predict their abundances (Millar and Nejad 1985; Herbst and Leung 1986; Millar, Leung and Herbst 1987). Since the majority of the observed species are neutral, then after initial production of ionization by photo and/or cosmic ray ionization followed by sequences of positive ion- neutral reactions which generate polyatomic ions, a charge neutralization process - usually dissociative electron-ion recombination - is invoked to produce the observed neutral molecules. For example, OH and H_2O are often assumed to be produced in the recombination with electrons of the observed interstellar ion, H_3O^+, which is believed to be produced in the reaction sequence (Wootten et al. 1986)

$$H^+ \underset{H}{\overset{O}{\rightleftharpoons}} O^+ \xrightarrow{H_2} OH^+ \xrightarrow{H_2} H_2O^+ \xrightarrow{H_2} H_3O^+ \xrightarrow{e} OH,\ H_2O \qquad (1)$$

$$H_2^+ \xrightarrow{H_2} H_3^+ \xrightarrow{O} OH^+$$

For the accurate prediction of the abundances of the observed species, values for the rate coefficients and product distributions of both the ion- neutral and dissociative recombination reactions are required. Many laboratory data are available for ion- neutral reactions (e.g. see Anicich and Huntress 1986; Ikezoe et al. 1987) and these have been included in detailed models (e.g., see Herbst and Leung 1986) but, much fewer data are available concerning dissociative recombination - particularly in relation to the neutral products (Adams and Smith 1988a). Although laboratory data are available for some ions not implicated in

interstellar syntheses (N_2^+, NO^+, CO_2^+ and H_2O^+; see, for example, Rowe et al. 1987, and the review by Adams and Smith 1988a), these data only relate to the atomic products of the recombination of these ions in unknown states of excitation (except for the case of N_2^+ ($v'' = 1$), Queffelec et al 1985).

Some effort has been made theoretically to predict the products of recombination. Detailed potential curves have been calculated for O_2^+ (Guberman 1983) and some curves are also available for HeH^+ (Michels 1989), H_3^+ (Michels and Hobbs 1984) and very recently HCO^+ (Kraemer and Hazi 1988). Herbst (1978) and Green and Herbst (1979) have applied phase space ideas to predict the reaction products of dissociative recombination, and Bates (1950, 1986, 1987) has considered which products would be likely in terms of the valence bonds which might break based on their bonding/anti-bonding character. However, for the case of H_3O^+, the Bates and Herbst approaches predict very different results. The energetically allowed reaction channels are (see Table 1):

$$H_3O^+ + e \longrightarrow H + H_2O \quad (2a)$$

$$\longrightarrow OH + H_2 \quad (2b)$$

$$\longrightarrow O + H + H_2 \quad (2c)$$

$$\longrightarrow OH + 2H \quad (2d)$$

Bates (1986) previously predicted that H_2O production (channel (2a)) is dominant, the other channels being minor, whereas Herbst calculated that OH production via channels (2b) (80%) and (2d) (10%) is dominant. These theories depend on appropriate crossings of the potential curve(s) for the neutralized excited polyatomic molecule and the repulsive potential energy curve(s) for the products. This has very recently been re-considered by Bates (1989) who concluded that channel (2b), producing OH and H_2, would be enhanced on the basis that there are likely to be more favourable curve crossings for those products which are molecular and

radical. Because these theoretical approaches are in the development phase, and not least because of the difficulty in calculating potential curves for polyatomic ions, quantitative experimental identification of the products is essential both to guide theory and to improve models of interstellar molecular synthesis. Reaction (2) is very critical to these models since if the fraction of the recombinations, f, resulting in OH production is small, then the dominant oxygen-containing species is H_2O, whereas if f is large, then the dominant oxygen containing species is O_2 (Millar et al. 1988). The effect of varying f in the models has been considered by Sternberg, Dalgarno and Lepp (1987) and Millar et al. (1988).

Our approach to this situation has been to determine f for the recombination of ground vibronic state H_3O^+ utilizing the flowing afterglow/Langmuir Probe (FALP) technique modified to include laser-induced fluorescence (LIF) detection of radical species (Adams, Herd and Smith 1989). In addition, we have determined the fraction of recombinations leading to OH for HCO_2^+, which is an observed interstellar ion (Thaddeus, Guelin and Linke 1981; Minh, Irvine and Ziurys 1988), and for N_2OH^+ .

II. EXPERIMENTAL

The FALP technique incorporates laser induced fluorescence (LIF) for the detection of molecular radicals and VUV absorption spectroscopy for the detection of atoms, and has been discussed in detail recently (Adams, et al. 1989) and will therefore only be mentioned briefly here. Ionization is created upstream in a flowing He carrier gas (at a typical pressure of 1.6 Torr) by a microwave discharge; then Ar and H_2 are sequentially added downstream to produce a non-recombining H_3^+/e afterglow plasma by the reactions

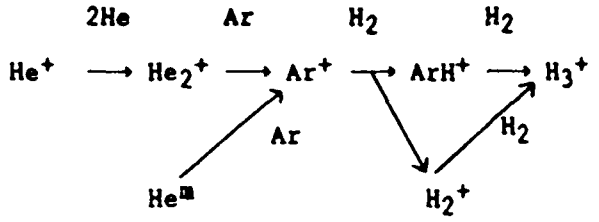

(5)

Further downstream, H_2O, CO_2 or N_2O are added and a recombining plasma is produced by proton transfer from H_3^+ e.g.

$$H_3^+ + H_2O \longrightarrow H_3O^+ + H_2 \qquad (6)$$

Any internal excitation of the product ion is rapidly quenched in the presence of excess reactant neutral by near-resonant proton transfer, e.g.

$$H_3O^{+*} + H_2O \longrightarrow H_3O^+ + H_2O^* \qquad (7)$$

At the initial electron densities (~1 X 10^{10} cm^{-3}) in the recombining plasma, the ions are efficiently neutralised to give products. Any OH $X^2\Pi(v''=0)$ resulting from the dissociative recombination reactions of H_3O^+, HCO_2^+ and N_2OH^+ with electrons is detected further downstream by laser excitation of the $A^2\Sigma(v'=1) \longleftarrow X^2\Pi(v''=0)$ rovibronic transition of OH and detection of fluorescence in the (1,1) band. An absolute calibration of the fluorescence intensity against OH $X^2\Pi(v''=0)$ number density was obtained and has been discussed in detail previously (Adams et al. 1989).

In order to ensure that the OH observed resulted from the recombination reaction, the OH fluorescence intensity, I_f, was measured as a function both of the flow of the added reactant gas (except in the case of H_2O for which it is difficult to vary the flow for large flows) and as a function of the electron density, $n_e(0)$, just upstream of the addition point of the gas. A recombining H_3O^+/electron plasma was also created by adding O_2 upstream into a pure He carrier gas and adding H_2

downstream whence the reaction sequence

$$He^+ \xrightarrow{O_2} O^+ \xrightarrow{H_2} OH^+ \xrightarrow{H_2} H_2O^+ \xrightarrow{H_2} H_3O^+ \qquad (8)$$

produced H_3O^+. Also, O_2^+ is produced in the initial reaction in sequence (8); however this ion is unreactive with H_2 and therefore could not contribute to OH production. In this case, I_f was then measured as a function of H_2 flow. The dependence of I_f on both reactant gas flow rate and $n_e(O)$ confirmed that OH is a product in the recombination of H_3O^+, HCO_2^+ and N_2OH^+ with electrons. All measurements were made at 300K.

III. RESULTS AND DISCUSSION

a) OH Products of Recombination: Comparison with Theory

Information obtained concerning the neutral products of the dissociative recombination of H_3O^+, HCO_2^+ and N_2OH^+ is given in Table 2 together with the recombination coefficients, α_e, which were determined previously at 300K (Smith and Adams 1984; Adams and Smith 1988b). The recombination of HCO^+ with electrons was also studied but an OH product was not observed even though this product channel is somewhat exothermic (-0.8 eV). This seems reasonable as it would require a bond to be formed between the H and O atoms which are separated by the central C-atom (in the FALP, utilization of the reaction $H_3^+ + CO$ produces HCO^+ and not the higher energy isomer HOC^+; Dixon, Komornicki and Kraemer, 1984). However, the absence of OH as a product did show that there were no significant extraneous sources of OH in the afterglow plasma.

In Table 2, the percentages of the recombinations which produce OH are separated into those resulting in the ground and the vibrationally

excited states of the electronic ($X^2\Pi$) ground state. These molecules in the ground electronic state are not necessarily primary products of the recombination reactions since, in the recombination of all three ionic species, the electronically excited $A^2\Sigma$ state of OH is accessible which can rapidly radiatively relax to the $X^2\Pi$ state (German 1975). It is worthy of note that the vibrationally excited levels of the $A^2\Sigma$ state ($v'>2$) can rapidly predissociate to O and H (Smith, Elmergreen and Brooks 1974). It should be noted that vibrational excitation in the reaction products is not important in modelling the chemistry of interstellar gas clouds since vibrationally excited states relax to the $v''=0$ level of the $X^2\Pi$ state in times much shorter than a collision time with even the most abundant species, H_2 (Langhoff et al. 1983). Thus, only the total fraction of the recombinations which lead to OH is significant, independent of its nascent state distribution. However, it is interesting to note that radiative vibrational relaxation within the $X^2\Pi$ state will result in infrared emissions which might be detectable in the directions towards interstellar gas clouds.

It is important to compare the experimentally determined product distributions with theoretical predictions in order to assess the validity of the various theoretical approaches to dissociative recombination. For the case of H_3O^+ recombination, (65±10)% of the recombinations result in the production of OH. Herbst (1978), considering only channels leading to the production of the electronic ground states of OH and H_2O (channels 2(b) and 2(d), and channel 2(a) respectively in Table 1), concluded that ~90% of the recombinations would result in OH production, the remaining ~10% producing H_2O. If the only energetically accessible electronically excited state of OH, the $A^2\Sigma$ state, had been included in the calculation, then OH production would presumably be even more strongly favoured compared to H_2O. Thus Herbst's

theory significantly overestimates the amount of OH production. The converse applies to the earliest theory of Bates (1986, 1987) which predicted that H_2O production would be very much dominant. This was substantiated by Millar et al. (1988) who extended the Bates theory by making quantum chemical calculations of the charge distributions in the recombining ions and predicted that H and H_2O (channel 2(a)) are the only products. This of course significantly underestimates the OH production. However, these two different theoretical approaches both rely on the existence of readily accessible repulsive potential curves to the predicted products. This has very recently been recognised by Bates (1989) who argues that there would be the greatest likelihood of favourable curve crossings if the products of the recombination were both molecular and radical. As far as the H_3O^+ + e recombination is concerned, this means that the products OH + H_2 would be more likely than previously thought.

Also, the phase space approach of Herbst requires that the potential surface of the neutralized ion be fully explored before dissociation into products. If many favourable curve crossings exist then this is unlikely to happen and this would influence the predicted product distribution. In view of this discussion, it appears that the availability of accessible curve crossings should be taken into account in theoretically predicting product distributions to be used in the models of molecular synthesis in interstellar clouds.

For the other two recombination reactions that we report here (i.e. HCO_2^+ + e and N_2OH^+ + e), no explicit theoretical predictions have been made. However, since the structures of HCO_2^+ and N_2OH^+ have been determined theoretically then the original Bates' theory (1986, 1987) can be used to make some predictions. The lowest energy form of HCO_2^+ has been shown theoretically to be $\overset{+}{H}OCO$ (Frisch, Schaefer and Binkley 1985;

Schaefer 1988) and thus the product channels H + CO_2 (channel 3(a), see Table 1) and OH + CO (channel 3(b)) would both be predicted, consistent with the experimental data for the production of OH (a (34±6)% product, see Table 2). That the channel giving the two molecular products (one being a radical, Bates 1989) is not dominant, might imply that some predissociating $A^2\Sigma$ state of OH is generated in the recombination reaction. In fact, in preliminary emission studies of this recombination reaction, weak $A^2\Sigma \rightarrow X^2\Pi$ emissions of OH have indeed been observed indicating that some of the OH is produced in the $A^2\Sigma$ state.

Rice, Lee and Schaefer (1986) calculated that the lowest energy form of N_2OH^+ is $N\overset{+}{N}OH$ and thus N_2 + OH (channel 4(b), see Table 1) would be expected as a product channel, again in accordance with the experimental data for the production of OH (a (31±5)% product, see Table 2), although again the channel leading to the two molecular products, one which is a radical (N_2 and OH) is not dominant. The other channel (4(f)) predicted on the basis of these theoretical ideas, N + NOH (or N + NO + H) would require the breaking of a nitrogen-nitrogen triple bond and is therefore considered to be unlikely. Similar arguments apply to channels 4(d) and 4(e) (see Table 1). Obviously, further experiments are necessary to determine the contribution to the product distribution due to atomic products (using VUV absorption and fluorescence spectroscopy) and to electronically excited products (using emission spectroscopy as mentioned above). Such experiments are in progress.

b) Interstellar Implications: H_3O^+ + e

The experimental data for this reaction indicate that 65% of the recombinations lead to OH (see Table 2), the remaining percentage being distributed in an as yet unknown manner between the other energetically

accessible product channels (see Table 1). As stated above these data were obtained at 300K, however the accessible curve crossings are unlikely to change significantly with decreasing temperature and thus it is not unreasonable to apply these results to low temperature interstellar gas cloud chemistry. Following the ideas of Millar et al. (1988), it is possible to clarify the situation as to the identity of the dominant oxygen- containing species in dense interstellar clouds. The implications of different product ratios of the H_3O^+ recombination reaction to interstellar chemistry have been discussed in detail by Sternberg et al. (1987) and by Millar et al. (1988) who considered possible scenarios for various fractions, f, of the H_3O^+ recombinations which produce OH. For an f = 0.65 in a cloud with an H_2 number density of 10^4 cm^{-3} at a temperature of 50K, a depletion factor for carbon and oxygen of 0.1, a cosmic ray ionization rate of $10^{-17}s^{-1}$ and a total metal fractional abundance of 1.5×10^{-8}, Sternberg et al. (1987) predicted in the steady state, the fractional abundances (relative to H_2) of H_3O^+, OH, H_2O, C^+, CH_4, C_2H_2, and C_3H_2 (these are listed in Table 3 together with the fractional abundances actually observed in various interstellar clouds). It can be seen that the calculated values for H_3O^+, OH and CH_4, within error, are in agreement with direct observations. However, the fractional abundance predicted for C_3H_2 (7.3×10^{-11}) is significantly smaller than observations. It should be noted that Millar et al. (1988) predict a fractional abundance of C_3H_2 in agreement with Sternberg et al. (1987) using a steady state model (both with f=0.1) but additionally predict much larger fractional abundances ($\sim10^{-7}$) using an early-time model. Nevertheless it is gratifying to see that, to a large degree, the direct observations are consistent with predictions based on the product distribution experimentally measured at 300K for the H_3O^+ recombination reaction, as reported in the present study.

In the earlier models of molecular synthesis (see Prasad and Huntress 1980; Graedel, Langer and Frerking 1982; Millar and Freeman 1984; Leung, Herbst and Huebner 1984; Herbst and Leung 1986), an f value of 0.5 (i.e. close to experimental value of 0.65) was fortuitously adopted. However, it should be noted that it was generally assumed in these models that the fraction of the recombinations which do not produce OH lead to the production of H_2O. There is no experimental evidence yet to support this assumption and, indeed, since the $A^2\Pi$ excited state of OH is accessible and predissociates for $v' \geq 2$ (Smith et al. 1974), it is possible that the production of O and H atoms (channel (2c)) could occur.

However, because OH is a dominant product from the recombination of H_3O^+, the dominant oxygen containing species in dense interstellar gas clouds should be O_2 (formed via the reaction of OH + O) rather than H_2O (Millar et al. 1988).

c) Interstellar Implications: HCO_2^+ + e

Much less effort has been directed towards the interstellar ion chemistry of HCO_2^+ compared to that of H_3O^+. The ion HCO_2^+ has been detected in Sgr.B2 (Thaddeus,Guelin and Linke 1981) with a fractional abundance of $\geq 10^{-10}$ (Minh et al. 1988) which is about two orders of magnitude greater than expected on the basis of molecular synthesis in cold quiescent interstellar gas clouds (Herbst and Leung 1986). The abundances of HCO_2^+ and CO_2 are closely linked by the proton transfer reactions:

$$H_3^+ + CO_2 \longrightarrow HCO_2^+ + H_2 \qquad (9)$$

$$N_2H^+ + CO_2 \longrightarrow HCO_2^+ + N_2 \qquad (10)$$

$$HCO_2^+ + CO \longrightarrow HCO^+ + CO_2 \qquad (11)$$

together with the more minor reactions

$$HCO_2^+ + H_2O\ (NH_3,\ etc) \longrightarrow H_3O^+\ (NH_4^+,\ etc) + CO_2 \qquad (12)$$

(Herbst et al. 1977). The abundances of H_3^+, N_2H^+ and CO are such that reactions (9) to (11) are the dominant production and loss processes for HCO_2^+ and CO_2 and thus effectively cycle CO_2 between its protonated and unprotonated forms with the number density ratio, R, = $[HCO_2^+]/[CO_2]$ being relatively unaffected by other overall production and loss processes (see reactions (15) to (19)). By considering that HCO_2^+ and CO_2 are in dynamic equilibrium, then

$$R = \frac{k_9[H_3^+] + k_{10}[N_2H^+]}{k_{11}[CO] + k_{12}[H_2O\ (NH_3\ etc.)]} \qquad (13)$$

The rate coefficients, k_9 and k_{10} have been measured at 300K (Ikezoe et al. 1987) and it is assumed that these are appropriate to interstellar cloud temperatures (a reasonable assumption for proton transfer reactions which proceed at or close to the collisional rate; note that for reactions (12), since H_2O and NH_3 have appreciable permanent dipole moments, then the collisional rate coefficients at interstellar temperatures will be appreciably greater than at 300K; Adams, Smith and Clary 1985). The rate coefficient for reaction (11) has not been measured but is confidently expected to be equal to the collisional value. Using these values of rate coefficients together with the fractional abundances of the species included in equation (13) as determined in the dense cloud model of Herbst and Leung (1986), then

$$R = \frac{[HCO_2^+]}{[CO_2]} = 10^{-5} \qquad (14)$$

It is now of interest to consider the overall loss processes for these coupled species, HCO_2^+ and CO_2, and to determine how effective

dissociative recombination is as a loss process. Loss processes for HCO_2^+ and CO_2 (Herbst et al. 1977; Prasad and Huntress 1979) are :

$$HCO_2^+ + O \longrightarrow HCO^+ + O_2 \quad (15)$$

$$HCO_2^+ + N \longrightarrow HCO^+ + NO \quad (16)$$

$$He^+ + CO_2 \longrightarrow CO^+ (80\%),\ CO_2^+(10\%),\ O^+(10\%) \quad (17)$$

$$C^+ + CO_2 \longrightarrow CO^+ + CO \quad (18)$$

$$H^+ + CO_2 \longrightarrow HCO^+ + O \quad (19)$$

as well as those dissociative recombination channels of the $HCO_2^+ + e$ reaction (reactions (3b) and (3c) in Table 1) which do not produce CO_2 and which comprise at least 34% of the recombinations. Consideration of these loss processes gives:

$$\frac{d[HCO_2^+]}{dt} + \frac{d[CO_2]}{dt} = -(k_{15}[O]+k_{16}[N])[HCO_2^+] - (k_{17}[He^+]+k_{18}[C^+] + k_{19}[H^+])[CO_2] - p\alpha_e[e][HCO_2^+] \quad (20)$$

where p is the fraction of the recombinations which generate products other than CO_2. The relative importance of these loss processes can be assessed by utilizing the value of R in equation (14), the fractional abundances of the various species in equation (19) as determined in the dense cloud model of Herbst and Leung (1986), and the known rate coefficients for the reactions. k_{17} and k_{18} have been determined to be $\sim 1 \times 10^{-9}$ $cm^3 s^{-1}$ and k_{19} to be 3×10^{-9} cm^3 s^{-1} at 300K (Ikezoe et al. 1987) and since they are close to their respective collisional rate coefficients they are not expected to vary significantly with temperature (since CO_2 does not have a dipole moment). The rate coefficients, k_{15} and k_{16} have not been measured, however, by consideration of similar exothermic atom reactions (Viggiano et al. 1980), the rate coefficients are expected to be a significant fraction (~20-50% at 300K) of their

collisional values. The recombination coefficient, α_e, for the HCO_2^+ + e reaction has been measured to be $3.4 \times 10^{-7} cm^3 s^{-1}$ at 300K (Adams and Smith 1988b), and in common with the α_e for other reactions, is expected to increase to ~ $1 \times 10^{-6} cm^3 s^{-1}$ at interstellar cloud temperatures (Adams and Smith 1988a). Application of these data to equation (19) shows that the HCO_2^+ + e recombination reaction will be a competitive loss process for HCO_2^+ and CO_2 for values of the product p.x(e) of approximately 10^{-8}, where x(e) is the fractional abundance of electrons relative to H_2. Thus, since $p \geq 0.35$, then x(e) ~ 3×10^{-8}, which is within the range of x(e) of 10^{-7} to 10^{-9} commonly used in models of interstellar gas clouds (Prasad and Huntress 1979; Graedel, Langer and Frerking 1982, Leung, Herbst and Huebner 1984; Herbst and Leung 1986; Millar et al. 1988). Therefore, dissociative recombination of HCO_2^+ is expected to be an important loss process for HCO_2^+ and thus for CO_2 in interstellar clouds. However, more detailed modelling is obviously required to establish the magnitude of the contribution of dissociative recombination to the loss of HCO_2^+/CO_2.

Finally, when the detailed product distributions of other recombination reactions have been determined, there could be unforeseen implications to interstellar molecular synthesis.

ACKNOWLEDGMENTS

We are grateful to the USAF and the SERC for financial support of this work. We also wish to thank Professor Sir David Bates for providing us with a preprint of his most recent theoretical paper on dissociative recombination.

TABLE 1

Exothermicities (eV) for Possible Channels of the Dissociative Recombination Reactions Indicated

Channel	Reaction (2) $H_3O^+ + e$	Reaction (3) $HOCO^+ + e$	Reaction (4) $NNOH^+ + e$
(a)	$H + H_2O + 6.4$	$H + CO_2 + 8.0$	$H + N_2O + 7.6$
(b)	$OH + H_2 + 5.8$	$OH + CO + 6.9$	$OH + N_2 + 10.4$
(c)	$O + H + H_2 + 1.5$	$O + H + CO + 2.5$	$O + H + N_2 + 6$
(d)	$OH + 2H + 1.3$		$OH + 2N + 0.6$
(e)			$NH + NO + 6.5$
(f)			$N + H + NO + 2.7$

NOTES. The energetics were calculated for the ground rovibronic states of the species indicated using data obtained from Rosenstock et al. (1977), Weast (1985) and McIntosh, Adams and Smith (1988).

TABLE 2

Percentage Product Distributions and Rate Coefficients, α_e, Measured at 300K for the Dissociative Recombination Reactions Indicated

$H_3O^+ + e$		$\overset{+}{H}OCO + e$		$N\overset{+}{N}OH + e$	
$OH(v''=0)+H_2(2H)$ 46%	65%	$OH(v''=0)+CO$ 17%	34%	$OH(v''=0)+N_2(2N)$ 14%	31%
$OH(v''>0)+H_2(2H)$ 19%		$OH(v''>0)+CO$ 17%		$OH(v''>0)+N_2(2N)$ 17%	
other products	35%	other products	66%	other products	69%
α_e[a], cm^3s^{-1}					
1.0×10^{-6}		3.4×10^{-7}		4.2×10^{-7}	

[a] Smith and Adams 1984; Adams and Smith 1988b.

TABLE 3

Comparison of Model Predictions (Sternberg et al. 1987) and Observed Fractional Abundances (Relative to H_2) of Several Interstellar Species

Species	Predicted Fractional Abundance	Observed Fractional Abundance	Source	Reference
H_3O^+	1.0×10^{-9}	$\sim10^{-9}$	OMC-1,SgrB2	Wootten et al. 1986
OH	5.8×10^{-8}	3×10^{-7}	TMC-1	Irvine et al. 1985, 1987
		6×10^{-8}	TMC-1	Leung et al. 1984
H_2O	7.8×10^{-7}	-	-	-
C^+	6.4×10^{-10}	-	-	-
CH_4	5.0×10^{-8}	$<8\times10^{-7}$	OMC-1	Knacke et al. 1985
C_2H_2	7.7×10^{-10}	-	-	-
C_3H_2	7.3×10^{-11}	2×10^{-8}	TMC-1	Irvine et al. 1987
		$>5\times10^{-9}$	"	Matthews and Irvine 1985
		5×10^{-10}	SgrB2	Thaddeus et al. 1987
		1×10^{-9}	"	Irvine et al. 1987
		7×10^{-11}	OMC-1	Thaddeus et al. 1985

NOTES. The predicted fractional abundances are those obtained using a value of 0.65 for the fraction of $H_3O^+ + e$ recombinations leading to OH in the chemical model of Sternberg et al. (1987).

REFERENCES

Adams, N.G. and Smith, D. 1988a, in *Rate Coefficients in Astrochemistry*, eds. T.J. Millar and D.A. Williams (Kluwer Academic Publishers, Dordrecht) pp.173-192.

Adams, N.G. and Smith, D. 1988b, *Chem. Phys. Lett.*, **144**, 11.

Adams, N.G., Smith, D. and Clary, D.C. 1985, *Ap. J. (Letters)*, **296**, L31.

Adams, N.G., Herd, C.R. and Smith, D. 1989, *J. Chem. Phys.*, submitted.

Anicich, V.G., and Huntress, W.T. Jr. 1986, *Ap.J. Suppl.*, **62**, 553.

Bates, D.R. 1950, *Phys.Rev.*, **78**, 492.

Bates, D.R. 1986, *Ap. J. (Letters)*, **308**, L45.

Bates, D.R. 1987, in *Modern Applications of Atomic and Molecular Processes* ed. A.E. Kingston (Plenum, London) pp 1-27.

Bates, D.R 1989, *Ap. J*, preprint.

Dixon, D.A., Komornicki, A. and Kraemer, W.P. 1984, *J. Chem. Phys.*, **81**, 3603.

Frisch, M.J., Schaefer, H.F.III and Binkley, J.S. 1985, *J. Phys. Chem.*, **89**, 2192.

German, K.R. 1975, *J. Chem. Phys.*, **63**, 5252.

Graedel, T.E., Langer, W.D. and Frerking, M.A. 1982, *Ap. J. Suppl.*, **48**, 321.

Green, S. and Herbst, E. 1979, *Ap. J.* **229**, 121.

Guberman, S.L, 1983, in *Physics of Ion-Ion and Electron-Ion Collisions*, eds. F. Brouillard and J.W. McGowan (Plenum, New York) pp. 167.

Herbst, E. 1978, *Ap. J.*, **222**, 508.

Herbst, E., and Leung, C.M. 1986 *M.N.R.A.S.*,**222**, 689.

Herbst, E., Green, S., Thaddeus, P. and Klemperer,W. 1977, *Ap. J.*, **215**, 503.

Ikezoe, Y., Matsuouka, S., Takebe, M., and Viggiano, A. 1987, *Gas Phase*

Ion Molecule Reactions Rate Constants through 1986. (Maruzen Company Ltd, Japan).

Irvine, W.M., Goldsmith, P.F., and Hjalmarson, A. 1987 in *Interstellar Processes*, eds. D.J. Hollenback and H.A. Thronson Jr. (Reidel, Dordrecht) pp. 561-609.

Irvine, W.M., Schloerb, F.P., Hjalmarson, A., and Herbst, E. 1985, in *Protostars and Protoplanets II* (University of Arizona Press, Tucson) pp. 579-620.

Knacke, R.F., Geballes, T.R., Roll, K.S. and Tokunaga, A.T. 1985, *Ap. J. (Letters)*, 298, L67.

Kraemer, W.P., and Hazi, A.U. 1988, *International Symposium on Dissociative Recombination*, May 29-31, 1988.

Langhoff, S.R., Jaffe, R.L., Lee, J.H., and Dalgarno, A. 1983 *Geophys. Res. Lett.*, 10, 896.

Leung, C.M., Herbst, E., and Huebner, W.F. 1984, *Ap. J. Suppl.*, 56, 231.

Matthews, H.E., and Irvine, W.M. 1985, *Ap. J. (Letters)*, 298, L61.

McIntosh, B.J., Adams, N.G., and Smith, D. 1988, *Chem. Phys. Lett.*, 148, 142.

Michels, H.H. 1989, in *Dissociative Recombination: Theory, Experiment and Applications*, eds. J.B.A. Mitchell and S.L. Guberman (World Scientific Publ. Co., New York).

Michels, H.H., and Hobbs, R.H. 1984, *Ap. J. (Letters)*, 286, L27.

Millar, T.J., and Freeman, A. 1984, *M.N.R.A.S.*, 207, 405.

Millar, T.J., and Nejad, L.A.M. 1985, *M.N.R.A.S.*, 217, 507.

Millar, T.J., Leung, C.M. and Herbst, E. 1987, *Astron. Ap.*, 183, 109.

Millar, T.J., DeFrees, D.J., McLean, A.D., and Herbst, E., 1988, *Astron. Astrophys.* 194, 250.

Minh, Y.C., Irvine, W.M., and Ziurys, L.M. 1988, *Ap. J.*, 334, 175.

Prasad, S.S. and Huntress, W.T. 1979, *Ap. J.*, 228, 123.

Prasad, S.S. and Huntress, W.T. 1980, *Ap. J.*, 239, 151.

Queffelec, J.L., Rowe, B.R., Morlais, M., Gomet, J.C. and Vallee, F. 1985, *Planet. Space Sci.*, 33, 263.

Rice, J.E., Lee, T.J. and Schaefer, H.F.III 1986, *Chem. Phys. Lett.*, 130, 333.

Rosenstock, H.M., Draxl, K., Steiner, B.W., and Herron, J.T. 1977, *J. Phys. Chem. Ref. Data*, 6, Suppl.1.

Rowe, B.R., Vallee, F., Queffelec, J.L., Gomet, J.C. and Morlais, M. 1987, *J. Chem. Phys.*, 88, 845.

Schaefer, H.F. III 1989 in "Ion and Cluster Ion Spectroscopy and Structure" Ed. J.P. Maier (Elsevier, Amsterdam) pp. 109-130.

Smith, D., and Adams, N.G. 1984, *Ap. J. (Letters)*, 284, L13.

Smith, W.H., Elmergreen, B.G. and Brooks, N.H. 1974, *J. Chem. Phys.*, 61, 2793.

Sternberg, A., Dalgarno, A., and Lepp, S. 1987, *Ap. J.*, 320, 676.

Thaddeus, P., Guelin, M., and Linke, R.A. 1981 *Ap. J. (Letters)*, 246, L41.

Thaddeus, P., Vrtilek, J.M. and Gottlieb, C.A. 1985, *Ap. J. (Letters)*, 299, 163.

Viggiano, A.A., Howorka, F., Albritton, D.L., Fehsenfeld, F.C., Adams, N.G., and Smith, D. 1980, *Ap. J.* 236, 492.

Weast, R.C. (ed.) 1985 *CRC Handbook of Chemistry and Physics* 66th Edn. (CRC Press, Boca Raton, Florida) p.

Wootten, A., Boulanger, F., Bogey, M., Combes, F., Encrenaz, P.J., Gerin, M., and Ziurys, L. 1986, *Astr. Ap.*, 166, L15.

N.G. Adams, C.R. Herd and D. Smith: School of Physics and Space Research, University of Birmingham, P.O. Box 363, Birmingham B15 2TT, U.K.

APPENDIX 7

A SELECTED ION FLOW TUBE STUDY OF THE REACTIONS OF THE PH_n^+ IONS (n = 0 TO 4) WITH SEVERAL MOLECULAR GASES AT 300K

D. SMITH, B.J. McINTOSH AND N.G. ADAMS

J.Chem.Phys., 90, 6213 (1989)

A selected ion flow tube study of the reactions of the PH_n^+ ions ($n = 0$ to 4) with several molecular gases at 300 K

David Smith, Bruce J. McIntosh, and Nigel G. Adams
School of Physics and Space Research, University of Birmingham, P.O. Box 363, Birmingham B15 2TT, England

(Received 21 October 1988; accepted 31 January 1989)

The reactions of ions in the series PH_n^+ ($n = 0$ to 4) have been studied at 300 K with CH_3NH_2, PH_3, NH_3, CH_3CCH, H_2S, C_2H_4, CH_3OH, COS, C_2H_2, O_2, H_2O, CH_4, HCN, CO_2, CO, and H_2 using a selected ion flow tube (SIFT) apparatus. The majority are fast binary reactions, the measured rate coefficients, k, being close to the respective collisional values, and for reactions involving polyatomic reactant molecules multiple product ions are observed. Most reaction mechanisms are represented in this large number of reactions including charge transfer, proton transfer, atom abstraction and especially evident is phosphorus atom insertion in which product ions such as H_nPN^+, H_nPO^+, H_nPS^+ and $H_nC_xP^+$ are formed. The reactions of the PH_n^+ ions ($n = 0$ to 2) with CO_2, CO, and H_2 proceed by the process of ternary association except for the P^+ reaction with CO_2, in which PO^+ is formed in a fast binary reaction. PH_4^+ reacts only with CH_3NH_2 and NH_3 by fast proton transfer, a process which is always rapid when it is exothermic. Upper limits to the heats of formation of HPO^+, H_2PO^+, $PC_2H_2^+$ and HCP have also been deduced from their observation as products of some of the reactions.

I. INTRODUCTION

In recent years, following our development of the selected ion flow tube (SIFT) technique,[1] we have carried out detailed studies of the reactions of positive ions in recognizable series with a number of molecular species. This work was stimulated by the growing interest in interstellar ion chemistry and the need for kinetic data to substantiate the quantitative ion-chemical models that describe the formation of the wide variety of molecules that have been detected in interstellar clouds.[2,3] Thus we have previously studied the reactions of ions in the series CH_n^+ ($n = 0$ to 4),[4-8] NH_n^+ ($n = 0$ to 4),[9] and SH_n^+ ($n = 0$ to 3),[10] with a variety of molecular species many of which are known to exist in interstellar clouds. Studies of this kind not only provide the critical kinetic data and product ion branching ratios for use in the chemical models but also have revealed, for example, interesting trends in reactivity with increasing hydrogenation of the reactant ions, insights into reaction mechanisms and thermodynamic data such as proton affinities and heats of formation of molecules (including radicals) which are difficult to obtain by other means.

The discovery of PH_3 in the Jovian atmosphere prompted Thorne *et al.*[11] to study the reactions of ions in the series PH_n^+ ($n = 0$ to 4) with H_2, CH_4, NH_3, and PH_3 and the reactions of P^+ and PH^+ with N_2, O_2, CO, CO_2, H_2O, and HCN using the ion cyclotron resonance (ICR) technique.

These studies followed up earlier ICR studies by Holtz *et al.*[12] of the reactions of PH_3 with several ionic species. The very recent discovery of PN molecules in the Orion molecular cloud[13] prompted us to study the reactions of the ions derived from phosphine, PH_n^+ ($n = 0$ to 4), with some 17 molecular species, most of which are known interstellar species, in order to explore the possible routes to the production of PN, and indeed other phosphorus-bearing molecules in interstellar clouds. However, in this paper we are not primarily concerned with the interstellar implications of the study but rather with the very interesting fundamental data provided on the kinetics, product ratios, reaction mechanisms, and thermochemistry which this survey of the reactions of PH_n^+ provides.

II. EXPERIMENTAL

The measurements were carried out in a SIFT apparatus in helium carrier gas at 300 K. This now standard technique has been described in detail previously, most recently in a review.[1] The PH_n^+ ions were created in a low pressure electron impact ion source, and after mass filtering, the P^+, PH^+, PH_2^+, PH_3^+, and PH_4^+, (the last mentioned being produced in the reactions of the primary ions with PH_3) were separately injected into the helium carrier gas at low laboratory energies (< 10 eV) to inhibit collisional dissociation of the ions. Nevertheless a small fraction (up to 10%) of the ions suffered collisional breakup at injection resulting in a small percentage of "unwanted ions" in the flow tube (P^+ from PH^+ and PH_2^+; PH^+ from PH_3^+). It is interesting to note that in the breakup of PH_2^+ and PH_3^+ the only significant products were those in which two H atoms (presumably in the form of an H_2 molecule) were formed. The slight distortion of the products and product distributions resulting from the presence of the unwanted ions were accounted for in the ion product distributions derived for each reaction. Reactant gases were introduced at a controlled flow rate into the carrier gas/ion swarm and the rate coefficients and the ion product distributions were determined in the usual manner.[1] The reactant vapors H_2O and CH_3OH were introduced as dilute mixtures in helium (2% and 5%, respectively) to inhibit dimerization and to facilitate accurate flow rate measurements. The HCN was also diluted by helium but to an uncertain dilution which we ascertained by measuring the apparent rate coefficients for the exothermic proton transfer

reactions of several ions (e.g., HCO^+ and N_2H^+) with the HCN in the mixture, reactions which invariably proceed at the collisional limiting rate for which the rate coefficient k_c can be readily calculated using the ADO theory.[14]

None of the PH_n^+ ions reacted with N_2 with a measurable rate coefficient and this offered the opportunity to use N_2 as a relaxant for any vibrational or electronic energy in the reactant ions, a technique we have used previously to ensure that metastable electronically and vibrationally excited reactant ions in SIFT experiments are relaxed to their ground state prior to reaction with the added gases.[15] No influence was apparent on the product ratios or the rate coefficients for selected test reactions, and so we judge that the reactant ions in these experiments are in their ground vibronic states (appropriate to 300 K).

III. RESULTS

All of the 16 molecular species included in this study react at varying rates with P^+, PH^+ and PH_2^+, but eight of the molecular species do not react with PH_3^+. Since only two neutrals (NH_3 and CH_3NH_2) react with PH_4^+, data on the PH_4^+ reactions are not included in the compilation of rate coefficients ($cm^3\,s^{-1}$ for two-body reactions and $cm^6\,s^{-1}$ for three-body association reactions) and percentage ion product distributions obtained for the many reactions given in Table I. Most reactions are fast binary reactions, the rate coefficients usually being essentially equal to or a significant fraction of k_c. However, exothermic binary reaction channels are not available for most molecules in the lower part of the table (HCN to H_2) and then the much slower (less efficient) process of ternary association is observed in several reactions. For these reactions both the effective binary rate coefficient at a helium pressure of 0.48 Torr and the equivalent ternary association rate coefficient are given. The reactant molecules are listed in Table I in order of increasing ionization energy from CH_3NH_2 (ionization energy is 8.97 eV as given below the molecule) to H_2 (ionization energy 15.43eV). Also given are the proton affinities above each reactant molecule given in units of kcal mol^{-1} as obtained from the accepted compilations.[16,17] Similarly, the recombination energies are given in eV below each reactant ion and the detachment energy of protons from the ions (which is equivalent to the proton affinity of the PH_{n-1} neutral species) is given above each ion in kcal mol^{-1}, except, of course, for P^+ ions. The proton affinities of P, PH, and PH_2 were obtained from Ref. 18. The value given for PA(PH_3) is the value obtained experimentally from proton transfer studies.[16] Thus from a glance at Table I, it is clear for which reactions charge transfer and proton transfer are energetically allowed. Also included in Table I are the collisional rate coefficients for the PH_2^+ reactions (which are essentially the same as those for the P^+, PH^+, and PH_3^+ reactions) calculated using the ADO theory.[14]

Typical data samples from SIFT experiments have been given before in other papers,[1,9] so here we give only one example to illustrate an extension to the usual analysis. In Fig. 1(a) the data are presented for the reaction

$$P^+ + C_2H_2 \rightarrow PC_2H^+ + H \quad (95\%) \qquad (1a)$$

$$\xrightarrow{He} PC_2H_2^+ \quad (5\%) \qquad (1b)$$

in the form of a semilog plot of the P^+ reactant ion count rate and the count rates of the product ions PC_2H^+ and $PC_2H_2^+$ as a function of the flow rate of the reactant gas C_2H_2. The slope of the linear P^+ decay provides a value for the overall rate coefficient for the reaction (1), i.e., k_1. In Fig. 1(b) the percentages of the product ions are plotted as a function of the C_2H_2 flow rate to obtain an ion product distribution in the normal manner.[1,9] (Note that the minority product is adduct ion $PC_2H_2^+$, which is presumably formed in a ternary collision between P^+, C_2H_2 and a He atom; we discuss the $PC_2H_2^+$ ion later.) During the study of this reaction, and indeed several other reactions in this series, it was clear that the product ion PC_2H^+ reacted rapidly with C_2H_2 as is obvious in Fig. 1(a) from the decrease in the PC_2H^+ count rate with increasing C_2H_2 flow at the larger flows. The reaction occurring is

$$PC_2H^+ + C_2H_2 \rightarrow PC_4H_2^+ + H \qquad (2a)$$

$$\xrightarrow{He} PC_4H_3^+. \qquad (2b)$$

Note that an adduct ion [channel (2b)] is formed in this reaction also. The curve of the PC_2H^+ count rate [PC_2H^+] versus C_2H_2 flow rate (giving rise to a C_2H_2 number density [N]) can be described by an expression of the form[19]

$$[PC_2H^+]_N = [P^+]_0 \frac{\alpha k_1}{(k_2 - k_1)} \times [\exp(-k_1[N]t) - \exp(-k_2[N]t)],$$

where $[P^+]_0$ is the count rate of P^+ primary ions at zero flow (zero N) of C_2H_2, k_1 and k_2 are the rate coefficients for reactions (1) and (2), α is a coefficient which accounts both for mass discrimination between P^+ and PC_2H^+ in the quadrupole detection system and for the nonunity branching ratio in reaction (1) and t is the reaction time given by the quotient of the length of the flow tube reaction zone and the ion swarm flow velocity. Since $[P^+]_0$, k_1 and t are known then by fitting the [PC_2H^+] versus [N] data using an iterative nonlinear least-squares procedure,[20] a value for k_2 (and indeed α) can be obtained. The computer generated fit to the experimental data points is shown in Fig. 1(c) which yields $k_2 = 9.1 \times 10^{-10}$ $cm^3\,s^{-1}$ and $\alpha = 0.64$. This approach to rate coefficient determinations is useful when the secondary ions (in this case PC_2H^+) cannot be formed in an ion source and injected into the SIFT in the usual way or when it is necessary to study the reactivity of a product ion of a specific ion-molecule reaction.

A similar approach to data reduction can be taken to determine the rate coefficient for a primary reaction in which a primary product or secondary product ion has the same mass/charge ratio as the primary reactant ion. Such is the case for the reactions of PH^+ with CH_3NH_2 (secondary product ion $CH_3NH_3^+$, see Table I) and PH_2^+ with CH_3OH (secondary product ion $CH_3OH_2^+$). In this case the distorted (nonlinear) decay plot of the reactant ion count rate is fitted to an appropriate expression[19] and provides values for the primary and secondary (where appropriate) reaction

TABLE I Rate coefficients and ion product distributions for the reactions of P^+, PH^+, PH_2^+, and PH_3^+ with a series of molecules at 300 K. The reactant molecules are listed in order of increasing ionization energy and these energies are given below each molecule in eV, above each molecules is given its proton affinity in kcal mol^{-1}. The proton detachment energies (kcal mol^{-1}) and recombination energies (eV) are given above and below the reactant ions, respectively. The measured binary rate coefficient in $cm^3 s^{-1}$ for each reaction is given in the form 1.3(− 9) (see the $P^+ + CH_3NH_2$ reaction) which means 1.3×10^{-9} $cm^3 s^{-1}$. Also given are the collisional rate coefficients k_c in $cm^3 s^{-1}$ as calculated by the Langevin or ADO theories (Ref. 14) as appropriate (k_c is essentially the same for all of the ions PH_n^+, $n = 0$ to 4). Ternary association rate coefficients in units of $cm^6 s^{-1}$ obtained at a fixed pressure of 0.48 Torr are indicated by an asterisk. The percentage of each product ion is given in parentheses after the ion. PH_4^+ ions reacted only with CH_3NH_2 and NH_3 (see the text) and so these data are not included in this table.

PA(kcal/mol)			149.8	160.2	169.5
	k_c	P^+	PH^+	PH_2^+	PH_3^+
IP(eV)	($cm^3 s^{-1}$)	10.486	10.18	9.82	9.87
214.1 CH_3NH_2 8.97	1.73(− 9)	1.3(− 9) $CH_2NH_2^+$ (68) PNH_3^+ (32)	1.8(− 9) $CH_2NH_2^+$ (38) PNH_3^+ (16) PNH_4^+ (46)	1.7(− 9) $CH_2NH_3^+$ (62) $CH_3NH_2^+$ (38)	1.9(− 9) $CH_3NH_3^+$
188.6 PH_3 9.98	1.37(− 9)	1.2(− 9) PH_2^+ (26) P_2H^+ (62) $P_2H_2^+$ (12)	1.3(− 9) PH_3^+ (18) PH_4^+ (9) P_2^+ (12) $P_2H_2^+$ (53) $P_2H_3^+$ (8)	1.1(− 9) PH_4^+ (5) P_2H^+ (17) $P_2H_3^+$ (78)	1.1(− 9) PH_4^+
204.0 NH_3 10.166	1.93(− 9)	1.8(− 9) NH_3^+ (52) PNH_3^+ (48)	2.1(− 9) NH_4^+ (19) PNH_2^+ (28) PNH_3^+ (53)	2.0(− 9) NH_4^+ (19) PNH_3^+ (81)	2.3(− 9) NH_4^+
182 CH_3CCH 10.36	1.55(− 9)	1.7(− 9) $C_2H_3^+$ (42) PCH_2^+ (52) $PC_3H_2^+$ (6)	1.7(− 9) $C_2H_4^+$ (19) $C_3H_3^+$ (17) $PC_2H_2^+$ (64)	1.6(− 9) $C_2H_3^+$ (43) PCH_2^+ (44) PCH_4^+ (7) $PC_3H_4^+$ (6)	1.6(− 9) $C_2H_3^+$ (91) PCH_2^+ (9)
170.2 H_2S 10.47	1.44(− 9)	1.4(− 9) H_2S^+ (31) PS^+ (12) HPS^+ (57)	1.5(− 9) H_2S^+ (9) HPS^+ (64) H_2PS^+ (27)	1.5(− 9) H_2PS^+	1.0(− 9) H_2S^+
162.6 C_2H_4 10.51	1.24(− 9)	1.2(− 9) $PC_2H_2^+$	1.2(− 9) PCH_2^+ (30) $PC_2H_3^+$ (70)	1.2(− 9) PCH_2^+ (12) $PC_2H_4^+$ (88)	4.7(− 10) C_2H_4 PH_3^+ Press. indep. $> 4.6(- 26)^*$
181.9 CH_3OH 10.85	1.88(− 9)	1.4(− 9) HPO^+	1.9(− 9) H_2PO^+	2.0(− 9) CH_2OH^+ (65) PCH_4^+ (8) H_2PO^+ (27)	1.9(− 9) $CH_3OH_2^+$
151 COS 11.184	1.38(− 9)	1.1(− 9) PO^+ (38) PS^+ (62)	1.3(− 9) HPS^+	9.9(− 10) H_2PS^+	4.6(− 11) H_3PS^+
153.3 C_2H_2 11.41	1.12(− 9)	1.3(− 9) PC_2H^+ (95) $PC_2H_2^+$ (5)	1.3(− 9) $PC_2H_2^+$	1.4(− 9) $PC_2H_2^+$	5.8(− 10) $PC_2H_3^+$
100.9 O_2 12.059	7.40(− 10)	5.6(− 10) PO^+	5.4(− 10) PO^+	7.8(− 11) PO^+	< 2(− 13)
165.1 H_2O 12.62	2.07(− 9)	5.5(− 10) PO^+ (10) HPO^+ (90)	1.2(− 9) HPO^+ (62) H_2PO^+ (17) H_3O^+ (21)	4.9(− 10) H_2PO^+ (67) H_3O^+ (33)	< 1(− 13)

TABLE I (continued).

PA(kcal/mol)			149.8	160.2	169.5
	k_c	P^+	PH^+	PH_2^+	PH_3^+
IP(eV)	($cm^3 s^{-1}$)	10.486	10.18	9.82	9.87
132.0	1.15(− 9)	9.6(− 10)	1.1(− 9)	1.1(− 9)	< 1(− 13)
CH_4		PCH_3^+	PCH_3^+ (95)	PCH_4^+	
12.62			PCH_4^+ (5)		
171.4	2.81(− 9)	1.4(− 10)	1.7(− 9)	1.4(− 9)	2.6(− 9)
HCN		HCN P^+	H_2CN^+ (95)	H_2CN^+ (72)	H_2CN^+
13.59			HCN PH^+ (5)	HCN PH_2^+ (28)	
		1.2(− 27)*	> 7.3(− 28)*	> 3.4(− 27)*	
130.9	8.68(− 10)	4.6(− 10)	8.6(− 12)	7.5(− 12)	< 1(− 13)
CO_2		PO^+	$CO_2 PH^+$	$CO_2 PH_2^+$	
13.769			5.9(− 28)*	5.1(− 28)*	
141.6	8.40(− 10)	3.5(− 13)	1.0(− 12)	2.9(− 12)	< 1(− 13)
CO		$CO P^+$	$CO PH^+$	$CO PH_2^+$	
14.013		2.4(− 29)*	7.0(− 29)*	1.9(− 28)*	< 8(− 30)*
101.3	1.53(− 9)	1.3(− 13)	4.3(− 13)	1.1(− 12)	< 1(− 13)
H_2		PH_2^+	PH_3^+	PH_4^+	
15.43		7.5(− 30)*	2.4(− 29)*	6.7(− 29)*	< 6(− 30)*

rate coefficients and α. The rate coefficients given in Table I for the PH^+ and PH_2^+ reactions given immediately above were obtained using this procedure.

IV. DISCUSSION AND CONSIDERATIONS OF INDIVIDUAL REACTIONS

The recombination energies of the PH_n^+ ions are relatively small and thus charge transfer is energetically allowed in only a few reactions. P^+ can charge transfer only with the first five molecules in Table I, PH^+ with the first three and PH_2^+ and PH_3^+ with only one, CH_3NH_2. Proton transfer is energetically favorable in about half of the reactions. Note that even when charge transfer and proton transfer are energetically allowed they do not always occur. The majority of the reactions in this wide series lead to the production of ions incorporating phosphorus bonded to carbon, nitrogen, oxygen or sulfur as appropriate.

A. Reactions of each primary species

(i) P^+ reactions: Even when charge transfer is energetically allowed (for CH_3NH_2, PH_3, NH_3, CH_3CCH, H_2S) it is the majority channel in only one case (the NH_3 reaction), although the $CH_2NH_2^+$ (with H_2) and the $C_2H_3^+$ (with CH) could be the products of dissociative charge transfer in the CH_3NH_2 and CH_3CCH reactions, respectively. In the large majority of the reactions the P atom is incorporated into the product ions with the release of stable neutral products (e.g., H_2, CO) or atomic radicals (e.g., H, O).

(ii) PH^+ reactions: Although proton transfer is energetically allowed for 10 of the 16 molecules it apparently occurs for only five (PH_3, NH_3, H_2S, H_2O, and HCN) and then only as a minority channel in all except the HCN reaction, for which there are no other exothermic binary channels. Most of these reactions are rapid and with often more than one product channel. Clearly, other reaction mechanisms are dominating proton transfer even when it is energetically allowed. In the proton transfer process

$$PH^+(^2\Pi) + X \rightarrow P(^4S_{3/2}) + XH^+, \qquad (3)$$

the X and XH^+ are invariably singlets and so spin inversion is required which presumably will tend to inhibit such reactions, although for the CH_3NH_2, PH_3, and NH_3 reactions, proton transfer is sufficiently exothermic for the ^2D state of the P atoms to be accessed and then spin inversion does not occur. It is perhaps significant, therefore, that although proton transfer does occur in the HCN reaction which is quite exothermic (> 20 kcal mol^{-1}), but for which spin inversion would be required, the rate coefficient for the reaction is significantly less than k_c (see Table I).

It should be noted that there is likely to be an excited $^4\pi$ state of PH^+ which is only slightly more energetic than the $^2\pi$ ground-state (by analogy with NH^+ for which there is a $^4\pi$ state only ~80 meV above the ground state[21]) and it is possible that an equilibrium concentration of $PH^+(^4\pi)$ may be present in the PH^+ ion swarm. If this were the case, it would not significantly effect the energetics of the PH^+ reactions but it could influence reactions because of spin restrictions. Note that it is not inconceivable that the 9% H_2S^+ product in the PH^+/H_2S reaction may be due to the reaction of $PH^+(^4\pi)$.

(iii) PH_2^+ reactions: Proton transfer is energetically allowed in nine reactions but is only observed in five (CH_3NH_2, PH_3, NH_3, H_2O, and HCN) and, again, it is a

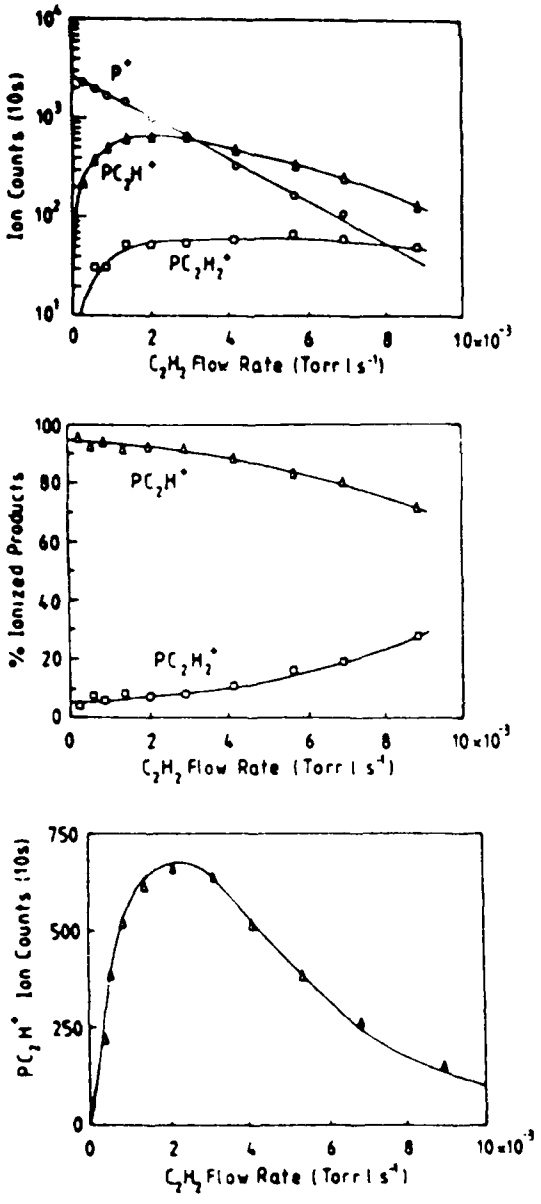

FIG. 1. Sample plots taken from this SIFT study of PH_n^+ reactions at 300 K. (a) Data obtained for the reaction of P^+ ions with C_2H_2, the P^+ primary ion (○) and the product ions PC_2H^+ (△) and $PC_2H_2^+$ (□) count rates (10 s sampling period) in semilogarithmic form are plotted against the C_2H_2 flow rate. The rate coefficient for the primary reaction is obtained from the slope of the linear plot. (b) The percentages of the product ion count rates are plotted as a function of the C_2H_2 flow rate and extrapolation to zero C_2H_2 flow provides the ion product distribution for the reaction (see Table I). (c) The count rate of the PC_2H^+ product ion given in (a) is plotted separately as a function of C_2H_2 flow rate. The continuous curve through the data points has been fitted according to the procedure outlined in the text and provides a value for the rate coefficient for the secondary reaction of PC_2H^+ with C_2H_2 of 9.1×10^{-10} cm^3 s^{-1}.

minority channel in each case except for HCN and the rate coefficient is only about half of k_c in this case. Again, spin inversion is required for proton transfer from the singlet PH_2^+ ($^1A_1$) to singlet state molecules producing singlet state ions and triplet $PH(^3\Sigma^-)$.

(iv) PH_3^+ reactions: Where proton transfer is energetically allowed (in seven reactions) it occurs essentially as the only product (the only exception is the CH_3CCH reaction in which an additional minor (9%) channel is observed) at or very close to the collision rate. So there are apparently no barriers to proton transfer from PH_3^+ and the production of the PH_2 radical and the closed shell (singlet) ions. Note that the observation that proton transfer occurs to H_2S but not to H_2O is consistent with the excepted value for the proton affinity of PH_2 of 169.5 kcal mol^{-1}.[18] In only three other reactions, the COS, C_2H_2, and C_2H_4 reactions, do new chemical bonding arrangements form. In the first of these, S-atom abstraction from the COS results, leaving the stable CO neutral and in the second the $PC_2H_3^+$ ion is produced which we discuss later in Sec. IV B (iii) together with the similar ion $PC_2H_2^+$. For the reaction between PH_3^+ and C_2H_4 association occurs with a very large rate coefficient; no variation of the effective binary rate coefficient with pressure was apparent and so only a lower limit to the ternary association rate coefficient can be given (Table I). We have noted in previous studies[22] that when a slightly endothermic (< 5 kcal mol^{-1}) binary channel is available then association is often very rapid and have argued that the occurrence of this endothermic step within the excited intermediate complex prolongs the lifetime of the complex and thus facilitates collisional association. This so-called "endothermic trapping" could be occurring here, since the proton transfer between PH_3^+ and C_2H_4 is endothermic by only about 6 kcal mol^{-1}.

Unlike P^+, PH^+, and PH_2^+, the radical PH_3^+ ions show little propensity to associate with those molecules in which no binary channels are available. This is presumably because the outer shell of the central P has a deficiency of only one electron and cannot act as a lone pair acceptor.

B. Reactions of individual reactant molecular species

Comparisons can be made of the analogous pairs of reactions, e.g., NH_3/PH_3, H_2S/H_2O, COS/CO_2, etc., and it is interesting to compare these by inspection of Table I. However, here we choose to briefly discuss the reactions in the following groupings although these groupings are artificial to a degree: (i) PH_3, (ii) N-containing molecules, (iii) Hydrocarbons, (iv) sulphur-containing molecules, (v) oxygen-containing molecules, and (vi) CO_2, CO, and H_2.

(i) PH_3 reactions: Ions involving P-P bonds are readily formed with the hydrogen deficient ions ($P_2H_n^+$, $n<3$) being most evident. All of the $P_2H_n^+$ ($n = 0$ to 3) react further with PH_3 (apparently by proton transfer producing PH_4^+) with very large rate coefficients (as indicated by the fitting of product ion curves as described in Sec. III). Values of $PA(P_2) \sim 158$ kcal mol^{-1} (Ref. 23) and $PA(P_2H_2) = 179$ kcal mol^{-1} (Ref. 24) derived from *ab initio* calculations would make proton transfer from P_2H^+ and $P_2H_3^+$ to PH_3 exothermic which is what we observe. The reactions of PH_n^+ ($n = 0$ to 4) with PH_3 have been studied also using the ICR technique[11]; some differences are evident between these data and the present SIFT results. Proton transfer channels were not observed in the PH^+ and PH_2^+ reactions in the ICR experiments. The ICR and SIFT rate coefficients for these reactions are reasonably consistent.

(ii) CH_3OH, H_2O, and HCN reactions: The propensity to form P-N bonds is very apparent in these reactions. They are all very fast reactions, even those association reactions of HCN which produce $HCNP^+$, $HCNPH^+$, and $HCNPH_2^+$ ions. The ions PNH_2^+ and PNH_3^+ are especially evident as product ions (as are the analogous $P_2H_2^+$ and $P_2H_3^+$ ions in the PH_3 reactions), this presumably being an indicator of the stability of these ions and the strength of the P-N bond. The rate coefficients and product distributions obtained for the NH_3 reactions in the ICR experiment[11] are similar to the SIFT results except that charge transfer between P^+ and NH_3 was not observed in the ICR experiment.

(iii) CH_3CCH, C_2H_4, C_2H_2, and CH_4 reactions: In all of the reactions with C_2H_4, C_2H_2, and CH_4 incorporation of a P atom into the product ion resulted with formation of P–C bonds. This also occurred, but not exclusively, in the CH_3CCH reactions (see Table I). The ion PCH_2^+, produced in some of the CH_3CCH and CH_4 reactions, is presumably protonated HCP (*ab initio* calculations indicate protonation occurs exclusively onto the C atom[25]). PCH_3^+ and PCH_4^+ [expected to be $CH_2 = PH_2^+$, i.e., P protonated $CH_2 = PH$ (Ref. 25)] are also efficiently formed in some of these CH_3CCH amd CH_4 reactions. In the reactions with the molecules containing two carbon atoms, the C–C bond is generally retained with P incorporation. All of these reactions have large rate coefficients, the ions $PC_2H_2^+$, $PC_2H_3^+$, and $PC_2H_4^+$ being major products. The facile production of $PC_2H_2^+$ suggests that it has a relatively low heat of formation and that it indeed has the predicted cyclic (aromatic) structure, i.e.,

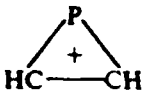

(Ref. 26). The production of the $C_2H_n^+$ ions in the CH_3CCH reactions presumably results in the elimination of the stable molecule HCP according to

$$PH_{n-1}^+ + CH_3CCH \rightarrow C_2H_n^+ + HCP \quad (n = 3 \text{ to } 5). \quad (4)$$

The ICR results[11] for the CH_4 reactions are similar to the present SIFT results except that a smaller value for the rate coefficient of the PH_2^+ reaction of 5.8×10^{-10} cm^3 s^{-1} was obtained in the ICR study.

(iv) H_2S and COS reactions: P-S bond formation was facile in these reactions, HPS^+ and H_2PS^+ being particularly evident. The COS reactions proceeded with the elimination of CO, thus

$$PH_n^+ + COS \rightarrow H_nPS^+ + CO \quad (5)$$

In only the P^+ reaction was a second channel evident ($PO^+ + CS$), an observation which we use to place a limit on the $\Delta H_f^\circ(PO^+)$ (see Sec. IV C).

(v) CH_3OH, O_2, and H_2O reactions: Production of P–O bonds in these reactions is facile. PO^+ ions are the exclusive products of the O_2 reactions, although the PH_2^+ reaction, in which H_2O is the likely neutral product, has an unusually small rate coefficient. Since the reaction is exothermic, this presumably indicates the presence of an activation barrier as does the absence of any of the three exothermic channels available for the reaction of $PH_3^+ + O_2$ (namely, to produce PO^+, HPO^+, and H_2PO^+). HPO^+ and H_2PO^+ are major product ions in the CH_3OH and H_2O reactions.

(vi) CO_2, CO, and H_2 reactions: PH_3^+ did not react at a measurable rate with any of these three molecules. The reactions of PH^+ and PH_2^+ with CO_2 to produce HPO^+ and H_2PO^+, respectively, are exothermic by at least 12 kcal mol^{-1} but these channels did not occur, instead these reactions proceeded via relatively slow ion/molecule association. The ternary association rate coefficients increase as the polyatomicity of the ion increases for the CO and H_2 reactions in accordance with the idea that a greater number of internal modes are available in which to share the binding energy thus prolonging the lifetime of the excited complex and increasing the probability of collisional stabilization.[22] In recent experiments, we have shown that these association reactions proceed much faster at 80 K in accordance with expectations. This work has some relevance to astrochemistry and this will be discussed in more detail in a subsequent paper.

C. Thermochemical limits derived from these studies

Detailed reaction surveys such as that summarized in Table I contain a wealth of "hidden" information. The observed production of an ionic species in a reaction in some cases can place a limit on its heat of formation, its proton affinity, etc., as we have described [see Sec. IV A (iii)]. Thus, we have derived limits for the heats of formation of HPO^+, H_2PO^+, $PC_2H_2^+$, and HCP. These data are given in Table II together with the reactions which were exploited to derive them.

V. CONCLUDING REMARKS

This detailed study of the reactions of PH_n^+ ions has not only provided a great deal of kinetic data but also some insight into the nature of these ion–molecule reactions. The propensity for phosphorus to form bonds with O, N, C, and S is very evident. Several particular ionic species are obvious as products of the reactions, notably ions like H_nPN^+, H_nPO^+, H_nPS^+, and $H_nC_mP^+$ and from their observation as products we have been able to derive thermodynamic quantities (heats of formation and proton detachment energies) for some. Regrettably, the structures of most of these ions are not known with any certainty, and we can only spec-

TABLE II. Estimates and limits of the heats of formation ΔH° of the ionic and neutral species indicated, obtained from consideration of the kinetics and energetics of the reactions shown in each case.

Reaction[a]	Deduction
$P^+ + H_2O \rightarrow HPO^+ + H$	$\Delta H_f^\circ(HPO^+) < 207$ kcal mol^{-1}
$PH^+ + H_2O \rightarrow H_2PO^+ + H$	$\Delta H_f^\circ(H_2PO^+) < 183$ kcal mol^{-1}
$PH^+ + C_2H_2 \rightarrow PC_2H_2^+ + H$	$\Delta H_f^\circ(PC_2H_2^+) < 295$ kcal mol^{-1}
$PH^+ + CH_3CCH \rightarrow C_2H_4^+ + HCP$	$\Delta H_f^\circ(HCP) < 81$ kcal mol^{-1} [b]

[a] ΔH_f° of neutral species from Refs. 16 and 27.
[b] JANAF (Ref. 27) estimates $\Delta H_f^\circ(HCP)$ to be 40 ± 15 kcal mol^{-1}.

ulate on these. However, it seems certain that the ion $PC_2H_2^+$ is probably cyclic and stable. Structural calculations for some of the product ions discussed above would be valuable.

If ions such as those mentioned above are formed in interstellar clouds by similar ion chemistry to that discussed here then they could be the precursors of neutral molecules such as PN which has recently been detected in the Orion molecular clouds[13] and others such as HCP, PO, PS, and PC_2H which, as yet, have not been detected. We discuss the formation of phosphorus-bearing molecules in interstellar clouds in a subsequent paper.

ACKNOWLEDGMENTS

Our thanks are due to the SERC and the USAF for providing financial support of this work.

[1] D. Smith and N. G. Adams, Adv. At. Mol. Phys. **24**, 1 (1987).
[2] E. Herbst and C. M. Leung, Mon. Not. R. Astron. Soc. **222**, 689 (1986).
[3] D. Smith, Philos. Trans. R. Soc. London Ser. A **323**, 269 (1987); **324**, 257 (1988).
[4] D. Smith and N. G. Adams, Int. J. Mass Spectrom. Ion Phys. **23**, 123 (1977).
[5] D. Smith and N. G. Adams, Chem. Phys. Lett. **47**, 145 (1977).
[6] N. G. Adams and D. Smith, Chem. Phys. Lett. **47**, 383 (1977).
[7] D. Smith and N. G. Adams, Chem. Phys. Lett. **54**, 530 (1978).
[8] N. G. Adams and D. Smith, Chem. Phys. Lett. **79**, 563 (1981).
[9] N. G. Adams, D. Smith, and J. F. Paulson, J. Chem. Phys. **72**, 288 (1980).
[10] D. Smith, N. G. Adams, and W. Lindinger, J. Chem. Phys. **75**, [illegible] (1981).
[11] L. R. Thorne, V. G. Anicich, and W. T. Huntress, Chem. Phys. Lett. **98**, 162 (1983).
[12] D. Holtz, J. L. Beauchamp, and J. R. Eyler, J. Am. Chem. Soc. **92**, 7045 (1970).
[13] L. M. Ziurys, Astrophys. J. **321**, L81 (1987).
[14] T. Su and M. T. Bowers, in *Gas Phase Ion Chemistry*, edited by M. T. Bowers (Academic, New York, 1979), Vol. 1, p. 83.
[15] D. Smith, N. G. Adams, K. Giles, and E. Herbst, Astron. Astrophys. **200**, 191 (1988).
[16] S. G. Lias, J. F. Liebman, and R. D. Levin, J. Phys. Chem. Ref. Data **13**, 695 (1984).
[17] S. G. Lias, J. F. Liebman, and R. D. Levin, J. Phys. Chem. **17**, Suppl. 8 (1988).
[18] J. Berkowitz, L. A. Curtiss, S. T. Gibson, J. P. Greene, G. L. Hillhouse, and J. A. Pople, J. Chem. Phys. **84**, 375 (1986).
[19] J. Glosik, A. B. Rakshit, N. D. Twiddy, N. G. Adams, and D. Smith, J. Phys. B **11**, 3365 (1978).
[20] P. R. Bevington, *Data Reduction and Error Analysis for the Physical Sciences* (McGraw-Hill, New York, 1969), p. 237.
[21] E. Herbst, D. J. DeFrees, and A. D. McLean, Astrophys. J. **321**, 898 (1987).
[22] E. E. Ferguson, D. Smith, and N. G. Adams, J. Chem. Phys. **81**, 742 (1984).
[23] M. T. Nyugen, Chem. Phys. Lett. **146**, 524 (1988).
[24] M. T. Nyugen, Chem. Phys. Lett. **135**, 73 (1987).
[25] L. L. Lohr, H. B. Schlegel, and K. Morokuma, J. Phys. Chem. **88**, 1981 (1984).
[26] J. R. Bews and C. Glideweil, J. Mol. Struct. **104**, 105 (1983).
[27] D. R. Stull and H. Prophet, Natl. Stand. Ref. Data Ser. Natl. Bur. Stand. **37** (1971).

APPENDIX 8

REACTIONS OF Kr^+, Kr_2^+, Xe^+ AND Xe_2^+ IONS WITH SEVERAL MOLECULAR GASES AT 300K

K. GILES, N.G. ADAMS AND D. SMITH

J.Phys.B., 22, 873 (1989)

J. Phys. B: At. Mol. Opt. Phys. 22 (1989) 873-883. Printed in the UK

Reactions of Kr^+, Kr_2^+, Xe^+ and Xe_2^+ ions with several molecular gases at 300 K

Kevin Giles, Nigel G Adams and David Smith

School of Physics and Space Research, University of Birmingham, PO Box 363, Birmingham B15 2TT, UK

Received 30 August 1988

Abstract. The reactions of the atomic ions Kr^+ and Xe^+ and the molecular ions Kr_2^+ and Xe_2^+ have been studied with several molecular gases at 300 K using a selected ion flow tube (SIFT). In some of the atomic ion reactions differential reactivity was observed between the spin-orbit states ($^2P_{3/2}$, $^2P_{1/2}$) of the ions and, when this was so, the lower energy $^2P_{3/2}$ state of both ions was observed to react more rapidly than the $^2P_{1/2}$ state, in accordance with the findings of previous work. Whereas charge transfer was the only reaction mechanism observed for the atomic ions, both charge transfer and inert gas/reactant molecule switching were observed in several reactions of the molecular ions, the latter process producing ions such as $KrCH_4^+$ and $XeC_2H_2^+$. By considering the kinetics of the near-thermoneutral charge transfer reactions of Kr_2^+ with N_2O and Xe_2^+ with COS, the dissociation energies of the molecular ions have been determined to be ≤ 1.15 eV for Kr_2^+ and ≤ 1.05 eV for Xe_2^+, both these upper-limit values being in good agreement with previous experimental and theoretical values.

1. Introduction

The reactions of the rare gas singly charged atomic ions He^+, Ne^+ and Ar^+ have been studied extensively at thermal energies (see the compilation of rate coefficients and ionic reaction products given by Ikezoe *et al* (1987)). The large recombination energies of these ions ensure that charge transfer reactions can occur with almost any molecular species, and in most cases dissociative charge transfer is allowed also. The ground electronic states of both Ne^+ and Ar^+ are split due to spin-orbit coupling; the difference in the energies of these states ($^2P_{3/2}$ (lower state) and $^2P_{1/2}$) is very small for Ne^+ (i.e. 0.097 eV) and differently reacting states of Ne^+ have not been observed. The difference in the energies of the $Ar^+(^2P_{3/2})$ and $Ar^+(^2P_{1/2})$ ions is also small (0.178 eV) but in this case a difference in the reactivity of the spin-orbit states of Ar^+ has been observed in experiments carried out at suprathermal energies utilising TESICO (Tanaka *et al* 1981), TEPICO (Guyon *et al* 1986) and crossed beam (Liao *et al* 1986) techniques. In addition there exists some evidence from one thermal energy flow tube experiment for differently reacting forms of Ar^+ ions.

The spin-orbit splittings of the ground electronic states of Kr^+ and Xe^+ are relatively large at 0.666 eV and 1.306 eV respectively and the recombination energies are relatively small ($Kr^+(^2P_{3/2}) = 13.999$ eV, $Xe^+(^2P_{3/2}) = 12.130$ eV), and so differences in the reactivity of the spin-orbit states for both ions are more likely. A study of the reactions of Kr^+ and Xe^+ with several molecular gases at 300 K in a selected ion flow tube (SIFT)

0953-4075/89/060873+11$02.50

some years ago showed that the $\frac{3}{2}$ and $\frac{1}{2}$ states do indeed react at very different rates with some gases, and the rate coefficients and the ionic products of the separate spin-orbit states were determined (Adams *et al* 1980). Charge transfer, as expected for rare gas ions, was the only process observed except for the reaction with H_2 for which charge transfer is quite clearly endothermic for both states of Kr^+ and Xe^+. However, reaction did occur between both Kr^+ states and H_2 to produce KrH^+ ions. The ionisation energies of CH_4(12.62 eV) and N_2O(12.89 eV) lie between the recombination energies of the $Xe^+(^2P_{3/2})$ and $Xe^+(^2P_{1/2})$ ions and so charge transfer with the lower energy $\frac{1}{2}$ state ion cannot occur; charge transfer was observed between the $Xe^+(^2P_{1/2})$ ions and CH_4 and N_2O. The most remarkable result of these experiments was that when a difference in the reactivity of the spin-orbit states of either Kr^+ or Xe^+ was observed then invariably the lower-energy $^2P_{3/2}$ ions reacted more rapidly (the rate coefficients and ionic products of some of these reactions are listed in table 1). This work by Adams *et al* (1980) was followed up by Jones *et al* (1982) who explained the difference in the reactivities of the spin-orbit states of Kr^+ by considering the correlation between reactant and product states, the approach taken to explain why the reactivity of the $^2P_{3/2}$ states of some neutral species, including Br and I atoms (isoelectronic with Kr^+ and Xe^+ ions), is often greater than the $^2P_{1/2}$ states (see the recent review by Dagdigian and Campbell (1987)).

The reactivities of the singly charged molecular ions He_2^+, Ne_2^+ and Ar_2^+ have been extensively studied and these, like their singly charged atomic counterparts, also are very reactive (see, for example, the papers by Bohme *et al* (1970), Collins and Lee (1980) and the papers cited in the compilation by Ikezoe *et al* (1987)). The recombination energies of these ions differ from those of their ground state atomic analogues by the dissociation energies, D_0, of the molecular ions ($D_0(He_2^+)$ = 2.45 eV (Khan and Jordan 1986), $D_0(Ne_2^+)$ = 1.31 eV, $D_0(Ar_2^+)$ = 1.30 eV (Michels *et al* 1978)) and are quite large. Charge transfer between these ions and most gases is therefore facile. The recombination energies of Kr_2^+ and Xe_2^+ are lower (about 13 eV and 11 eV respectively, see §3.2) and so they are expected to react with fewer species, but to our knowledge no studies of the reactivities of these molecular ions have been carried out.

We report in this paper the results of a study of the reactions of $Kr^+(^2P_{3/2}, ^2P_{1/2})$, $Xe^+(^2P_{3/2}, ^2P_{1/2})$, $Kr_2^+(A\,^2\Sigma_{1/2}^+)$ and $Xe_2^+(A\,^2\Sigma_{1/2}^+)$ with several molecular gases at 300 K using the SIFT technique. The atomic ion studies extend those of Adams *et al* (1980) to involve several more reactant gases. Charge transfer, as expected, commonly occurs but, additionally, the molecular ion reactions reveal that rare gas atom/reactant molecule exchange (switching) occurs in several reactions. From the results of this study, the recombination energies of the ground states of the Kr_2^+ and Xe_2^+ ions and their dissociation energies have been determined and are compared with previous experimental and theoretical determinations.

2. Experimental details

The SIFT technique has been described previously, most recently in a detailed review paper (Smith and Adams 1987). Briefly, ions are generated in an ion source, selected according to their mass-to-charge ratio using a quadrupole mass filter and injected into helium carrier gas (at a pressure of typically 0.5 Torr) which is constrained to flow along a stainless steel tube by the action of a large mechanical pump. Reactant gases are introduced into the carrier gas/ion swarm and the reactant ions and the

Table 1. A compilation of the rate coefficients (in $cm^3 s^{-1}$, e.g. for the $Kr^+(^2P_{3/2})$ reaction with NH_3, the rate coefficient is given as 7.0(−10) which is 7.0×10^{-10} $cm^3 s^{-1}$) and the product ion distributions (percentages given in parentheses after the particular product ion, unless only a single product ion is observed) for the reactions of both spin-orbit states of Kr^+ and Xe^+ and the reactions of Kr_2^+ and Xe_2^+ with 13 molecular gases, determined in a SIFT apparatus at 300 K. The recombination energies of the ion species and the ionisation energies of the reactant molecules in electron volts are given below each species. Also indicated, in square brackets, are the 300 K collisional rate coefficients for each reaction (for references see text). For the sake of completeness, the previous data due to Adams *et al* (1980) for the reactions of Kr^+ and Xe^+ with NH_3, H_2S, COS, O_2, CH_4, N_2O, CO_2 and CO are also included. Where no reaction is observed the rate coefficient is indicated as < 1(−12) $cm^3 s^{-1}$.

	Kr^+		Kr_2^+	Xe^+		Xe_2^+
Reactant molecule	$^2P_{3/2}$ 14.00	$^2P_{1/2}$ 14.67	12.87	$^2P_{3/2}$ 12.13	$^2P_{1/2}$ 13.44	11.11
NH_3 10.17	NH_3^+		NH_3^+	NH_3^+		NH_3^+
	7.0(−10)	4.9(−10)	1.6(−9)	8.3(−10)	1.8(−10)	1.4(−9)
	[1.71(−9)]		[1.64(−9)]	[1.66(−9)]		[1.62(−9)]
H_2S 10.47	H_2S^+(35) KrH^+(20) KrH^+(35) S^+(45) S^+(30) SH^+(35)		H_2S^+	H_2S^+		H_2S^+
	1.0(−9)	1.0(−9)	8.2(−10)	9.9(−10)	9.9(−10)	1.0(−9)
	[1.19(−9)]		[1.11(−9)]	[1.13(−9)]		[1.08(−9)]
C_2H_4 10.51	$C_2H_3^+$(45) $C_2H_2^+$(45) $C_2H_4^+$(10)		$C_2H_4^+$	$C_2H_3^+$(25) $C_2H_4^+$(75)		$C_2H_4^+$
	7.4(−10)	7.4(−10)	7.9(−10)	8.5(−10)	8.5(−10)	9.7(−10)
	[1.05(−9)]		[9.86(−10)]	[1.01(−9)]		[9.61(−10)]
C_3H_8 10.95	$C_2H_3^+$(5) $C_2H_4^+$(15) $C_2H_5^+$(60) $C_3H_3^+$(10) $C_3H_6^+$(10)		$C_2H_4^+$(30) $C_2H_5^+$(25) $C_3H_6^+$(5) $C_3H_7^+$(30) $C_3H_8^+$(10)	$C_3H_6^+$(30) $C_3H_7^+$(65) $C_3H_8^+$(5)		$C_3H_8^+$
	9.8(−10)	9.8(−10)	8.1(−10)	8.8(−10)	8.8(−10)	8.6(−10)
	[1.09(−9)]		[9.94(−10)]	[1.02(−9)]		[9.57(−10)]
COS 11.18	COS^+		COS^+	COS^+		$XeCOS^+$(85) COS^+(15)
	4.3(−10)	9.6(−11)	8.5(−10)	8.7(−10)	~2.0(−11)	6.5(−10)
	[1.07(−9)]		[9.57(−10)]	[9.88(−10)]		[9.12(−10)]
C_2H_2 11.41	—		$C_2H_2^+$	$C_2H_2^+$		$XeC_2H_2^+$
	< 1(−12)	< 1(−12)	9.2(−10)	5.0(−10)	3.5(−11)	8.9(−10)
	[9.59(−10)]		[9.00(−10)]	[9.18(−10)]		[8.79(−10)]
C_2H_6 11.51	$C_2H_4^+$(65) $C_2H_5^+$(35)		$C_2H_4^+$(35) $C_2H_5^+$(5) $C_2H_6^+$(60)	$C_2H_4^+$(55) $C_2H_5^+$(10) $C_2H_6^+$(35)		$XeC_2H_6^+$
	9.8(−10)	9.8(−10)	9.0(−10)	9.2(−10)	9.2(−10)	6.8(−10)
	[1.05(−9)]		[9.79(−10)]	[1.00(−9)]		[9.52(−10)]
O_2 12.06	O_2^+	—	O_2^+	O_2^+		—
	4.7(−11)	< 1(−12)	4.3(−10)	1.0(−10)	1.1(−10)	< 1(−12)
	[6.15(−10)]		[5.71(−10)]	[5.83(−10)]		[5.55(−10)]

Table 1. (continued)

Reactant molecule	Kr^+		Kr_2^+	Xe^+		Xe_2^+
	$^2P_{3/2}$	$^2P_{1/2}$		$^2P_{3/2}$	$^2P_{1/2}$	
	14.00	14.67	12.87	12.13	13.44	11.11
CH_4	CH_4^+	CH_3^+ (90)	$KrCH_4^+$ (40)	—	CH_4^+	—
12.62		CH_4^+ (10)	CH_4^+ (60)			
	1.0 (−9)	1.0 (−9)	7.1 (−10)	< 1 (−12)	9.0 (−10)	< 1 (−12)
		[1.03 (−9)]	[9.88 (−10)]		[1.00 (−9)]	[9.72 (−10)]
HCl	HCl^+		$KrHCl^+$ (90)	—	HCl^+	$XeHCl^+$
12.74			HCl^+ (10)			
	3.4 (−11)	3.3 (−12)	1.0 (−9)	< 1 (−12)	4.0 (−11)	3.1 (−11)
		[1.13 (−9)]	[1.04 (−9)]		[1.07 (−9)]	[1.01 (−9)]
N_2O	N_2O^+		KrN_2O^+ (40)	—	N_2O^+	—
12.89			N_2O^+ (60)			
	4.0 (−10)	1.5 (−11)	6.2 (−10)	< 1 (−12)	6.3 (−10)	< 1 (−12)
		[7.61 (−10)]	[6.93 (−10)]		[7.01 (−10)]	[6.67 (−10)]
CO_2	CO_2^+		—	—		—
13.77	6.3 (−10)	6.3 (−10)	< 1 (−12)	< 1 (−12)	< 1 (−12)	< 1 (−12)
		[7.01 (−10)]	[6.38 (−10)]		[6.57 (−10)]	[6.14 (−10)]
CO	CO^+		$KrCO^+$	—		$XeCO^+$
14.01	2.0 (−10)	2.8 (−11)	3.8 (−10)	< 1 (−12)	< 1 (−12)	1.9 (−12)
		[7.14 (−10)]	[6.68 (−10)]		[6.57 (−10)]	[6.51 (−10)]

product ions of reaction are monitored by a downstream quadrupole mass filter/detection system. Rate coefficients and ion product distributions (branching ratios) appropriate to the temperature of the reaction (the carrier gas temperature) are derived by relating the detected ion count rates to the flow rate of the reactant gas. All the experiments reported here were carried out at 300 K.

The atomic ions Kr^+ and Xe^+ were created from the rare gases in both low-pressure and high-pressure electron impact ion sources. In the low pressure source the ions suffer no collisions with their parent gases, whereas in the high-pressure source they may undergo many collisions depending on the pressure of the rare gas. The ratios of the currents of ions in both the $^2P_{3/2}$ and $^2P_{1/2}$ states that emerged from the low-pressure ion source were observed to be close to that expected on the basis of the statistical weights of the states ($(2J+1)$, i.e. 2:1 in favour of the $^2P_{3/2}$ state), whereas greater fractions of the lower-energy $^2P_{3/2}$ states emerged from the high-pressure source as the result of quenching of the high-energy state in collisions with the parent gas atoms. The fraction of each state in the carrier gas is evident from their differing reactivity with some reactant gases; an example of this is given in figure 1 for the reaction of $Xe^+(^2P_{3/2}, ^2P_{1/2})$ with C_2H_2. A straightforward analysis of the data provides the fraction of the ions in each state and the separate rate coefficients for the reactions (for further discussion of this see Adams *et al* (1980) and Adams and Smith (1988)).

The molecular ions Kr_2^+ and Xe_2^+ necessarily have to be generated in the high-pressure source. They are generated in both binary collisions of Kr and Xe with excited parent atoms (associative ionisation, e.g., $Kr + Kr^* \rightarrow Kr_2^+ + e$ (Samson and Cairns 1966)) and in ternary collisions between the atomic ions and ground state atoms (e.g. $Kr^+ + 2Kr \rightarrow Kr_2^+ + Kr$ (Smith *et al* 1972)). No convincing evidence for more than one

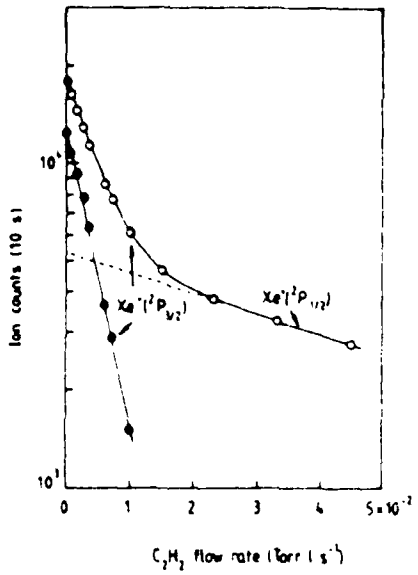

Figure 1. A semilogarithmic plot of the count rate of $Xe^+(^2P_{3/2}, ^2P_{1/2})$ ions versus the flow rate of C_2H_2 reactant gas obtained in the SIFT study (open circles). The slope of the line at the larger flow rates provides a value for the rate coefficient for the reaction of $Xe^+(^2P_{1/2})$ with C_2H_2. The linear plot (full circles) is derived by subtracting the count rates indicated by the dashed extrapolated line from the $Xe^+(^2P_{3/2}, ^2P_{1/2})$ count rate at the same flow rate of C_2H_2, and the slope of the line provides a value for the rate coefficient for the reaction of $Xe^+(^2P_{3/2})$ with C_2H_2. A bi-exponential fitting procedure using a microcomputer was used also to determine the separate rate coefficients with identical results.

reacting species of either Kr_2^+ or Xe_2^+ was obtained. In several of the reactions of these molecular ions, parallel charge transfer and rare gas atom/reactant molecule switching were observed (generating ions such as, for example, $KrHCl^+$ from the $Kr_2^+ + HCl$ reaction). To determine the branching ratio into the charge transfer and switching channels it was necessary to account for the several isotopic forms of the product ions containing the rare gas atoms. The measured rate coefficients are considered to be accurate to ±20%.

3. Results

In the previous study (Adams *et al* 1980) the rate coefficients and product ions for the reactions of Kr^+ and Xe^+ with NH_3, H_2S, COS, O_2, CH_4, N_2O, CO_2 and CO were determined. In some of these reactions the differing reactivities of the $^2P_{3/2}$ and $^2P_{1/2}$ states were very obvious; in others the rate coefficients were indistinguishable at the collisional limiting (maximum) value of the rate coefficient, k_c (calculated using well known theory (Su and Bowers 1979)). We have now extended this study of atomic ion reactions to include the hydrocarbon reactant gases C_2H_2, C_2H_4, C_2H_6 and C_3H_8 and also HCl, and the reactions of the molecular ions Kr_2^+ and Xe_2^+ have been studied with these gases and those mentioned above, amounting to 13 gases in all. The rate coefficients and ion product distributions for both the atomic and molecular ion reactions are given in table 1, together with the previous data for comparison. The layout of the table involves some simple logic. The reactant molecules are ordered

according to their ionisation energies (given below each molecule in eV) from the smallest, NH_3, to the largest, CO. The accurately known recombination energies for the $^2P_{3/2}$ and $^2P_{1/2}$ states of each atomic ion and those for the ground state of the molecular ions are also given, the latter being more precisely defined by the present studies (see § 3.2). The organisation of the table places the most exothermic charge transfer reactions (for ground state products) in the top left-hand corner and the least exothermic (and some endothermic) charge transfer reactions at the bottom right-hand corner. The thermicities for all the individual reaction channels have been obtained using thermochemical data from Rosenstock *et al* (1977). It has been assumed in calculating the reaction energetics that when two hydrogen atoms are released in the hydrocarbon reactions they appear as an H_2 molecule (three H atoms appear as H_2 and H) thus releasing the H-H bond energy. If this were not the case then all of such reaction channels observed to proceed would have been very endothermic, and so the rate data together with the thermicities is proof that H_2 formation does indeed occur in every case. The thermicity of each reaction is not included in the table to avoid making it too complicated. The thermicities for those very interesting reactions that are close to thermoneutral and which provide data on the recombination energies of Kr_2^+ and Xe_2^+ are given in § 3.2, where individual reactions are discussed.

3.1. Reactions of Kr^+ and Xe^+ with C_2H_4, C_3H_8, C_2H_2, C_2H_6 and HCl

The reactions of Kr^+ and Xe^+ with the other molecules included in the table have been discussed previously (Adams *et al* 1980) and so they are not discussed here. In those studies, the product ions of the reactions of the separate spin-orbit states were determined using filter gases to selectively remove either the $\frac{3}{2}$ or the $\frac{1}{2}$ state ions from the flow tube. This procedure inevitably introduces another reactive ionic species into the flow tube (e.g. when N_2O is used to 'filter out' $Xe^+(^2P_{1/2})$ from a mixture of both spin-orbit state ions, N_2O^+ is produced) which can produce other ions in reaction with the reactant gas and confuse the determination of product ion distributions. This was not too severe a problem for the 'simpler molecules' included in the Adams *et al* (1980) study, but was too severe for the hydrocarbon molecules included in this study, where, with the exception of C_2H_2, charge transfer and dissociative charge transfer were observed to occur, producing several product ions. So the product ions resulting from the separate reactions of each spin-orbit state could not be identified with much certainty. To circumvent this problem, two procedures were attempted with limited success. They were: (i) to add a small amount of filter gas (e.g. N_2O) to the high-pressure ion source containing the rare gas in order to destroy one state of the atomic ion and thus, hopefully, to introduce only one state into the flow tube (whilst this does reduce the fraction of the more reactive ion it is not sufficiently effective to allow unambiguous determination of product ions of one spin-orbit state only); (ii) to obtain the atomic ions by injecting the molecular ions (formed in the high pressure ion source) at the maximum lab. energy (50 eV) into the helium carrier gas in the flow tube, thus causing dissociation. Both the Kr^+ and Xe^+ ions formed in this way were in their lowest-energy $\frac{3}{2}$ states as shown by measuring the rate coefficients for their reactions with appropriate gases (e.g. N_2O, COS, see table 1). Fragmentation to the $\frac{3}{2}$ state is to be expected if the molecular ions are in their ground states or low-lying excited states (Dehmer and Dehmer 1978) and, indeed, this observation is taken as proof that the Kr_2^+ and Xe_2^+ ions extracted from the high-pressure ion source are predominantly in their ground states. Unfortunately, only a small fraction ($\sim\frac{1}{4}$) of the molecular ions could be

dissociated in this manner and thus a mixture of atomic and molecular ions was present in the flow tube to confuse the product ion distributions.

So, no attempt has been made in these studies to associate particular ion products of the reactions of Kr^+ and Xe^+ with particular spin-orbit states, except that in some cases it is clear that particular ion products can only be generated by the $\frac{1}{2}$ state because of energy constraints. For example, the reactions of $Xe^+(^2P_{3/2}, ^2P_{1/2})$ with C_2H_4 proceed to the following products:

$$Xe^+(^2P_{3/2}, ^2P_{1/2}) + C_2H_4 \rightarrow C_2H_2^+ + H_2 + Xe\ (-1.09, 0.22) \quad (1a)$$

$$\rightarrow C_2H_4^+ + Xe\ (1.62, 2.93). \quad (1b)$$

The numbers in brackets are the thermicities of the reactions in electron volts (eV) for the reactions of the $^2P_{3/2}$ and $^2P_{1/2}$ states of the Xe^+ respectively, the negative number indicating an endothermic channel. Thus, $C_2H_2^+$ can only generated from the $Xe(^2P_{1/2})$ ions, whereas $C_2H_4^+$ could be generated by both states of the Xe^+. All three products of the Kr^+ reactions with C_2H_4 can be produced by both spin-orbit states of the Kr^+. Note that the rate coefficients are not discernably different for the reactions of the individual spin states of Kr^+ and Xe^+ with C_2H_4, C_3H_8 and C_2H_6. All the reactions are efficient i.e. the rate coefficients are large fractions of the respective collisional rate coefficients (given in square brackets below the measured values in table 1) and multiple products are observed. For the reaction:

$$Xe^+(^2P_{3/2}, ^2P_{1/2}) + C_3H_8 \rightarrow C_3H_6^+ + H_2 + Xe\ (1.10, 2.41) \quad (2a)$$

$$\rightarrow iso\text{-}C_3H_7^+ + H + Xe\ (0.51, 1.82) \quad (2b)$$

$$\rightarrow C_3H_8^+ + Xe\ (1.18, 2.49) \quad (2c)$$

the major product (65%) is $C_3H_7^+$. However, production of $n\text{-}C_3H_7^+$ (i.e. $CH_3CH_2CH_2^+$) from $Xe^+(^2P_{3/2})$ (which represents about 66% of the total Xe^+ signal in the flow tube) is endothermic by 0.20 eV. Thus at least half of the $C_3H_7^+$ product ions must originate from $Xe^+(^2P_{3/2})$ and are presumably $iso\text{-}C_3H_7^+$ (i.e. $CH_3CH^+CH_3$), the production of which from the $Xe^+(^2P_{3/2})$ ions is exothermic by 0.51 eV. Also, due to energetic constraints, the small $C_2H_3^+$ product of the Xe^+ reaction with C_2H_6 must be generated from the $Xe^+(^2P_{1/2})$ ions.

The most unexpected result of these reactions involving hydrocarbon molecules is the unreactivity of C_2H_2 with both states of Kr^+ ions. This result was checked and double-checked and is an extremely unusual result for the reactions of energetic ions with polyatomic molecules, which are normally very efficient. This may be due to unfavourable Franck-Condon factors connecting C_2H_2 with the accessible (highly vibrationally excited) states of $C_2H_2^+$ ions. This result is especially surprising since Kr_2^+ rapidly charge transfers with C_2H_2 (see table 1) and so also does $Xe^+(^2P_{3/2})$. It is perhaps significant that amongst the hydrocarbon molecules included in this study, C_2H_2 is the only one that reacts at different rates with the two states of Xe^+. Again, as before, it is the $\frac{1}{2}$ state which reacts more rapidly whenever differential reactivity is observed and when both charge transfer channels are exothermic:

$$Xe^+(^2P_{3/2}, ^2P_{1/2}) + C_2H_2 \rightarrow C_2H_2^+ + Xe(0.72, 2.03). \quad (3)$$

Differential reactivity is also observed for the reactions of both Kr^+ and Xe^+ with HCl. Charge transfer between both states of Kr^+ ions and HCl is exothermic, and

again the $\frac{1}{2}$ state reacts more rapidly (see table 1). However, charge transfer is exothermic only for the reaction of the $\frac{1}{2}$ state of Xe^+ with HCl,

$$Xe^+(^2P_{3/2}, ^2P_{1/2}) + HCl \rightarrow HCl^+ + Xe(-0.61, 0.70) \tag{4}$$

and only this state is observed to react at a significant rate.

3.2. *Reactions of Kr_2^+ and Xe_2^+*

The smaller recombination energies of these molecular ions relative to their atomic counterparts renders charge transfer endothermic with several of the molecules included in this study (this is especially so for Xe_2^+). However, when charge transfer is energetically allowed it occurs efficiently, usually producing only the parent ion of the reactant molecule although there are obvious exceptions to this in which dissociative charge transfer occurs leading to multiple products (e.g. the reactions with C_3H_8 and C_2H_6—see table 1). Of much greater interest is the observation that when charge transfer is endothermic or near-thermoneutral, product ions comprising the reactant molecule and an inert gas atom appear. These atom/reactant molecule exchange or 'switching' reactions are exemplified by

$$Xe_2^+ + C_2H_2 \rightarrow XeC_2H_2^+ + Xe \tag{5}$$

in which the single product ion $XeC_2H_2^+$ is formed. Charge transfer is endothermic by 0.3 eV in this case. A single switching product is also observed for the reactions of Xe_2^+ with C_2H_6 and HCl which are also endothermic to charge transfer. However, in the reactions of Kr_2^+ with CH_4 and HCl charge transfer is exothermic by 0.25 eV and 0.13 eV respectively and in these reactions the charge transfer and switching products are both observed (see table 1). In two reactions charge transfer is apparently slightly endothermic (as determined from the available thermochemical data) yet the charge transfer products are significant parts of the product distributions (along with the switching products), these being:

$$Kr_2^+ + N_2O \rightarrow N_2O^+ + 2Kr_2\ (60\%) \tag{6a}$$

$$\rightarrow KrN_2O^+ + Kr\ (40\%) \tag{6b}$$

and the reaction:

$$Xe_2^+ + COS \rightarrow COS^+ + 2Xe_2\ (15\%) \tag{7a}$$

$$\rightarrow XeCOS^+ + Xe\ (85\%). \tag{7b}$$

Note that we assume that the least endothermic neutral products, i.e. Kr_2 and Xe_2, are formed in reactions (6*a*) and (7*a*) respectively, and this has implications for the dissociation energies derived below for Kr_2^+ and Xe_2^+.

The rate coefficients of the charge transfer reactions (6*a*) and (7*a*) obtained as the percentages of the total rate coefficient in each case are 3.7×10^{-10} cm^{3}s^{-1} and 9.8×10^{-11} cm^{3}s^{-1} respectively. These rate coefficients can be used to define a lower-limit to the recombination energies, R_e, of the Kr_2^+ and Xe_2^+ ions on the assumption that the measured rate coefficients, $k(300)$, are lower than the respective collisional values, $k_c(300)$, only by virtue of the endothermicities of the reactions. Thus the application of the Boltzmann relationship, $k(300) = k_c(300)\exp(-\Delta E/300k_b)$, where k_b is the Boltzmann constant, provides an upper-limit value for the endothermicity, ΔE. Then the R_e of the reactant ion (Kr_2^+ or Xe_2^+ here) is smaller than the ionisation energy, I_e,

of the reactant molecule by an amount ΔE. Thus for reaction (6*a*), ΔE takes a maximum value of 0.022 eV and the $R_e(Kr_2^+) \geqslant (I_e(N_2O) - 0.022) = 12.872$ eV (using 12.89(4) eV as the accurate value for $I_e(N_2O)$ (Rosenstock *et al* 1977)). Using this lower-limit value of $R_e(Kr_2^+)$ an upper limit to the dissociation energy, $D_e(Kr_2^+)$, of the Kr^+-Kr ion can be obtained. Thus $D_0(Kr_2^+)$ is given by $R_e(Kr^+(^2P_{3/2})) + D_0(Kr_2) - R_e(Kr_2^+)$, i.e. $(13.999 + 0.016 - 12.872) = 1.143$ eV or, more correctly, $D_0(Kr_2^+) \leqslant 1.15$ eV. The value for $D_0(Kr_2)$, and also that for $D_0(Xe_2)$ (see below), were obtained from Dehmer and Dehmer (1978). This compares favourably with the value of 1.15 ± 0.02 eV deduced by Ng *et al* (1977) from their studies of the photoionisation threshold of Kr_2 neutral dimers (their similar work on Xe_2 dimers is referred to below). Combining these two experimental determinations, a most likely value for $D_0(Kr_2^+)$ is the value indicated by the present studies as an upper-limit value, i.e. 1.15 eV. These experimental values together with the available theoretically determined D_0, due to Michels *et al* (1978) and Christiansen *et al* (1981), are given in table 2.

Using the kinetic data obtained for reaction (7*a*), ΔE takes a maximum value of 0.064 eV and thus, as before, $R_e(Xe_2^+) \geqslant (I_e(COS) - 0.064) = 11.110$ eV ($I_e(COS)$ is taken to be 11.17(4) eV for this calculation, i.e. the lower limit of the reported value, 11.184 ± 0.01 eV (Rosenstock *et al* 1977), to enable an upper limit to $D_0(Xe_2^+)$ to be determined). This value is in agreement with the lower limit of the appearance potential of Xe_2^+, determined to be 11.10 eV by Laporte *et al* (1983). Then the upper limit to $D_0(Xe_2^+)$, the dissociation energy of Xe^+-Xe, is given by $R_e(Xe^+(^2P_{3/2})) + D_0(Xe_2) - R_e(Xe_2^+)$, i.e. $(12.130 + 0.023 - 11.110) = 1.043$ eV; so $D_0(Xe_2^+) \leqslant 1.05$ eV. This is acceptable with the value derived by Ng *et al* (1976) of 1.03 ± 0.01 eV given in table 2. Again as for our value of $D_0(Kr_2^+)$, our value for $D_0(Xe_2^+)$ is somewhat smaller than the theoretical value of Michels *et al* (1978). So our judgement is that $D_0(Xe_2^+)$ is nearly equal to 1.05 eV.

It is interesting to note that the reaction

$$Xe_2^+ + C_3H_8 \rightarrow C_3H_8^+ + 2Xe/Xe_2 \tag{8}$$

is only exothermic by 0.16 eV yet the measured rate coefficient is close to the collisional

Table 2. The bond dissociation energies of ground state Kr_2^+ and Xe_2^+ ions in electron volts derived from experimental studies and from theory. Those derived from the present work (a) are considered to be strict upper-limit values for both ions. Other sources are as follows.

[b] Ng *et al* (1977): photoionisation of Kr_2 molecules.
[c] Pratt and Dehmer (1982): photoionisation of Kr_2 molecules.
[d] Abouaf *et al* (1978): photodissociation of Kr_2^+ ions.
[e] Ng *et al* (1976): photoionisation of Xe_2 molecules.
[f] Michels *et al* (1978)
[g] Christiansen *et al* (1981).

Kr_2^+		Xe_2^+	
Experiment	Theory	Experiment	Theory
$\leqslant 1.15$[a]	1.18[f]	$\leqslant 1.05$[a]	1.06[f]
1.15 ± 0.02[b]	1.13[g]	1.03 ± 0.01[e]	1.05[g]
1.150 ± 0.004[c]			
1.176 ± 0.02[d]			

value (see table 1) giving some credence to our assumption that for $\Delta E = 0$, the measured k can approach k_c for many ion-molecule reactions.

4. Concluding remarks

The present studies of the reactions of Kr^+ and Xe^+ follow the pattern of previous studies in that where differential reactivity of the $^2P_{3/2}$ and $^2P_{1/2}$ spin-orbit states of these ions is observed, it is the lower-energy $^2P_{3/2}$ state which reacts more rapidly. A similar result has previously been obtained for the reactions of the spin-orbit states of the isoelectronic halogen atoms.

Our comprehensive studies of the reactions of Kr_2^+ and Xe_2^+ ions is the first reported. Whereas only charge transfer is observed in the reactions of the atomic ions, both charge transfer and inert gas atom/reactant molecule switching is observed in the molecular ion reactions generating ions such as $KrCH_4^+$ and $XeC_2H_2^+$. Secondary reactions occur between the latter ions and the reactant gas generating dimer ions such as $C_2H_2^+ . C_2H_2$. These interesting reactions will be discussed in a further publication.

Making reasonable assumptions regarding the kinetics of the near-thermoneutral charge transfer reactions of Kr_2^+ with N_2O and Xe_2^+ with COS we have determined upper-limit values of the dissociation energies of these inert gas molecular ions. The values are in excellent agreement with the values derived from photoionisation studies of the neutral dimer molecules Kr_2 and Xe_2 and close to the derived theoretical values.

These studies demonstrate again that studies of ion-molecule reactions at thermal energies can provide accurate thermochemical data on ions (see the discussion of this in the paper by Smith *et al* (1981)). These studies of Kr_2^+ and Xe_2^+ reactions may also be of interest to those researching into the processes occurring in rare gas lasers (Laudenslager 1979).

Acknowledgments

Our thanks are due to SERC and USAF for providing financial support of this work.

References

Abouaf R, Huber B A, Cosby P C, Saxon R P and Moseley J T 1978 *J. Chem. Phys.* **68** 2406
Adams N G and Smith D 1988 *Techniques for the Study of Ion-Molecule Reactions* ed J M Farrar and W Saunders Jr (New York: Wiley) p 165
Adams N G, Smith D and Alge E 1980 *J. Phys. B: At. Mol. Phys.* **13** 3235
Bohme D K, Adams N G, Mosesman M, Dunkin D B and Ferguson E E 1970 *J. Chem. Phys.* **52** 5094
Christiansen P A, Pitzer K S, Lee Y S, Yates J H, Ermler W C and Winter N W 1981 *J. Chem. Phys.* **75** 5410
Collins C B and Lee F W 1980 *J. Chem. Phys.* **72** 5381
Dagdigian P J and Campbell M L 1987 *Chem. Rev.* **87** 1
Dehmer P M and Dehmer J L 1978 *J. Chem. Phys.* **69** 125
Guyon P M, Govers T R and Baer T 1986 *Z. Phys.* D **4** 89
Ikezoe Y, Matsuoka S, Takebe M and Viggiano A 1987 *Gas Phase Ion-Molecule Reaction Rate Constants Through 1986* (The Mass Spectroscopy Society of Japan, Tokyo, 112 Japan)
Jones T T C, Birkinshaw K, Jones J D C and Twiddy N D 1982 *J. Phys. B: At. Mol. Phys.* **15** 2439
Khan A and Jordan K D 1986 *Chem. Phys. Lett.* **128** 368
Laporte P, Saile V, Reininger R, Asaf U and Steinberger I T 1983 *Phys. Rev.* A **28** 3613

Laudenslager J B 1979 *Kinetics of Ion-Molecule Reactions* ed P Ausloos (New York: Plenum) p 405
Liao C L, Shao J D, Xu R, Flesch G D, Li Y G and Ng C Y 1986 *J. Chem. Phys.* **85** 3874
Michels H H, Hobbs R H and Wright L A 1978 *J. Chem. Phys.* **69** 5151
Ng C Y, Trevor D J, Mahan B H and Lee Y T 1976 *J. Chem. Phys.* **65** 4327
—— 1977 *J. Chem. Phys.* **66** 446
Pratt S T and Dehmer P M 1982 *Chem. Phys. Lett.* **87** 533
Rosenstock H M, Draxl K, Steiner B W and Herron J T 1977 *J. Phys. Chem. Ref. Data* **6** suppl 1
Samson J A R and Cairns R B 1966 *J. Opt. Soc. Am.* **56** 1140
Smith D and Adams N G 1987 *Adv. At. Mol. Phys.* **24** 1
Smith D, Adams N G and Lindinger W 1981 *J. Chem. Phys.* **75** 3365
Smith D, Dean A G and Plumb I C 1972 *J. Phys. B: At. Mol. Phys.* **5** 2134
Su T and Bowers M T 1979 *Gas Phase Ion Chemistry* vol 1, ed M T Bowers (New York: Academic) p 83
Tanaka K, Durup J, Kato T and Koyano I 1981 *J. Chem. Phys.* **74** 5561